ATTACHMENT 2

FINAL STEAM DRYER STRESS REPORT

CONTINUUM DYNAMICS, INCORPORATED REPORT NO. 12-18NP

(NON-PROPRIETARY)

Certain information, considered proprietary by Continuum Dynamics, Inc., has been deleted from the document in this Attachment. The deletions are identified by double square brackets ([[ ]]).

This Document Does Not Contain Continuum Dynamics, Inc. Proprietary Information

CDI Report No. 12-18NP

Stress Evaluation of Nine Mile Point Unit 2 Steam Dryer at 115% CLTP

Revision 0

Prepared by

Continuum Dynamics, Inc.
34 Lexington Avenue
Ewing, NJ 08618

Prepared under Purchase Order No. 4500428093 for

Westinghouse Electric Company LLC
1000 Westinghouse Drive
Cranberry Township, PA 16066

Prepared by

Alexander H. Boschitsch

Approved by

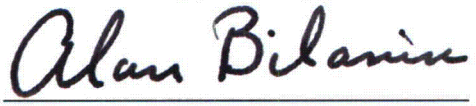

Alan J. Bilanin

October 2012

This report complies with Continuum Dynamics, Inc. Nuclear Quality Assurance Program currently in effect.

Executive Summary

The stresses resulting from acoustic loads at the 115% CLTP operating condition (also referred to herein as the extended power uprate or EPU condition) are calculated for the Nine Mile Point Unit 2 (NMP2) steam dryer using a finite element model and frequency-based analysis methodology. The finite element model of the steam dryer is identical to the one previously described in [1] and incorporates the modifications [1, 2] to the steam dryer previously deemed necessary to meet an alternating stress ratio SR-a>2 at EPU. Like the acoustic load analysis, the stress calculation is carried out in the frequency domain using the harmonic methodology described in Section 2. The stress analysis is consistent with those carried out in the U.S. for prior dryer qualification to EPU conditions. The resulting stresses are assessed for compliance with the ASME B&PV Code 2007 [3], Section III, subsection NG, for the load combination corresponding to normal operation (the Level A Service Condition).

The acoustic loads are prepared using the acoustic circuit model (ACM) version 4.1 [4]. This most recent version reflects biases and uncertainties obtained during re-benchmarking against available Quad Cities (QC) data carried out under the requirement that identical filtering methods be used on both QC data and new plant signal measurements. The ACM acoustic load predictions are obtained using main steam line strain gage measurements acquired at 115% CLTP conditions [5]. Other than the removal of known non-acoustic discrete frequencies (e.g., electrical noise at multiples of 60 Hz) and the application of coherence filtering (which was also invoked when processing the QC data) no other filtering methods are used. Further details of the acoustic load processing procedure are given in [4].

It is required that the alternating stress ratios at EPU be above a target level of 2.0. In order to meet this target, modifications to the dryer detailed in Section 5 of [1] and also in [6], were implemented. The modifications fall into the following groups:

(1) Welds connecting the lifting rod braces to the vane bank side plates. These locations experienced high stress before modification that were addressed by a combination of localized reinforcement plates (the two upper-most braces) and increased weld size (lower-most brace).
(2) Welds lying on the inward edge of the middle hood reinforcement strip. A $1/8^{th}$ inch thick reinforcement plate has been added onto the portion of the middle hood lying outboard of the closure plate.
(3) Inner hood/hood support welds. A total of four 15 lb masses were placed on the centermost inner hoods.
(4) Miscellaneous locations at: (i) the bottoms of the drain channels, (ii) ends of tie bars and (iii) the hood/hood support/base plate junctions which were predicted to have alternating stress ratios slightly below 2.0 at EPU before modifications were installed.
(5) Closure plate attachment welds that experienced high stresses due to vibration of the closure plate. These stresses were alleviated by attaching reinforcement ribs to suppress the adverse resonant responses.

To obtain refined estimates of the linearized stresses at selected high stress locations
[[

(3)]]

A stress evaluation of the entire post-reinforcement NMP2 steam dryer shows that at nominal EPU operation (no frequency shift) the minimum alternating stress ratio (SR-a) anywhere on the steam dryer is SR-a=3.09. The loads used to obtain this value account for all the end-to-end biases and uncertainties in the loads model [5] and finite element analysis. To account for uncertainties in the modal frequency predictions of the finite element model, the stresses are also computed for loads that are shifted in the frequency domain by ±2.5%, ±5%, ±7.5% and ±10%. The minimum alternating stress ratio encountered at any frequency shift is found to be SR-a=2.49 occurring at the +7.5% shift and occurring on the inner vane bank welded end plate/side plate junction. The stress ratio due to maximum stresses (SR-P) is dominated by static loads and is SR-P=1.25 with all frequency shifts considered.

The assessment shows that with the modifications in place the NMP2 steam dryer meets the required stress margin at EPU operation.

During power ascension testing NMP identified two off-normal loading conditions associated with the operational lineup of the RCIC system. Therefore additional stress evaluation is performed using both estimated and measured loads obtained with the RCIC line isolated at the EPU condition. The resulting limiting alternating stress ratio is shown to be SR-a=2.05 so that the target stress margin is maintained.

Table of Contents

Section Page

1. Introduction and Purpose

Current licensing procedures to qualify the Nine Mile Point Unit 2 (NMP2) nuclear plant for operation at Extended Power Uprate (EPU) operating condition require a stress assessment of the steam dryer to ensure adequate stress margins under the increased loads. The steam dryer loads due to acoustic pressure fluctuations in the main steam lines (MSLs) are potentially damaging and the cyclic stresses from these loads can produce fatigue cracking if loads are sufficiently high. The industry has addressed this problem with physical modifications to the dryers, as well as a program to define steam dryer loads and their resulting stresses. The EPU qualification process includes stress evaluations using both current licensed thermal power (CLTP) and EPU acoustic loads. The CLTP loads are acquired first and, by appropriate scaling, used to estimate EPU loads before power ascension takes place. A stress evaluation is carried out for these scaled loads to establish adequate stress margin and, if required, to design dryer modification to meet these margins. Details of these CLTP-based stress evaluations are documented in [1]. Since the methods for estimating EPU loads from ones measured at CLTP are subject to inherent conservatisms and approximations a confirmatory stress calculation is also required that uses actual loads measured at EPU conditions. The present report documents this confirmatory stress evaluation for the NMP2 steam dryer by calculating the maximum and alternating stresses generated using strain gage MSL pressure measurements acquired at EPU operation as documented in [5] (data file name: 20120721142636).

The load combination considered here corresponds to normal operation (the Level A Service Condition) and includes fluctuating pressure loads developed from NMP2 main steam line data, and weight. The fluctuating pressure loads, induced by the flowing steam, are predicted using a separate acoustic circuit analysis of the steam dome and main steam lines [8]. Level B service conditions, which include seismic loads, are not included in this evaluation. Stress ratios are obtained by comparing these stresses (appropriately adjusted at welds) against allowable values and used to ensure compliance with the ASME Code (ASME B&PV Code, Section III, subsection NG) and to confirm that the alternating stress ratio, SR-a>2, as required under current licensing requirements.

The current stress evaluation of the NMP2 steam dryer is performed using acoustic loads generated using a revised Acoustic Circuit Model (ACM) Rev. 4.1 [4]. The development of this revision was motivated primarily by a requirement for consistent usage of noise filtering strategies during both model calibration against available data and application of the model to plants. Other than the removal of known non-acoustic discrete frequencies (e.g., electrical noise at multiples of 60 Hz) and the application of coherence filtering (which was also invoked when processing the Quad Cities data) no other filtering methods are used. In particular, no noise subtraction using low power data is performed. Further details of the ACM Rev. 4.1 calibration activity are provided in [4]. Its application to obtain NMP2 steam dryer acoustic loads is detailed in [5]. As described in [4] re-benchmarking the ACM against available Quad Cities data produced updated estimates of the acoustic speed and damping in the acoustics description and also revised biases and uncertainties due to changes in the model, coherence-based noise filtering and comparison method. The biases and uncertainties used for the present load estimates are based on the comparison with QC data at 790MWe using 16 sensors.

The stress analysis is carried out in the frequency domain, which confers a number of useful computational advantages over a time-accurate transient analysis including the ability to assess the effects of frequency scaling in the loads without the need for additional finite element calculations. The analysis develops a series of unit stress solutions corresponding to the application of a unit pressure at a MSL at specified frequency, f. Each unit solution is obtained by first calculating the associated acoustic pressure field using a separate analysis that solves the damped Helmholtz equation within the steam dryer [9]. This pressure field is then applied to a finite element structural model of the steam dryer and the harmonic stress response at frequency, f, is calculated using the commercial ANSYS 10.0 finite element analysis software. This stress response constitutes the unit solution and is stored as a file for subsequent processing. Once all unit solutions have been computed, the stress response for any combination of MSL pressure spectrums (obtained by Fast Fourier Transform of the pressure histories in the MSLs) is determined by a simple matrix multiplication of these spectrums with the unit solutions. Details of the frequency-based stress evaluation methodology are contained in

In order to qualify the NMP2 steam dryer for EPU operation it is required that the limiting alternating stress ratio at EPU be above a target level of 2.0. In previous stress evaluations [10] it was determined that when the estimated EPU acoustic loads were impressed on the original steam dryer configuration, the predicted alternating stress ratios at several locations fell below the target level. Therefore, modifications to the steam dryer have been implemented to ensure that all locations meet or exceed the target stress ratio. Briefly, the groups and associated modifications consist of the following:

Group 1: The lifting rod bracket/side plate welds. High membrane stresses were predicted on the end of the existing weld. For the upper and middle brackets the modification to alleviate these stresses consists of reinforcements plates welded to the vane bank side plate and brace. For the lower-most brackets a simple increase in the weld size from ¼" to ½" suffices to reduce the stress to acceptable levels.

Group 2: The middle hood reinforcement strip that previously experienced a high stress due to vibration of the outboard section of the middle hood. This stress has been alleviated by overlaying a 1/8" curved plate over the portion of the middle hood located between the existing reinforcement strip and the closure plate.

Group 3: The inner hood/hood support welds that were previously subject to high stresses resulting from the inner hood vibrations. To reduce these stresses a total of four 15 lb masses are placed on the central inner hood panels (the two panels connecting to the central hood support) 18" below the top of the vane bank surface.

Group 4: A collection of locations that were previously determined to be slightly under the target stress ratios. These locations included:
(a) Middle hood/hood support welds. These stress locations are similar to the ones on the inner hood/hood support welds and are alleviated in a similar manner by adding a total of four 10 lb masses to the central sections of the middle hoods.

(b) Bottoms of the drain channel/skirt welds. These welds have been reinforced by thickening the length and wrapping the weld around the junction terminus and continuing it for 1" along the interior side.

(c) Outer hood/hood support/cover plate junctions. A stress relief cut-out hole optimized to minimize the alternating stresses has been added to the support plate.

Group 5: The closure plate attachment welds that, in the original configuration, encountered high stresses due to a strong 128 Hz vibration of the closure plate. These stresses have been addressed by attaching reinforcement ribs to suppress and increase the frequency of the adverse resonant response.

These modifications are fully accounted for in the current stress evaluation by updating the unit solutions of the complete dryer over the 30-250 Hz frequency range including the stiffened closure plate, the masses added to the inner and middle hoods, and the 1/8" thick reinforcement plate placed over the middle hood section outboard of the closure plate. Below 30 Hz the original un-modified steam dryer unit solutions are used. This is acceptable since the dynamic response of the dryer below this frequency is small; it is also conservative since no credit is taken for the stress reductions realized by these modifications. Other reinforcements such as the modified channel/skirt weld are localized [[

(3)]]

The frequency-based harmonic stress evaluation methodology, finite element model and post-processing procedures ([[(3)]]) are fully identical to those described in the previous NMP2 steam dryer stress evaluation using CLTP loads scaled to EPU conditions [1] and are described in Sections 2-4. The modifications made to the dryer are described in Section 5. The present stress report is distinguished from previous ones in that the acoustic signals are obtained at actual EPU conditions rather than inferred from CLTP measurements. The results in terms of stress intensity distributions and stress ratios together with PSDs of the dominant stress components are given in Section 6.

This stress evaluation shows that the limiting alternating stress ratio on the dryer at EPU is SR-a=2.49. The limiting peak stress ratio due to maximum membrane and bending stresses including static contributions is SR-P=1.25. These values show that the present modified steam dryer meets the required stress margin at EPU operation.

During power ascension testing NMP identified two off-normal loading conditions associated with the operational lineup of the reactor core isolation cooling (RCIC) system that create either a 92.5 Hz or 89.25 Hz content on the MSL B line. To predict the stresses resulting from this load real time analyses were performed using both estimated and measured EPU loads obtained from the test data. These calculations (Section 6.4) show that the limiting alternating stress ratio is SR-a=2.05 thus confirming that the required stress margin is sustained.

2. Methodology & Evaluation Procedures

2.1 Overview

Based on previous analysis undertaken at Quad Cities Units 1 and 2, the steam dryer can experience strong acoustic loads due to the fluctuating pressures in the MSLs connected to the steam dome containing the dryer. C.D.I. has developed an acoustic circuit model (ACM) that, given a collection of strain gage measurements of the fluctuating pressures in the MSLs, predicts the acoustic pressure field anywhere inside the steam dome and on the steam dryer [4, 8, 9, 11]. The ACM is formulated in frequency space and contains two major components that are directly relevant to the ensuing stress analysis of concern here. [[

(3)]]

[[

[3]]]

[[

[3]]]

2.2 [[[3]]]

[[

[3]]]

[[

(3)]]

2.3 Computational Considerations

Focusing on the structural computational aspects of the overall approach, there are a number of numerical and computational considerations requiring attention. The first concerns the transfer of the acoustic forces onto the structure, particularly the spatial and frequency resolutions. The ANSYS finite element program inputs general distributed pressure differences using a table format. This consists of regular 3D rectangular (i.e., block) $n_x \times n_y \times n_z$ mesh where n_α is the number of mesh points in the i-th Cartesian direction and the pressure difference is provided at each mesh point (see Section 3.10). These tables are generated separately using a program that reads the loads provided from the ACM software, distributes these loads onto the finite element mesh using a combination of interpolation procedures on the surface and simple diffusion schemes off the surface (off-surface loads are required by ANSYS to ensure proper interpolation of forces), and written to ASCII files for input to ANSYS. A separate load file is written at each frequency for the real and imaginary component of the complex force.

The acoustic field is stored at 5 Hz intervals from 0 to 250 Hz. While a 5 Hz resolution is sufficient to capture frequency dependence of the acoustic field (i.e., the pressure at a point varies gradually with frequency), it is too coarse for representing the structural response especially at low frequencies. For 1% critical structural damping, one can show that the frequency spacing needed to resolve a damped resonant peak at natural frequency, f_n, to within 5% accuracy is $\Delta f = 0.0064 \times f_n$. Thus for f_n=10 Hz where the lowest structural response modes occur, a frequency interval of 0.064 Hz or less is required. In our calculations we require that 5% maximum error be maintained over the range from f_n=5 Hz to 250 Hz resulting in a finest frequency interval of 0.0321 Hz at the low frequency end (this adequately resolves all structural modes up to 250 Hz). Since there are no structural modes between 0 to 5 Hz, a 0.5 Hz spacing is used over this range with minimal (less than 5%) error. The unit load, $\hat{\mathbf{f}}_n(\omega, \mathbf{R})$, at any frequency, ω_k, is obtained by linear interpolation of the acoustic solutions at the two nearest frequencies, ω_i and ω_{i+1}, spaced 5 Hz apart. Linear interpolation is sufficient since the pressure load varies slowly over the 5 Hz range (linear interpolation of the structural response would not be acceptable over this range since it varies much more rapidly over the same interval). Details regarding the frequency resolution have been provided in [13].

Solution Management

[[

(3)]]

[[

[3]]]

Structural Damping

In harmonic analysis one has a broader selection of damping models than in transient simulations. A damping factor, z, of 1% critical damping is used in the structural analysis. In transient simulations, this damping can only be enforced exactly at two frequencies (where the damping model is "pinned"). Between these two frequencies the damping factor can by considerably smaller, for example 0.5% or less depending on the pinning frequencies. Outside the pinning frequencies, damping is higher. With harmonic analysis it is straightforward to enforce very close to 1% damping over the entire frequency range. In this damping model, the damping matrix, **D**, is set to

$$\mathbf{D} = \frac{2z}{\omega}\mathbf{K} \tag{7}$$

where **K** is the stiffness matrix and ω the forcing frequency. When comparing the response obtained with this model against that for a constant damping ratio, the maximum difference at any frequency is less than 0.5%, which is far smaller than the 100% or higher response variation obtained when using the pinned model required in transient simulation.

Load Frequency Rescaling

One way to evaluate the sensitivity of the stress results to approximations in the structural modeling and applied loads is to rescale the frequency content of the applied loads. In this procedure the nominal frequencies, ω_k, are shifted to $(1+\lambda)\omega_k$, where the frequency shift, λ, ranges between $\pm 10\%$, and the response recomputed for the shifted loads. The objective of the frequency shifting can be explained by way of example. Suppose that in the actual dryer a strong structural-acoustic coupling exists at a particular frequency, ω^*. This means that the following conditions hold simultaneously: (i) the acoustic signal contains a significant signal at ω^*; (ii) the structural model contains a resonant mode of natural frequency, ω_n, that is near ω^*; and (iii) the associated structural mode shape is strongly coupled to the acoustic load (i.e., integrating the product of the mode shape and the surface pressure over the steam dryer surface produces a significant modal force). Suppose now that because of discretization errors and modeling idealizations that the predicted resonance frequency differs from ω^* by a small amount (e.g., 1.5%). Then condition (ii) will be violated and the response amplitude therefore significantly diminished. By shifting the load frequencies one re-establishes condition (ii) when $(1+\lambda)\omega^*$ is

near ω_n. The other two requirements also hold and a strong structural acoustic interaction is restored.

[[

(3)]]

Evaluation of Maximum and Alternating Stress Intensities

Once the unit solutions have been obtained, the most intensive computational steps in the generation of stress intensities are: (i) the FFTs to evaluate stress time histories from (5); and (ii) the calculation of alternating stress intensities. [[

(3)]]

The high computational penalty incurred in calculating the alternating stress intensities is due to the fact that this calculation involves comparing the stress tensors at every pair of points in the stress history. This comparison is necessary since in general the principal stress directions can vary during the response, thus for N samples in the stress history, there will be (N-1)N/2 such pairs or, for N=64K (the number required to accurately resolve the spectrum up to 250 Hz in 0.01 Hz intervals), 2.1×10^9 calculations per node each requiring the determination of the roots to a cubic polynomial. [[

(3)]]

[[2.4 **(3)]]**

[[

(3)]]

[[

(3)]]

2.5 Flaw Evaluation

As part of the steam dryer stress assessment for EPU operation an evaluation of existing flaws discovered in the outer hood/hood support/base plate junctions is required to establish whether or not flaw propagation will occur at EPU conditions. If growth of the existing indications cannot be readily ruled out then a modification to the existing locations is required. Performing the flaw evaluation and designing the stress relief cutout required the combined use of several analysis methods which are summarized here. The flaw growth assessment is

performed jointly by CDI and Structural Integrity Associates (SIA). CDI provided a high resolution sub-model that includes details of the local welds together with the perimeter loads and inertial and body forces as described above. CDI also conducted supporting calculations to estimate the RMS stresses and determine whether the behavior at these locations is symptomatic of load- or displacement-controlled stresses. Finally a modified sub-model of this location with a circular cutout in the hood support was developed as a contingency repair in the event that arresting of further crack growth at EPU operation cannot be assured under the current (unmodified) configuration. The sizing and placement of the circular cut-out is described in [7] and [[(3)]]. With these results, SIA conducted the flaw evaluation using a combination of analytical methods and finite element modeling using crack elements as described in [16].

Load- or Displacement-Controlled Stresses

The detailed flaw evaluation requires an assessment of whether the stress at the crack is primarily load- or displacement-controlled as this distinction warrants different criteria for establishing crack growth. In a load-controlled configuration the applied load essentially remains constant as the structure displaces. In a displacement-controlled configuration the forces experienced by the load are relieved as the structure displaces.

The distinction can be explained by way of example and reference to Figure 1 which depicts a structure similar to the hood support. The structure contains a flaw as shown and the right hand edge is either: (i) loaded with a constant force or (ii) required to move by a specified displacement. The former case would arise if the edge is directly loaded; the second situation arises when the hood response is dominated by the response of adjacent structures. Suppose that the displacement at the location indicated is monitored as the flaw length is increased. In a load-controlled configuration – case (i) - the monitored displacement is expected to increase as the flaw grows. Conversely in the displacement-controlled setting the monitored displacement will only be weakly affected by the flaw length and will either remain approximately the same or decrease with increasing flaw size.

For the outer hood/hood support/cover plate junction it is noted that the 1/4" outer hood support connects to the much thicker (1/2") outer hoods on the left edge and to the massive outer vane banks on the right edge. Since the outer hoods connect directly to the vane banks it can be surmised that acoustic forcing of the outer hoods will produce motions in the combined outer hood + vane bank assembly. Because of the comparatively stiff outer hoods and massive vane banks (compared to the hood support), the motions of this assembly is anticipated to be only weakly affected by a flaw at this junction.

To verify this behavior for a complex structure such as the dryer where multiple load paths exist, a practical means of establishing whether the forces transmitted to the hood support plates are displacement-limited is required. To this end the global finite element model is used and elements along the hood/hood support weld line progressively disconnected to simulate flaws of different lengths. Thus one begins with the fully connected model and evaluates the displacements at selected locations on the hood support and connected components when subjected to the ACM Rev. 4.1 acoustic loads. These locations are chosen to lie between 3-9

inches away from the high stress location as shown in Figure 2. The lowest finite element in the hood support that is adjacent to the outer hood/hood support weld is then disconnected. The nearest middle hood/hood support is similarly disconnected and the displacements at the same locations recalculated. Next this process is repeated by disconnecting the two lowest finite elements along the weld (i.e., the one disconnected previously and the one immediately above it also adjacent to the weld) and re-evaluating the displacements; then disconnecting the three lowest elements, etc. The displacements are then plotted as a function of disconnection length to see whether the displacements generally increase with disconnection length which is indicative of load-controlled behavior, or whether the displacements remain constant or reduce with disconnection length which implies displacement-controlled response. These plots are presented in Figure 3. From these plots the response at the outer hood/hood support/cover plate is consistent with displacement-controlled behavior as all displacements tend to reduce with crack length or plateau to constant values.

At the middle hood/hood support/base plate junction, the displacement amplitudes all decrease gradually or plateau except for the middle hoods themselves whose amplitudes continue to grow. This is indicative of a vibration mode that continues to grow as the restraint provided by the hood support is reduced. For the hood support itself however, where the dominant stress occur, the displacements at 2A and 2B are generally level or diminishing with crack length (see Figure 3) indicating that the hood support stress is also displacement-controlled.

The stress at the flaw tip is also recorded as a function of crack length to corroborate whether or not the stress is displacement-controlled. Generally, one would expect to observe a reduction in this stress as the crack is extended. This observation is indeed borne out as shown in Figure 4. This plot records the maximum unit solution stress at the flaw tip as a function of displacement length where the maximum is taken over all frequencies and MSL forcings.

Finally, it is noted that the displacement-controlled stress behavior at all hood/hood support/base plate junctions is supported by field observations at explained at length in [16]. Essentially, for a load-controlled stress state the observed flaws would have grown to considerably longer lengths. Instead, the flaws which are believed to have been initiated by residual stresses, have grown to approximately 2" on the outer hood supports and 0.5" at the middle and some inner hood supports and stopped. This is fully consistent with a displacement-controlled stress situation and also corroborates the analysis conducted in [16] which predicts crack growth to approximately 2" during the first operational cycle and subsequent arrest of the crack as the crack tip stress field diminishes. While the evaluation in [16] focuses on the outer hood support, this evaluation constitutes the bounding flaw assessment for all (outer, middle and inner) hood support junctions given that the highest junction stresses occur on the outer hood supports and all locations evidence displacement-controlled stress behavior near the flaws.

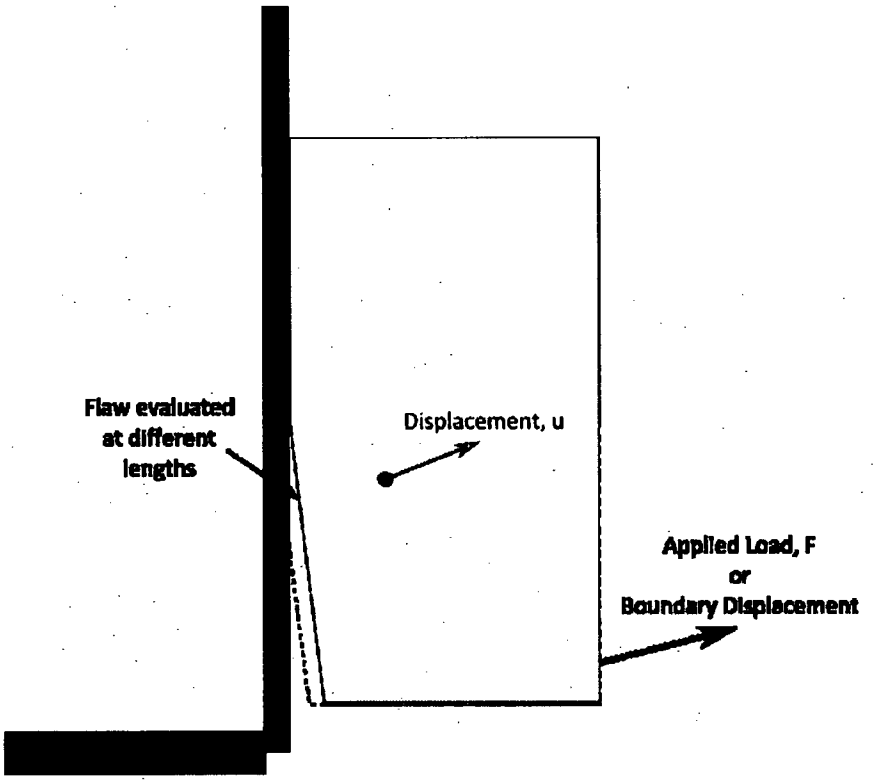

Figure 1. Conceptual arrangement of hood support geometry for the determining whether the limiting stresses are load- or displacement-controlled.

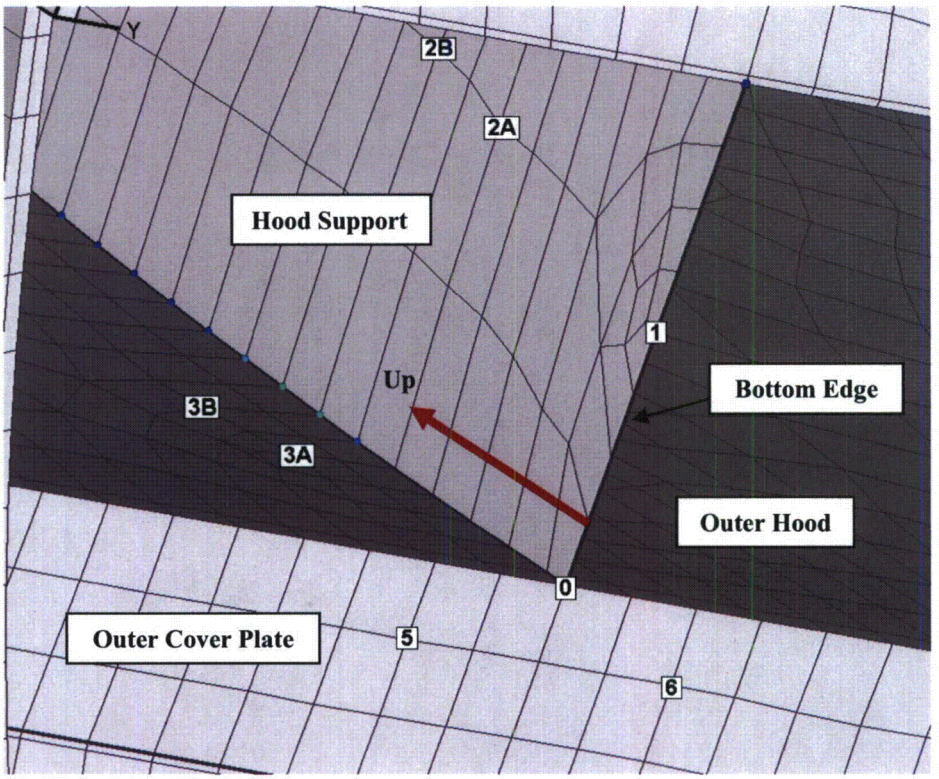

Figure 2. Depiction from below of locations near the outer hood/hood support/cover plate high stress point where displacements are recorded. Location 0 lies at the high stress location. Location 1 lies on the bottom edge of the hood support whereas locations 2A and 2B lie approximately 9" and 13" respectively above location 1. Locations 3A and 3B reside on the outer hood at approximately the same heights as 2A and 2B; Locations 4A and 4B are similarly placed on the outer hood and are located behind the hood support and thus obscured by the hood support in this view. Finally locations 5 and 6 are on the outer cover plate. Precise values are given in Table 1. Analogous locations are erected about the middle hood/hood support junction.

Table 1. Coordinates of Locations 0-6 in Figure 2.

Index	node	x	y	z
0	95267	-102.75	28.39	0
1	14954	-94.875	28.39	0
2A	14789	-93.7966	28.39	10.0558
2B	14840	-93.7159	28.39	13.6998
3A	79184	-102.624	23.9483	9.44825
3B	78999	-102.495	23.689	13.4162
4A	77836	-102.617	33.8335	9.70184
4B	77835	-102.48	34.3628	13.8147
5	48374	-105.543	24.76	0
6	48388	-106.358	32.0303	0

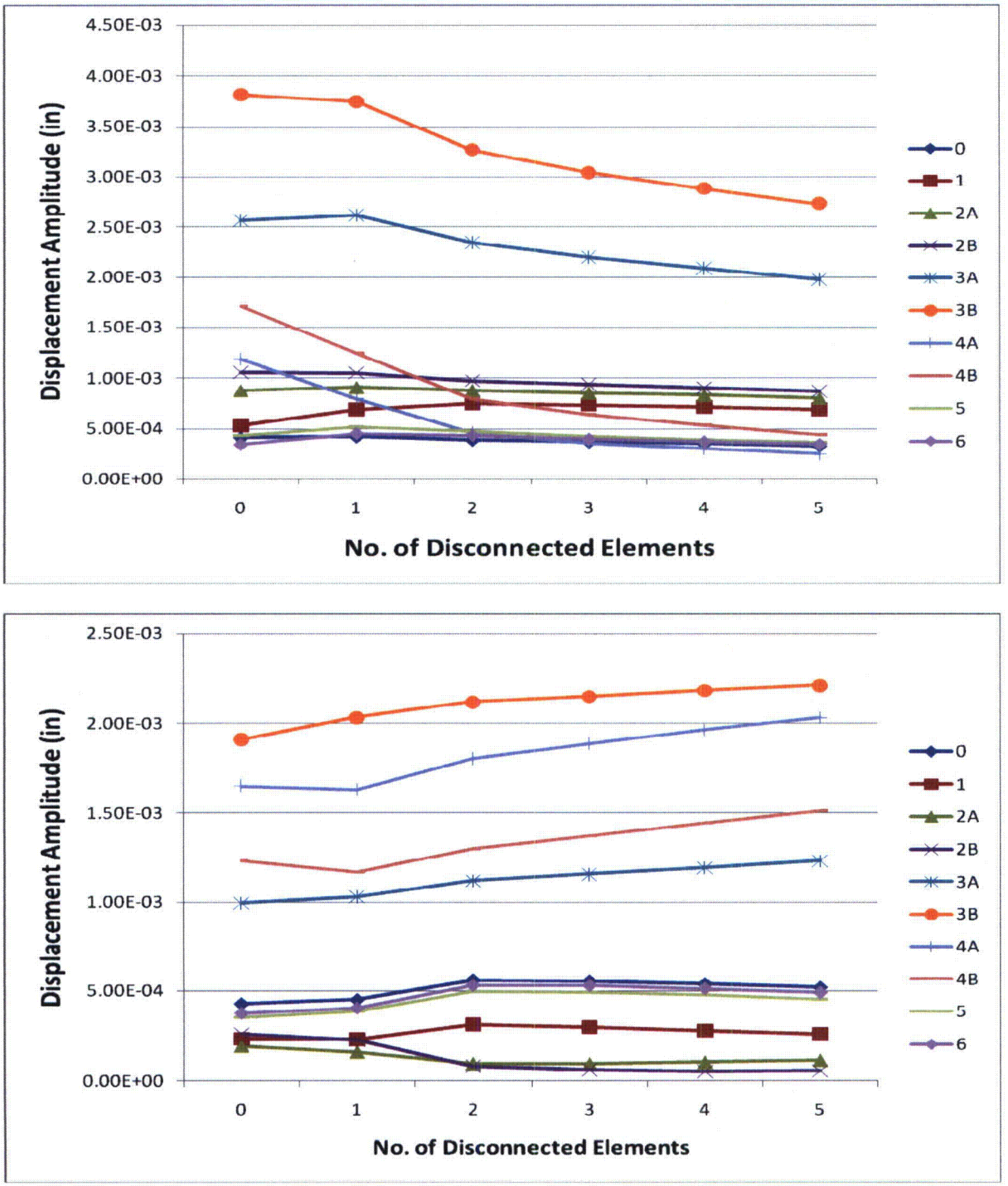

Figure 3. Variation of displacement amplitudes at the locations depicted in Figure 2 as a function of the number of disconnected elements along the hood/hood support weld line. Top – outer hood; bottom – middle hood.

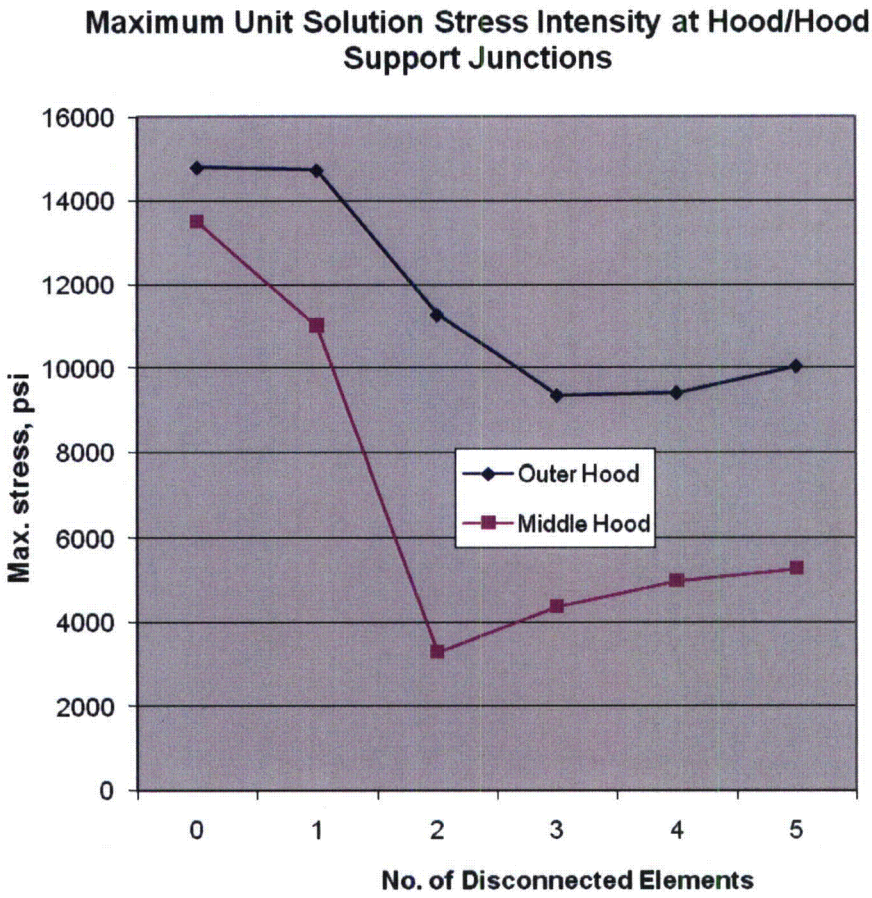

Figure 4. Variation of the maximum unit solution stress at the tip of the disconnection line as a function of the number of disconnected elements. The maximum of the stress intensity is taken over all MSL loadings and frequencies.

Sizing and Positioning the Stress Relief Cut-Out Hole

If the flaw evaluation shows insufficient margin a means of reducing the stress is needed. The option considered here is the insertion of a semi-circular stress relief cutout hole. The cut-out hole is optimized by adjusting the position and radius of the hole to minimize the overall stress ratio. The optimization process is carried out using a shell-based sub-model to expedite the overall design process. [[

(3)]]

3. Finite Element Model Description

A description of the ANSYS model of the nine Mile Point Unit 2 steam dryer follows.

3.1 Steam Dryer Geometry

A geometric representation of the Nine Mile Point Unit 2 steam dryer was developed from available drawings (provided by Constellation Energy Group and included in the design record file, DRF-C-279C) within the Workbench module of ANSYS. The completed model is shown in Figure 5. This model includes on-site modifications to the Nine Mile Point Unit 2 steam dryer. These are as follows.

On-Site Modifications

(i) The top tie rods are replaced with thicker ones.
(ii) Inner side plates are replaced with thicker ones.
(iii) Middle hoods are reinforced with additional strips.
(iv) Lifting rods are reinforced with additional gussets.
(v) Per FDDR KG1-0265 the support conditions are adjusted to ensure that the dryer is supported 100% on the seismic blocks.

These additional modifications have been incorporated into the NMP2 steam dryer model and are reflected in the results presented in this report. The affected areas are shown in Figure 6.

Modifications Implemented for EPU Operation

In [17] several modifications were proposed to meet target EPU stress margins using a previous acoustic loads model (ACM Rev. 4.0) without noise subtraction. These modifications are now superseded here by the ones below and detailed in Section 5 that are obtained by on the basis of acoustic loads processed using the ACM Rev. 4.1 analysis. These planned modifications include:

(vi) Reinforcement strips are added to the closure plates.
(vii) Reinforcements to the upper-most and middle lifting rod braces are made in the form of additional strengthening plates.
(viii) Increase the attachment weld size of the lower-most lifting rod brace from ¼" to ½".
(ix) A $1/8^{th}$ in curved plate is placed over the middle hood section lying outboard of the closure plate.
(x) Four 15 lb masses are added to the central inner hood panels.
(xi) Stress relief cut-outs are added to the outer hood/hood support/base plate junctions to alleviate local stresses.
(xii) A wrap-around weld is added to the bottom of the drain channel/skirt weld.
(xiii) Four 10 lb masses are added to the central middle hood panels.

All of the modifications summarized here and detailed in Section 5 are implemented in the results produced in Section 6.

Reference Frame

The spatial coordinates used herein to describe the geometry and identify limiting stress locations are expressed in a reference frame whose origin is located at the intersection of the steam dryer centerline and the plane containing the base plates (this plane also contains the top of the upper support ring and the bottom edges of the hoods). The y-axis is parallel to the hoods, the x-axis is normal to the hoods pointing from MSL C/D to MSL A/B, and the z-axis is vertical, positive up.

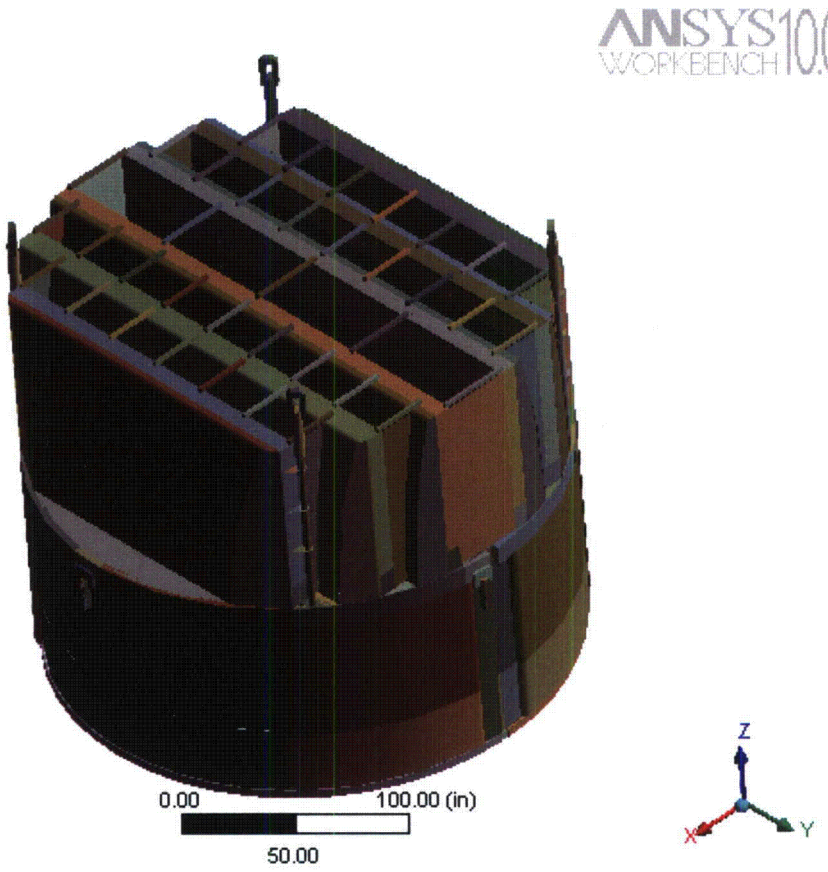

Figure 5. Overall geometry of the Nine Mile Point Unit 2 steam dryer model.

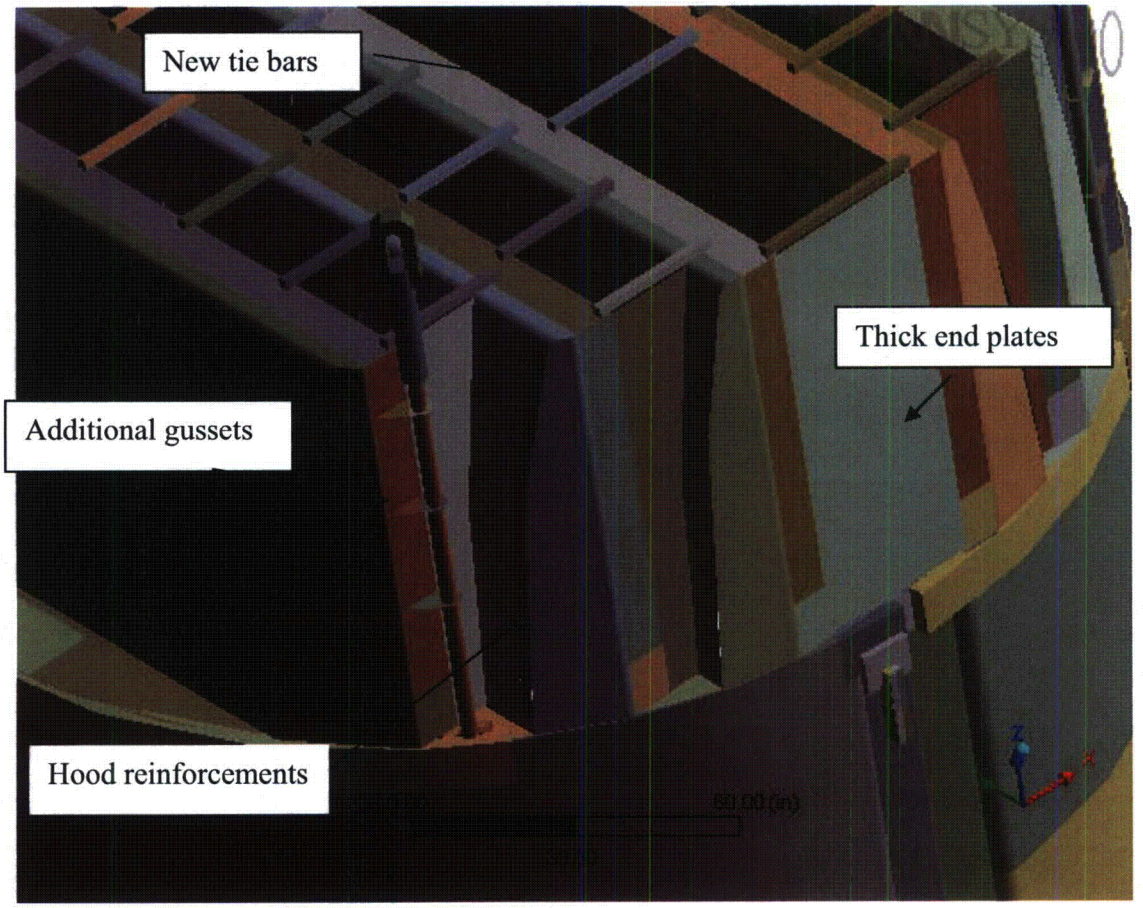

Figure 6. Existing on-site modifications accounted for in the model and associated geometrical details.

3.2 Material Properties

The steam dryer is constructed from Type 304 stainless steel and has an operating temperature of 550°F. Properties used in the analysis are summarized below in Table 2.

Table 2. Material properties.

	Young's Modulus (10^6 psi)	Density (lbm/in^3)	Poisson Ratio
stainless steel	25.55	0.284	0.3
structural steel with added water inertia effect	25.55	0.856	0.3

The structural steel modulus is taken from Appendix A of the ASME Code for Type 304 Stainless Steel at an operating temperature 550°F. The effective properties of perforated plates and submerged parts are discussed in Sections 3.4 and 3.6. Note that the increased effective density for submerged components is only used in the harmonic analysis. When calculating the stress distribution due to the static dead weight load, the unmodified density of steel (0.284 lbm/in^3) is used throughout.

Inspections of the NMP Unit 2 dryer have revealed IGSCC cracks in the upper support ring (USR) and skirt. A separate analysis of these cracks [18] has been performed to determine whether: (i) they will propagate further into the structure and (ii) their influence upon structural response frequencies and modes must be explicitly accounted for. To establish (i) the stress calculated in the global stress analysis is used in conjunction with the crack geometry to calculate the stress intensity factor which is then compared to the threshold stress intensity. For the USR and skirt cracks the highest stress intensity factors are 1.47 ksi-in$^{0.5}$ and 2.75 ksi-in$^{0.5}$ respectively; both values are below the threshold value (3 ksi-in$^{0.5}$) implying that fatigue crack growth will not occur.

To determine (ii) the change in modal response frequencies due to the presence of a flaw is predicted by analytical means (in the case of the USR) or using finite element analysis (for the skirt). In each case, the flaw size used in these calculations is increased to ensure conservative estimates (for example, in the case of the skirt flaws extending up to ½ the panel width are considered). For the USR, the change in modal frequencies due to the presence of the cracks is less than 0.5%. For the skirt, using a conservative estimate for the crack to panel width of 0.3 (the measured value is less than 0.17) the change in modal frequency is also less than 0.5%. In both cases such small changes in modal frequencies are considered negligible and are readily accounted for when performing frequency shifting.

3.3 Model Simplifications

The following simplifications were made to achieve reasonable model size while maintaining good modeling fidelity for key structural properties:

- Perforated plates were approximated as continuous plates using modified elastic properties designed to match the static and modal behaviors of the perforated plates. The

perforated plate structural modeling is summarized in Section 3.4 and Appendix C of [19].

- The drying vanes were replaced by point masses attached to the corresponding trough bottom plates and vane bank top covers (Figure 8). The bounding perforated plates, vane bank end plates, and vane bank top covers were explicitly modeled (see Section 3.5).

- The added mass properties of the lower part of the skirt below the reactor water level were obtained using a separate hydrodynamic analysis (see Section 3.6).

- [[

  (3)]]

- Four steam dryer support brackets that are located on the reactor vessel and spaced at 90° intervals were explicitly modeled (see Section 3.9).

- Most welds were replaced by node-to-node connections; interconnected parts share common nodes along the welds. In other locations the constraint equations between nodal degrees of freedom were introduced as described in Section 3.9.

3.4 Perforated Plate Model

The perforated plates were modeled as solid plates with adjusted elastic and dynamic properties. Properties of the perforated plates were assigned according to the type and size of perforation. Based on [20], for an equilateral square pattern with given hole size and spacing, the effective moduli of elasticity were found.

The adjusted properties for the perforated plates are shown in Table 3 as ratios to material properties of structural steel, provided in Table 2. Locations of perforated plates are classified by steam entry / exit vane bank side and vertical position.

Tests were carried out to verify that this representation of perforated plates by continuous ones with modified elastic properties preserves the modal properties of the structure. These tests are summarized in Appendix C of [19]and compare the predicted first modal frequency for a cantilevered perforated plate against an experimentally measured value. The prediction was obtained for 40% and 13% open area plates (these are representative of the largest and lowest open area ratios of the perforated plates at NMP2, as seen in Table 3) using the analytical formula for a cantilevered plate and the modified Young's modulus and Poisson's ratio given by O'Donnell [20]. The measured and predicted frequencies are in close agreement, differing by less than 3%.

[[

(3)]]

[[

[3]]

[[

[3]]

Figure 7. [[[3]]

Table 3. Material properties of perforated plates.

[[

[3]]]

3.5 Vane Bank Model

The vane bank assemblies consist of many vertical angled plates that are computationally expensive to model explicitly, since a prohibitive number of elements would be required. These parts have significant weight which is transmitted through the surrounding structure, so it is important to capture their gross inertial properties. Here the vane banks are modeled as a collection of point masses located at the center of mass for each vane bank section (Figure 4). The following masses were used for the vane bank sections, based on data found on provided drawings:

inner banks, 1618 lbm, 4 sections per bank;
middle banks, 1485 lbm, total 4 sections per bank; and
outer banks, 1550 lbm, 3 sections per bank.

These masses were applied to the base plates and vane top covers using the standard ANSYS point mass modeling option, element MASS21. ANSYS automatically distributes the point mass inertial loads to the nodes of the selected structure. The distribution algorithm minimizes the sum of the squares of the nodal inertial forces, while ensuring that the net forces and moments are conserved. Vane banks are not exposed to main steam lines directly, but rather shielded by the hoods.

The collective stiffness of the vane banks is expected to be small compared to the surrounding support structure and is neglected in the model. In the static case it is reasonable to expect that this constitutes a conservative approach, since neglecting the stiffness of the vane banks implies that the entire weight is transmitted through the adjacent vane bank walls and supports. In the dynamic case the vane banks exhibit only a weak response since (i) they have large inertia so that the characteristic acoustically-induced forces divided by the vane masses and inertias yield small amplitude motions, velocities and accelerations; and (ii) they are shielded from acoustic loads by the hoods, which transfer dynamic loads to the rest of the structure. Thus, compared to the hoods, less motion is anticipated on the vane banks so that

approximating their inertial properties with equivalent point masses is justified. Nevertheless, the bounding parts, such as perforated plates, side panels, and top covers, are retained in the model. Errors associated with the point mass representation of the vane banks are compensated for by frequency shifting of the applied loads.

3.6 Water Inertia Effect on Submerged Panels

Water inertia was modeled by an increase in density of the submerged structure to account for the added hydrodynamic mass. This added mass was found by a separate hydrodynamic analysis (included in DRF-C-279C supporting this report) to be 0.143 lbm/in^2 on the submerged skirt area. This is modeled by effectively increasing the material density for the submerged portions of the skirt. Since the skirt is 0.25 inches thick, the added mass is equivalent to a density increase by 0.572 lbm/in^3. This added water mass was included in the ANSYS model by appropriately modifying the density of the submerged structural elements when computing harmonic response. For the static stresses, the unmodified density of steel is used throughout.

3.7 Structural Damping

Structural damping was defined as 1% of critical damping for all frequencies. This damping is consistent with guidance given on pg. 10 of NRC RG-1.20 [24].

3.8 Mesh Details and Element Types

Shell elements were employed to model the skirt, hoods, perforated plates, side and end plates, trough bottom plates, reinforcements, base plates and cover plates. Specifically, the four-node, Shell Element SHELL63, was selected to model these structural components. This element models bending and membrane stresses, but omits transverse shear. The use of shell elements is appropriate for most of the structure where the characteristic thickness is small compared to the other plate dimensions. For thicker structures, such as the upper and lower support rings, solid brick elements were used to provide the full 3D stress. The elements SURF154 are used to assure proper application of pressure loading to the structure. Mesh details and element types are shown in Table 4 and Table 5.

The mesh is generated automatically by ANSYS with refinement near edges. The maximum allowable mesh spacing is specified by the user. Here a 2.5 inch maximum allowable spacing is specified with refinement up to 1.5 inch in the following areas: drain pipes, tie rods, the curved portions of the drain channels and the hoods. Details of the finite element mesh are shown in Figure 9. Numerical experiments carried out using the ANSYS code applied to simple analytically tractable plate structures with dimensions and mesh spacings similar to the ones used for the steam dryer, confirm that the natural frequencies are accurately recovered (less than 1% errors for the first modes). These errors are compensated for by the use of frequency shifting.

3.9 Connections between Structural Components

Most connections between parts are modeled as node-to-node connections. This is the correct manner (i.e., within the finite element framework) of joining elements away from discontinuities. At joints between shells, this approach omits the additional stiffness provided by the extra weld material. Also, locally 3D effects are more pronounced. The latter effect is accounted for using weld factors. The deviation in stiffness due to weld material is negligible, since weld dimensions are on the order of the shell thickness. The consequences upon modal

frequencies and amplitude are, to first order, proportional to t/L where t is the thickness and L a characteristic shell length. The errors committed by ignoring additional weld stiffness are thus small and readily compensated for by performing frequency shifts.

When joining shell and solid elements, however, the problem arises of properly constraining the rotations, since shell element nodes contain both displacement and rotational degrees of freedom at every node whereas solid elements model only the translations. A node-to-node connection would effectively appear to the shell element as a simply supported, rather than (the correct) cantilevered restraint and significantly alter the dynamic response of the shell structure.

To address this problem, constraint equations are used to properly connect adjacent shell- and solid-element modeled structures. Basically, all such constraints express the deflection (and rotation for shell elements) of a node, $\mathbf{R}_1$, on one structural component in terms of the deflections/rotations of the corresponding point, $\mathbf{P}_2$, on the other connected component. Specifically, the element containing $\mathbf{P}_2$ is identified and the deformations at $\mathbf{P}_2$ determined by interpolation between the element nodes. The following types of shell-solid element connections are used in the steam dryer model including the following:

1. Connections of shell faces to solid faces (Figure 10a). While only displacement degrees of freedom are explicitly constrained, this approach also implicitly constrains the rotational degrees of freedom when multiple shell nodes on a sufficiently dense grid are connected to the same solid face.
2. Connections of shell edges to solids (e.g., connection of the bottom of closure plates with the upper ring). Since solid elements do not have rotational degrees of freedom, the coupling approach consisted of having the shell penetrate into the solid by one shell thickness and then constraining both the embedded shell element nodes (inside the solid) and the ones located on the surface of the solid structure (see Figure 10b). Numerical tests involving simple structures showed that this approach and penetration depth reproduce both the deflections and stresses of the same structure modeled using only solid elements or ANSYS' bonded contact technology. Continuity of rotations and displacements is achieved.

The use of constraint conditions rather than the bonded contacts advocated by ANSYS for connecting independently meshed structural components confers better accuracy and useful numerical advantages to the structural analysis of the steam dryer including better conditioned and smaller matrices. The smaller size results from the fact that equations and degrees of freedom are eliminated rather than augmented (in Lagrange multiplier-based methods) by additional degrees of freedom. Also, the implementation of contact elements relies on the use of very high stiffness elements (in penalty function-based implementations) or results in indefinite matrices (Lagrange multiplier implementations) with poorer convergence behavior compared to positive definite matrices.

The steam dryer rests on four support blocks which resist vertical and lateral displacement. The support blocks contact the seismic blocks welded to the USR so that 100% of the dryer weight is transmitted through the seismic blocks per the FDDR KG1-265. Because the contact region between the blocks and steam dryer is small, the seismic blocks are considered free to

rotate about the radial axis. Specifically nodal constraints (zero relative displacement) are imposed over the contact area between the seismic blocks and the support blocks. Two nodes on each support block are fixed as indicated in Figure 11. One node is at the center of the support block surface facing the vessel and the other node is 0.5" offset inside the block towards the steam dryer, half way to the nearest upper support ring node. This arrangement approximates the nonlinear contact condition where the ring can tip about the block.

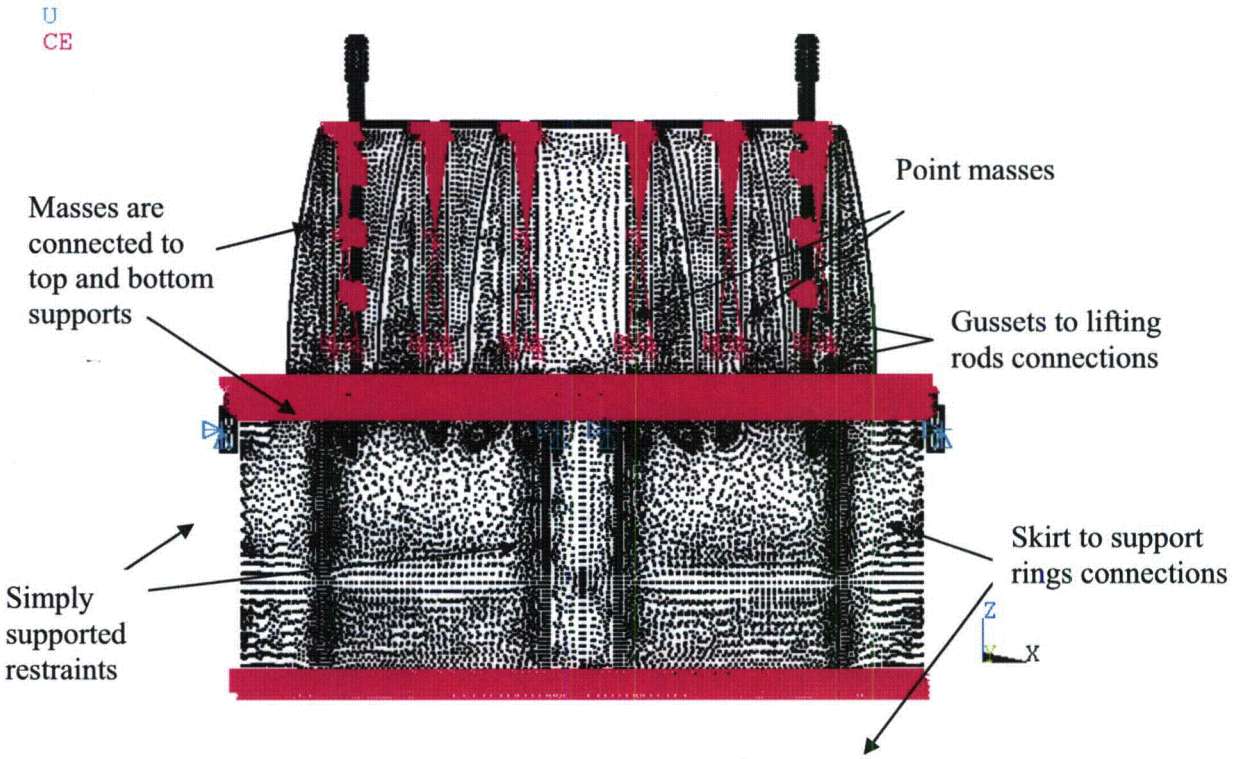

Figure 8. Point masses representing the vanes. The pink shading represents where constraint equations between nodes are applied (generally between solid and shell elements, point masses and nodes and [[[3]]]).

Table 4. FE Model Summary.

Description	Quantity
Total Nodes[1]	159,793
Total Elements	124,496

1. Not including additional damper nodes and elements.

Table 5. Listing of Element Types.

Generic Element Type Name	Element Name	ANSYS Name
20-Node Quadratic Hexahedron	SOLID186	20-Node Hexahedral Structural Solid
10-Node Quadratic Tetrahedron	SOLID187	10-Node Tetrahedral Structural Solid
4-Node Elastic Shell	SHELL63	4-Node Elastic Shell
Mass Element	MASS21	Structural Mass
Pressure Surface Definition	SURF154	3D Structural Surface Effect
Damper element	COMBIN14	Spring-Damper

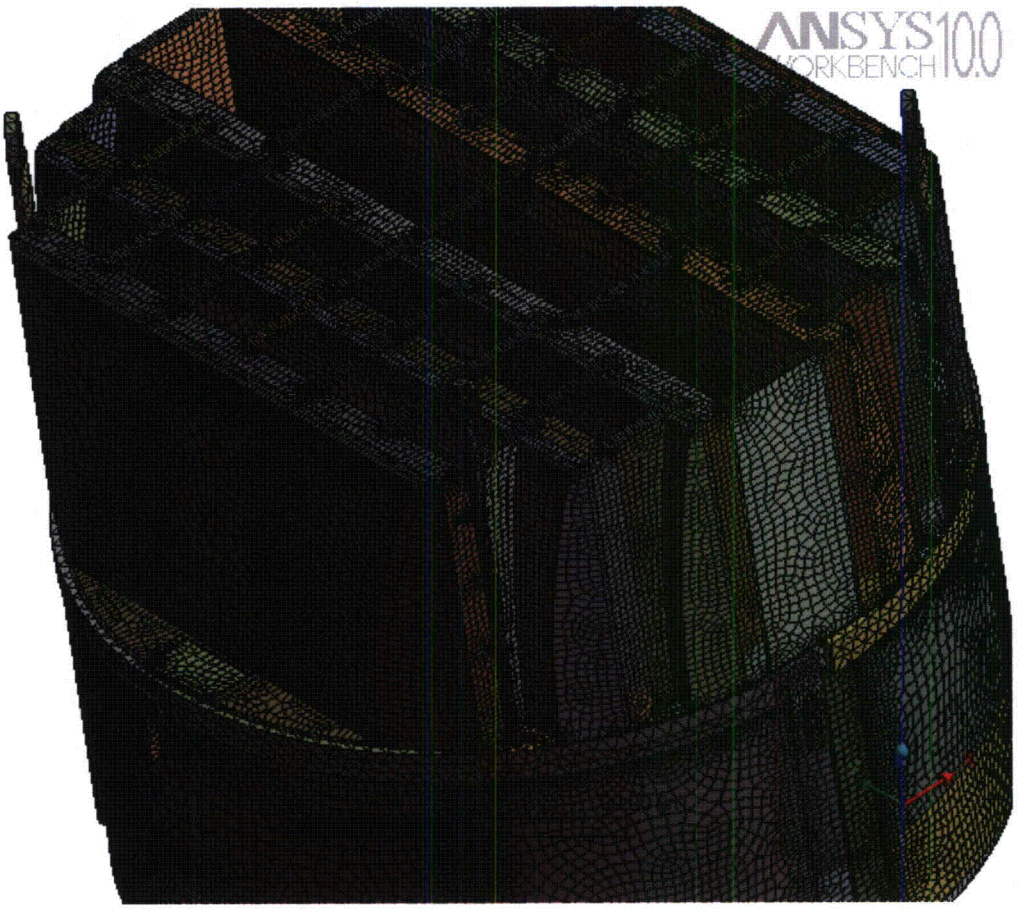

Figure 9a. Mesh overview.

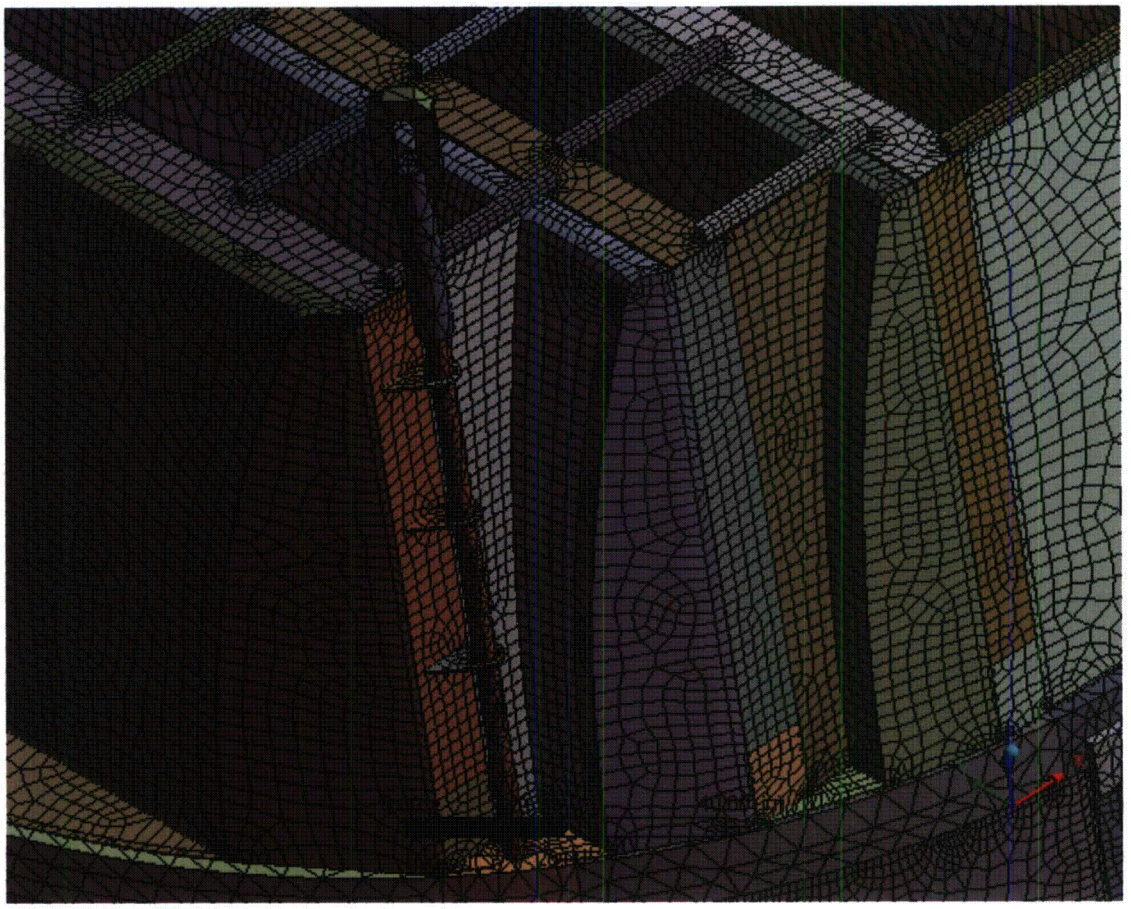

Figure 9b. Close up of mesh showing on-site modifications.

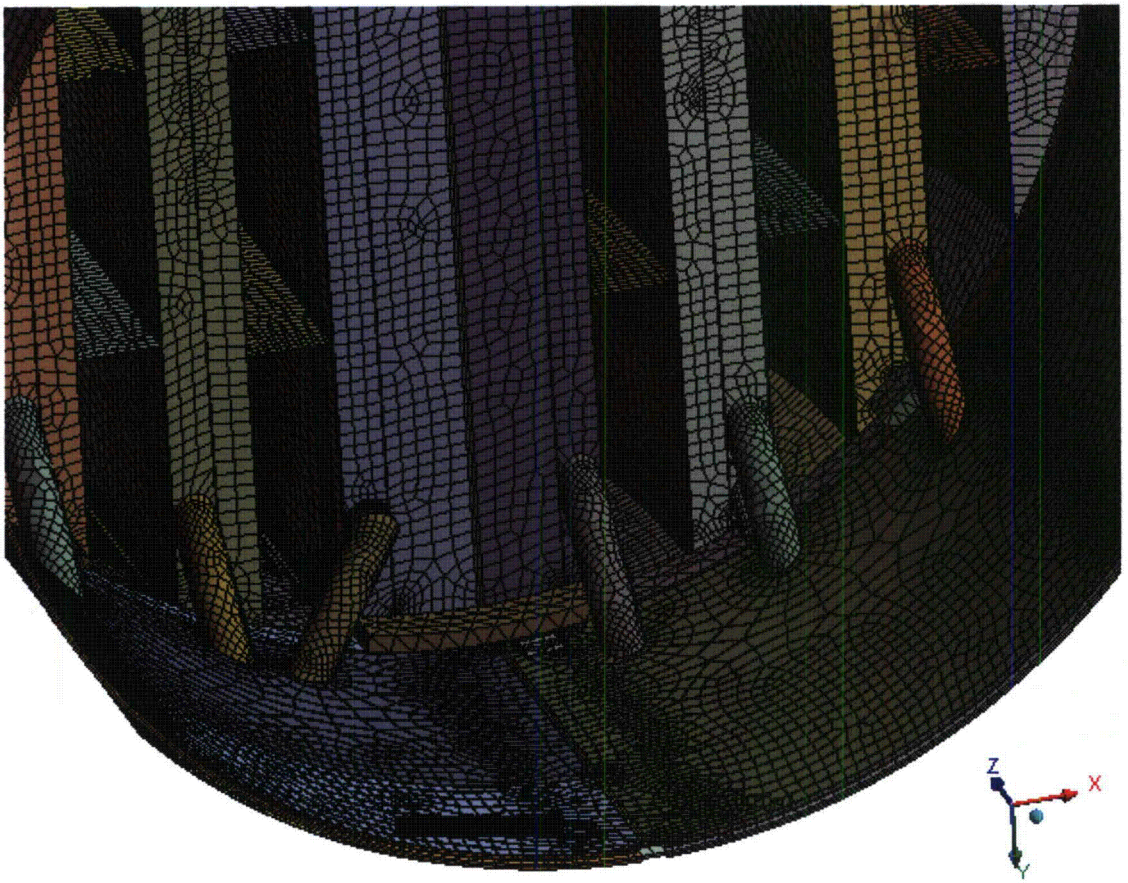

Figure 9c. Close up of mesh showing drain pipes and hood supports.

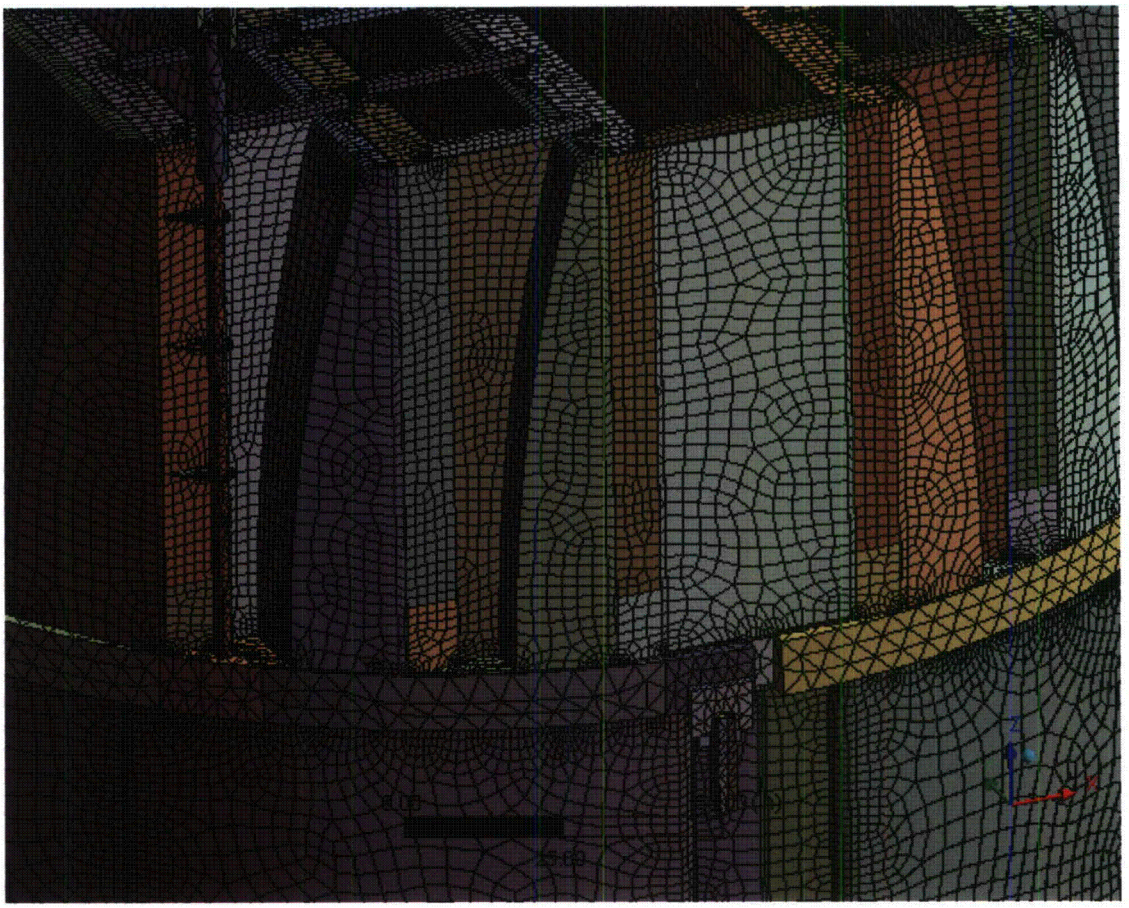

Figure 9d. Close up of mesh showing node-to-node connections between various plates.

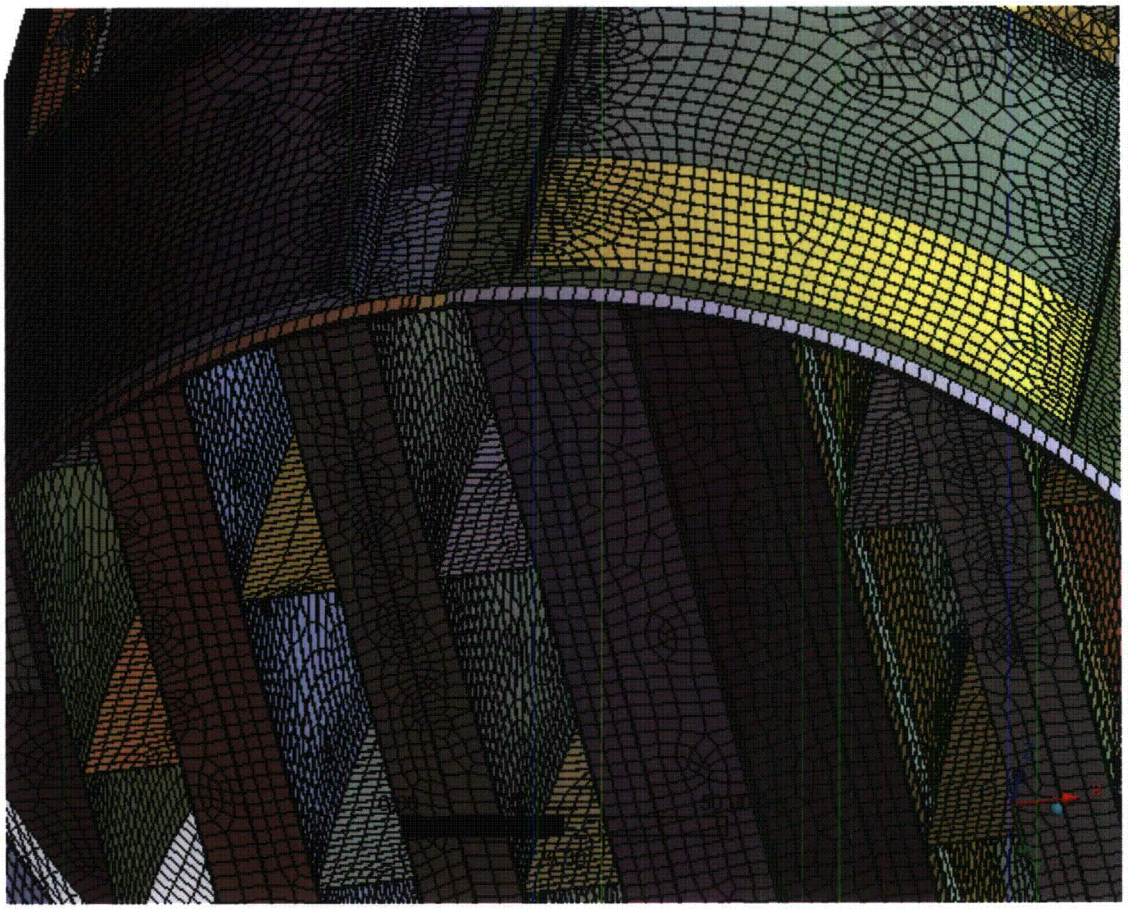

Figure 9e. Close up of mesh showing node-to-node connections between the skirt and drain channels; hood supports and hoods; and other parts.

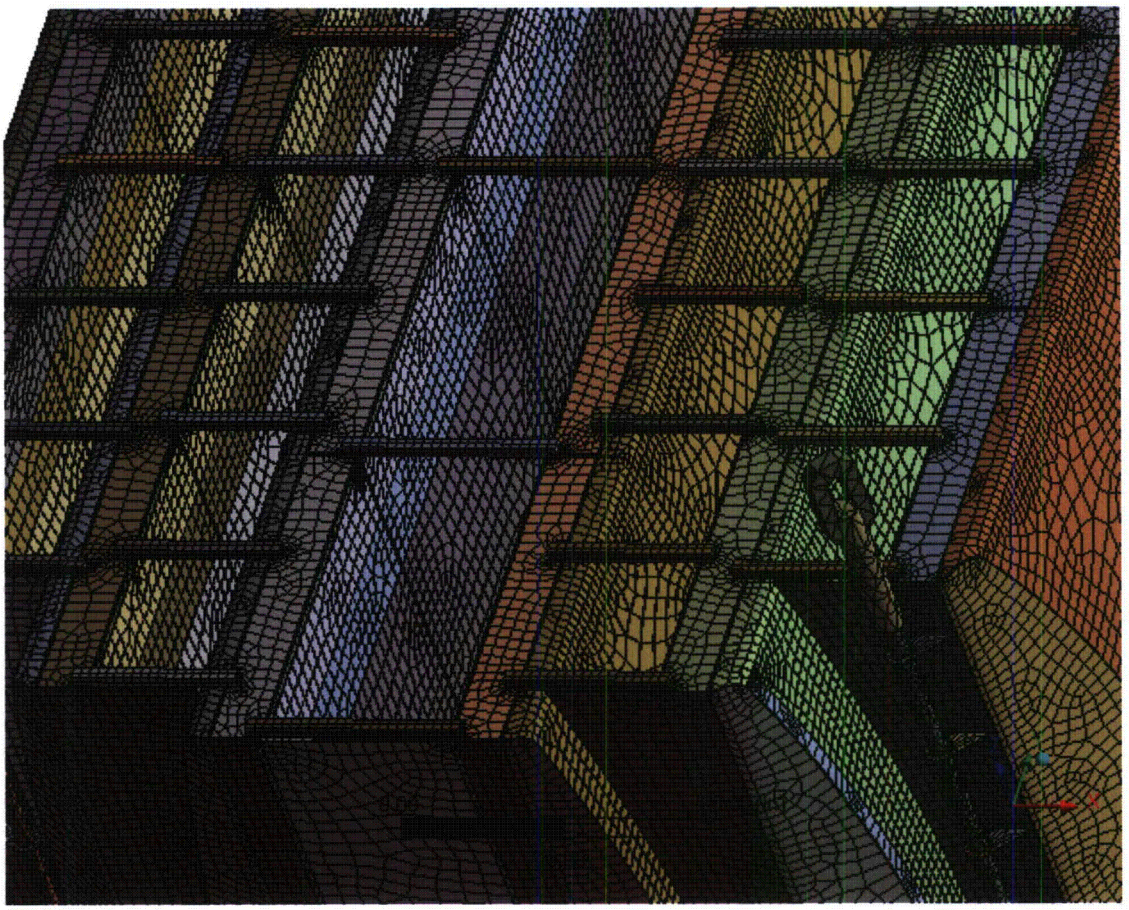

Figure 9f. Close up view of tie bars.

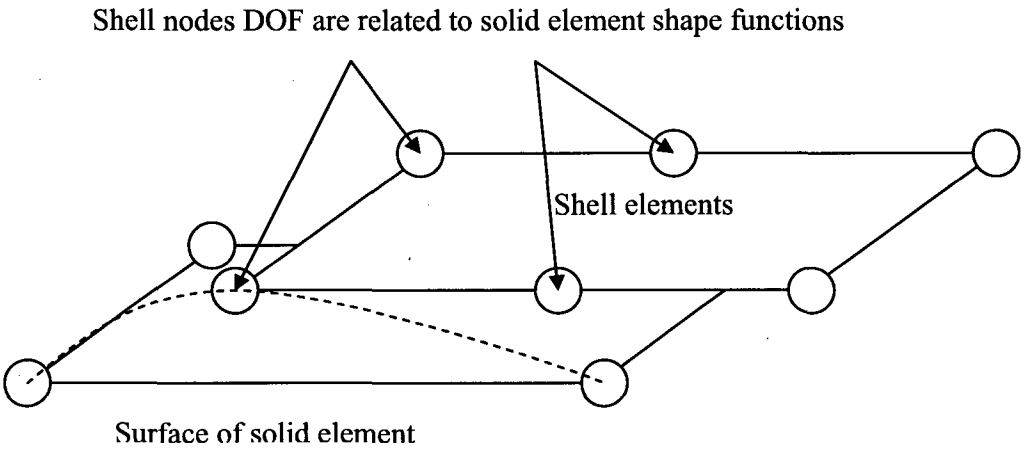

Figure 10a. Face-to-face shell to solid connection.

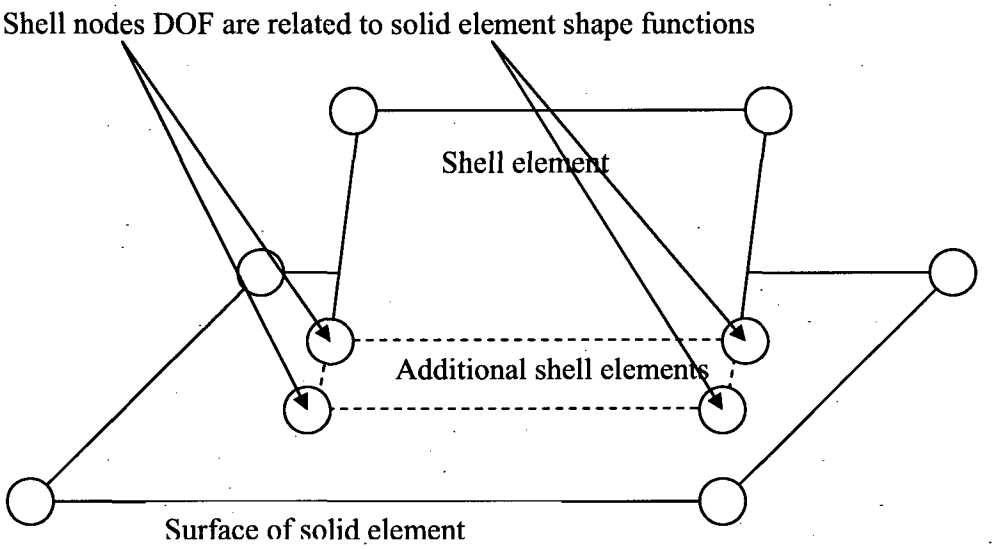

Figure 10b. Shell edge-to-solid face connection.

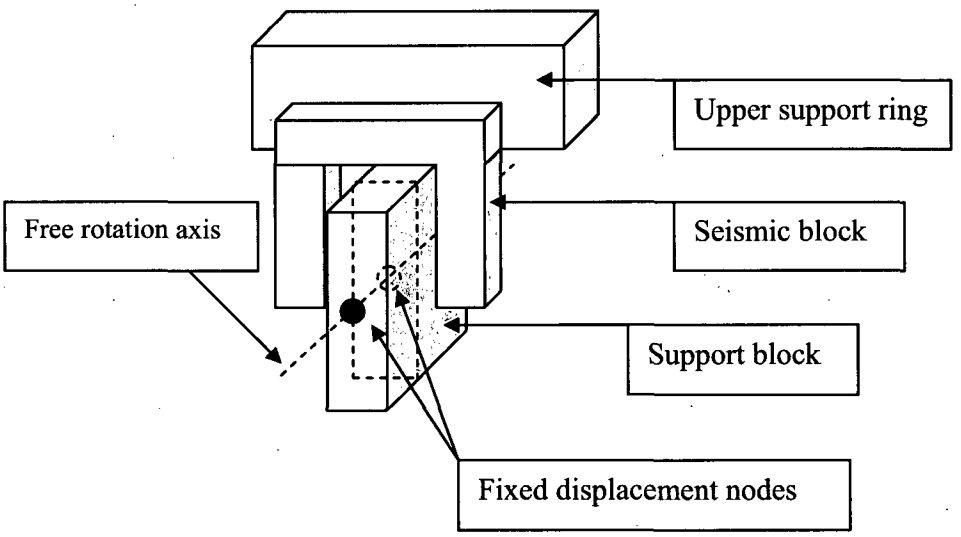

Figure 11. Boundary conditions. Inside node is half way between outer surface of support block and upper support ring.

3.10 Pressure Loading

The harmonic loads are produced by the pressures acting on the exposed surfaces of the steam dryer. At every frequency and for each MSL, the pressure distribution corresponding to a unit pressure at the MSL inlet is represented on a three-inch grid lattice grid (i.e., a mesh whose lines are aligned with the x-, y- and z-directions) that is superimposed over the steam dryer surface. This grid is compatible with the 'Table' format used by ANSYS to 'paint' general pressure distributions upon structural surfaces. The pressures are obtained from the Helmholtz solver routine in the acoustic analysis [9].

In general, the lattice nodes do not lie on the surface, so that to obtain the pressure differences at the surface it is necessary to interpolate the pressure differences stored at the lattice nodes. This is done using simple linear interpolation between the 8 forming nodes of the lattice cell containing the surface point of interest. Inspection of the resulting pressures at selected nodes shows that these pressures vary in a well-behaved manner between the nodes with prescribed pressures. Graphical depictions of the resulting pressures and comparisons between the peak pressures in the original nodal histories and those in the final surface load distributions produced in ANSYS, all confirm that the load data are interpolated accurately and transferred correctly to ANSYS.

The harmonic pressure loads are only applied to surfaces above the water level, as indicated in Figure 12. In addition to the pressure load, the static loading induced by the weight of the steam dryer is analyzed separately. The resulting static and harmonic stresses are linearly combined to obtain total values which are then processed to calculate maximum and alternating stress intensities for assessment in Section 5.

[[

[3]]] This is useful since revisions in the loads model do not necessitate recalculation of the unit stresses.

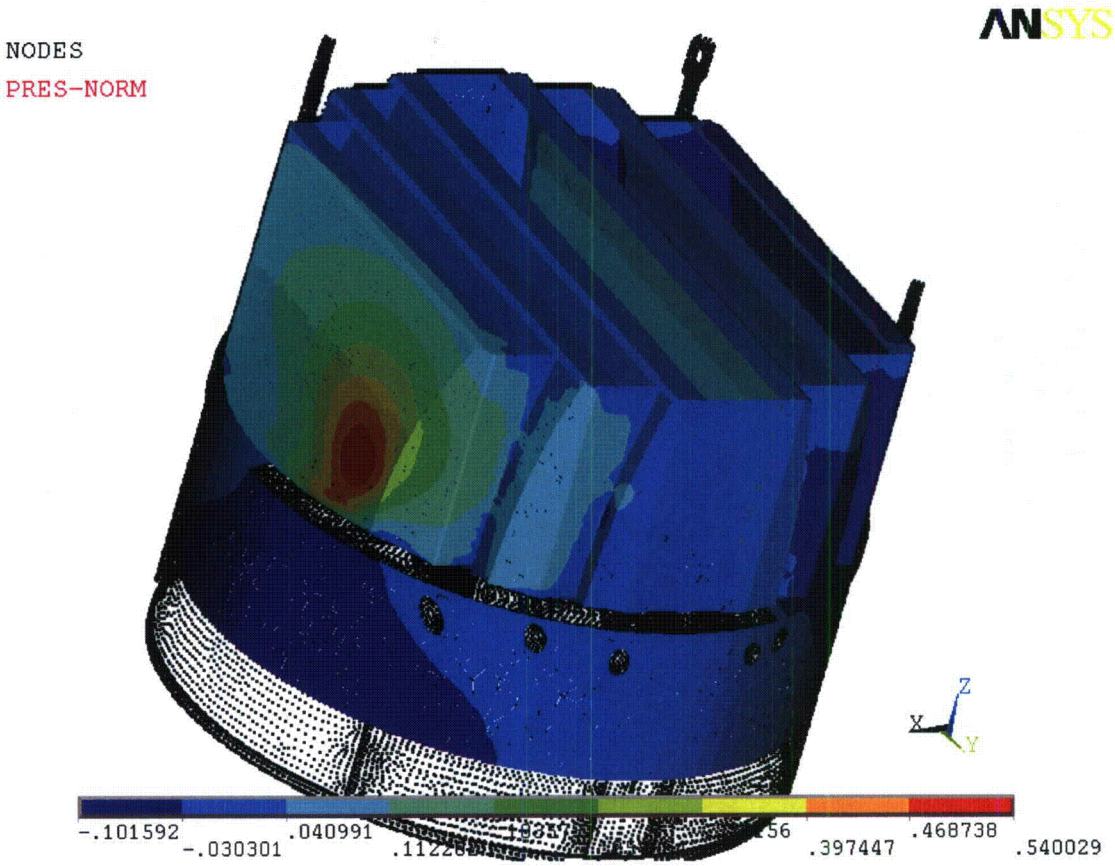

Figure 12a. Real part of unit pressure loading MSL A (in psid) on the steam dryer at 50.1 Hz. No loading is applied to the submerged surface and lifting rods.

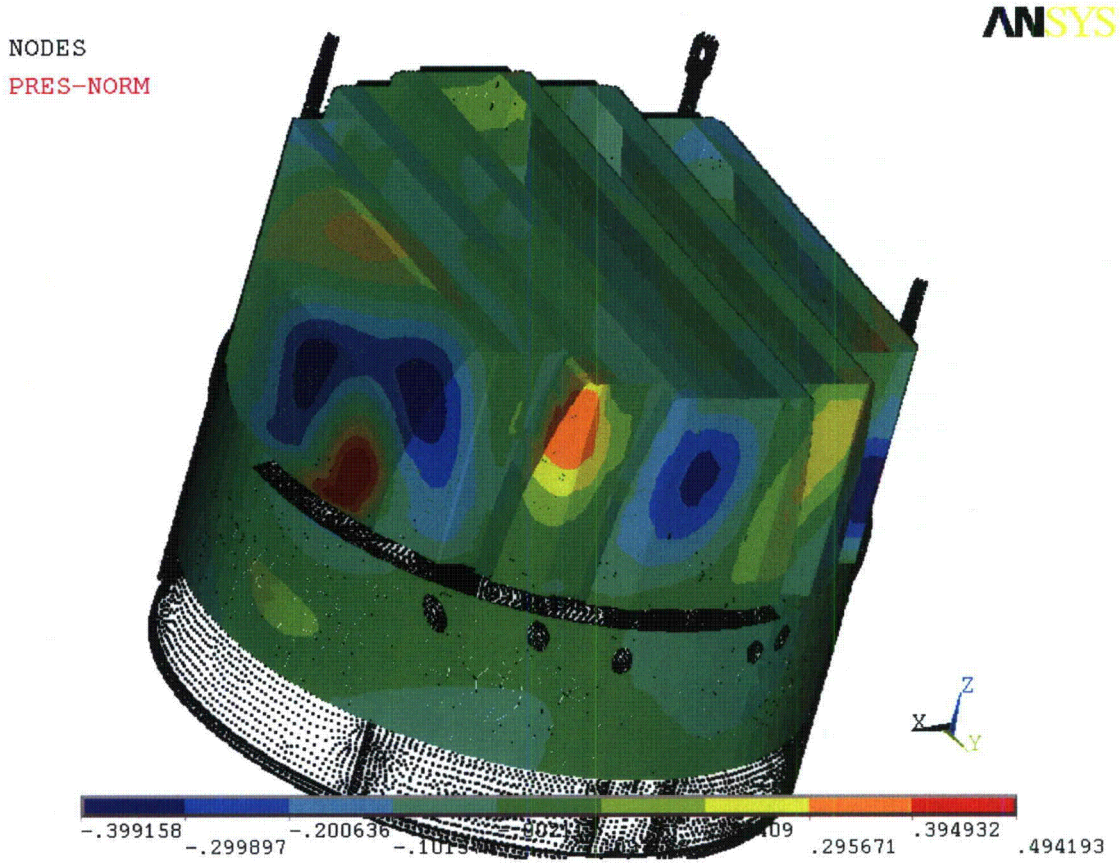

Figure 12b. Real part of unit pressure loading MSL A (in psid) on the steam dryer at 200.45 Hz. No loading is applied to the submerged surface and lifting rods.

4. Structural Analysis

The solution is decomposed into static and harmonic parts, where the static solution produces the stress field induced by the supported structure subjected to its own weight and the harmonic solution accounts for the harmonic stress field due to the unit pressure of given frequency in one of the main steam lines. All solutions are linearly combined, with amplitudes provided by signal measurements in each steam line, to obtain the final displacement and stress time histories. This decomposition facilitates the prescription of the added mass model accounting for hydrodynamic interaction and allows one to compare the stress contributions arising from static and harmonic loads separately. Proper evaluation of the maximum membrane and membrane+bending stresses requires that the static loads due to weight be accounted for. Hence both static and harmonic analyses are carried out.

4.1 Static Analysis

The results of the static analysis are shown in Figure 13. The locations with highest stress include the inner vane bank connection to inner base plate near support brackets with stress intensity 9,598 psi. There are four locations with artificial stress singularity, which are excluded from the analysis. The static stresses one node away are used at these locations as more realistic estimate of local stress. These locations are at the connections of the inner end plate to the inner base plate at the ends of the cut-out, as shown in Figure 13c.

4.2 Harmonic Analysis

The harmonic pressure loads were applied to the structural model at all surface nodes described in Section 3.10. Typical stress intensity distributions over the structure are shown in Figure 14. Stresses were calculated for each frequency, and results from static and harmonic calculations were combined.

To evaluate maximum stresses, the stress harmonics including the static component are transformed into a time history using FFT, and the maximum and alternating stress intensities for the response, evaluated. According to ASME B&PV Code, Section III, Subsection NG-3216.2 the following procedure was established to calculate alternating stresses. For every node, the stress difference tensors, $\boldsymbol{\sigma}'_{nm} = \boldsymbol{\sigma}_n - \boldsymbol{\sigma}_m$, are considered for all possible pairs of the stresses $\boldsymbol{\sigma}_n$ and $\boldsymbol{\sigma}_m$ at different time levels, t_n and t_m. Note that all possible pairs require consideration since there are no "obvious" extrema in the stress responses. However, in order to contain computational cost, extensive screening of the pairs takes place (see Section 2.3) so that pairs known to produce alternating stress intensities less than 250 psi are rejected. For each remaining stress difference tensor, the principal stresses S_1, S_2, S_3 are computed and the maximum absolute value among principal stress differences, $S_{nm} = \max\{|S_1 - S_2|, |S_1 - S_3|, |S_2 - S_3|\}$, obtained. The alternating stress at the node is then one-half the maximum value of S_{nm} taken over all combinations (n,m), i.e., $S_{alt} = \frac{1}{2}\max_{n,m}\{S_{nm}\}$. This alternating stress is compared against allowable values, depending on the node location with respect to welds.

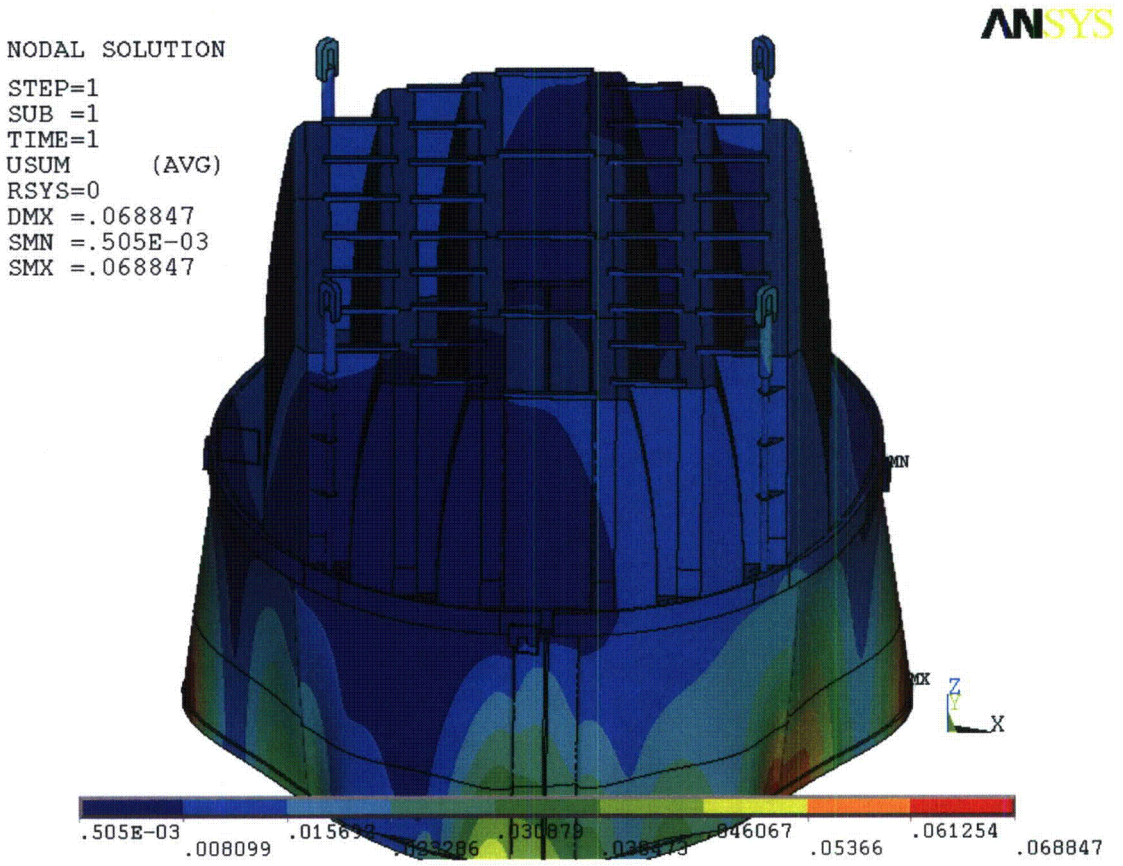

Figure 13a. Overview of static calculations showing displacements (in inches). Maximum displacement (DMX) is 0.069". Note that displacements are amplified for visualization.

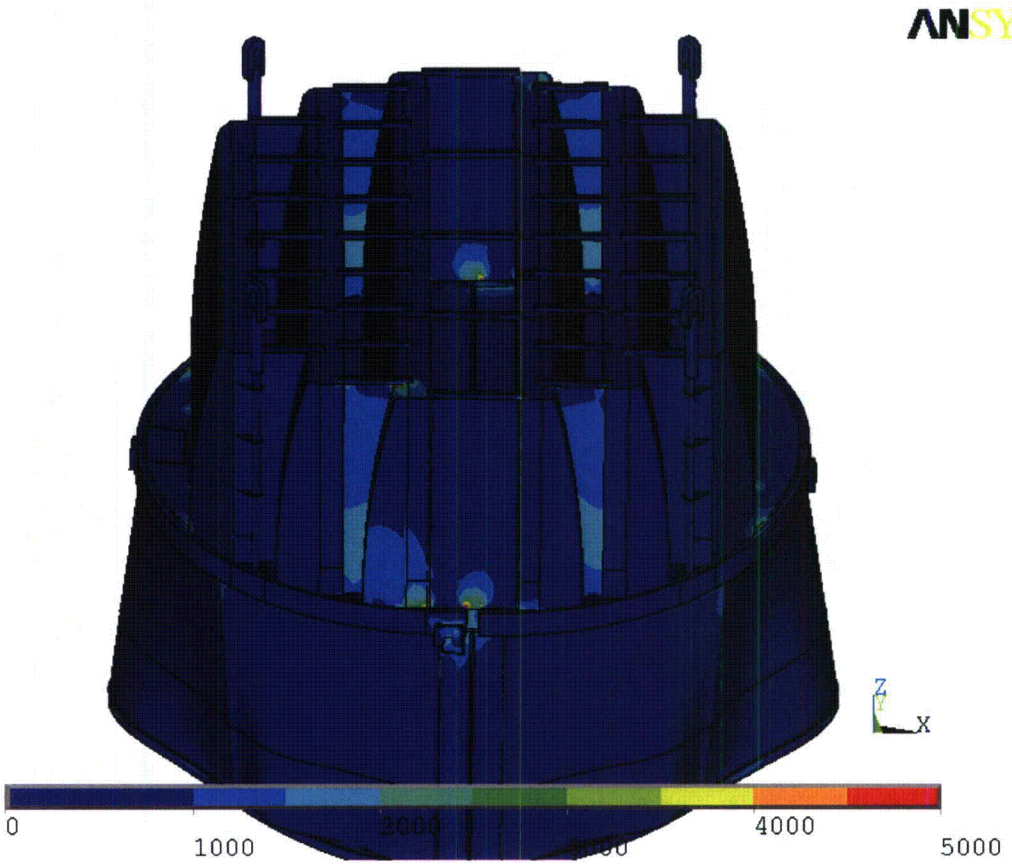

Figure 13b. Overview of static calculations showing stress intensities (in psi). Maximum stress intensity (SMX) is 9,598 psi. Note that displacements are amplified for visualization

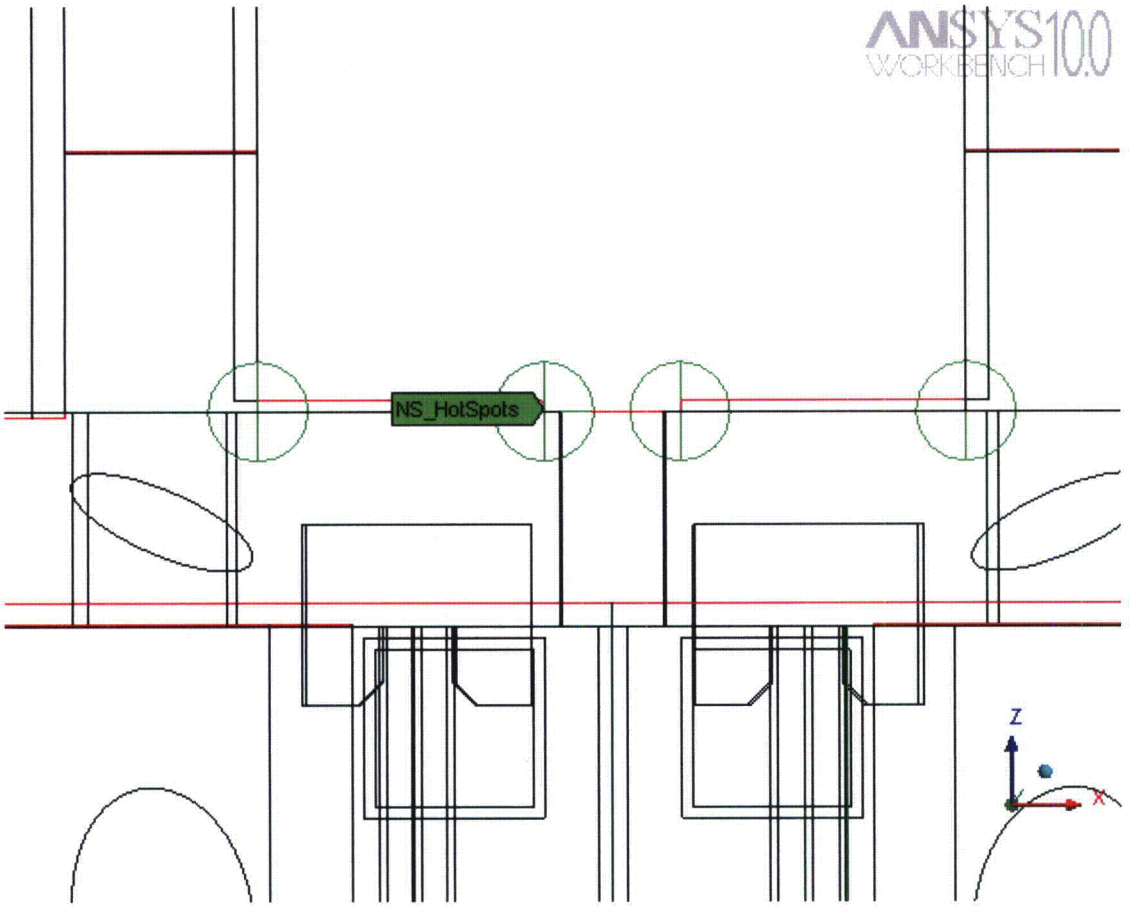

Figure 13c. Stress singularities. Model is shown in wireframe mode for clarity.

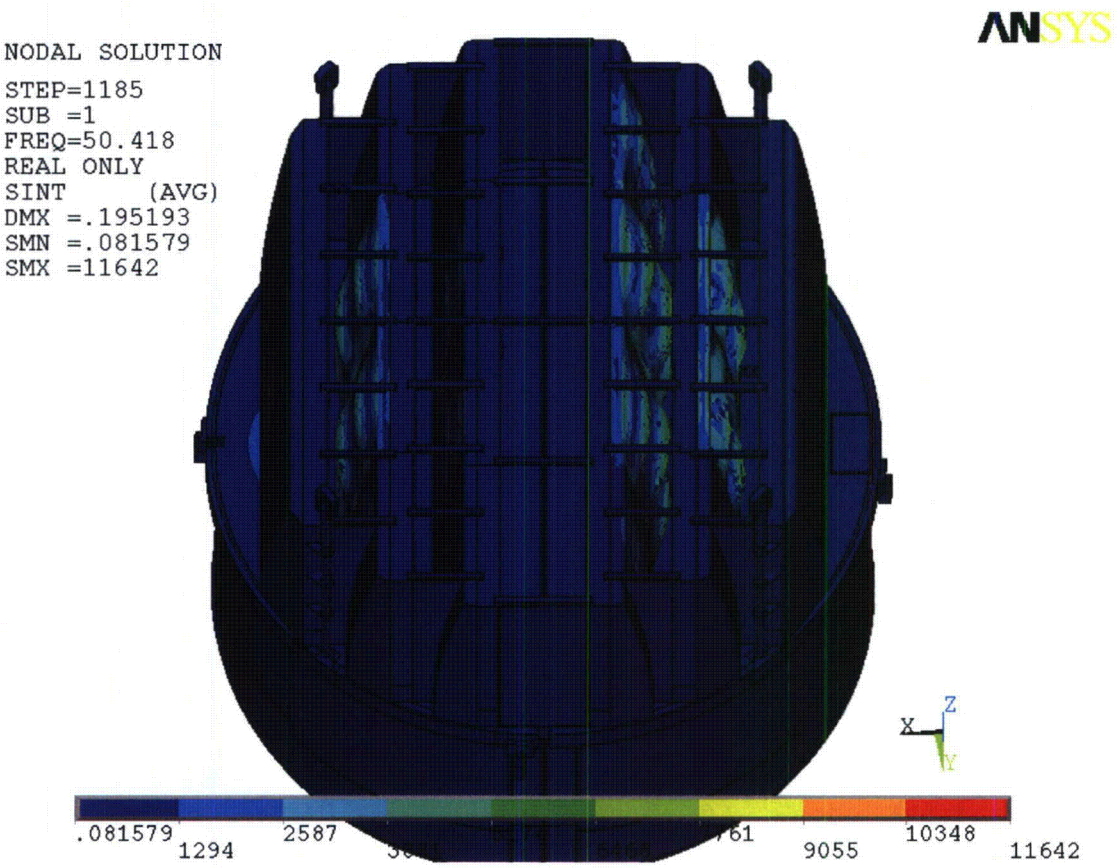

Figure 14a. Overview of harmonic calculations showing real part of stress intensities (in psi) along with displacements. Unit loading MSL A at 50.1 Hz (oriented to show high stress locations at the hoods).

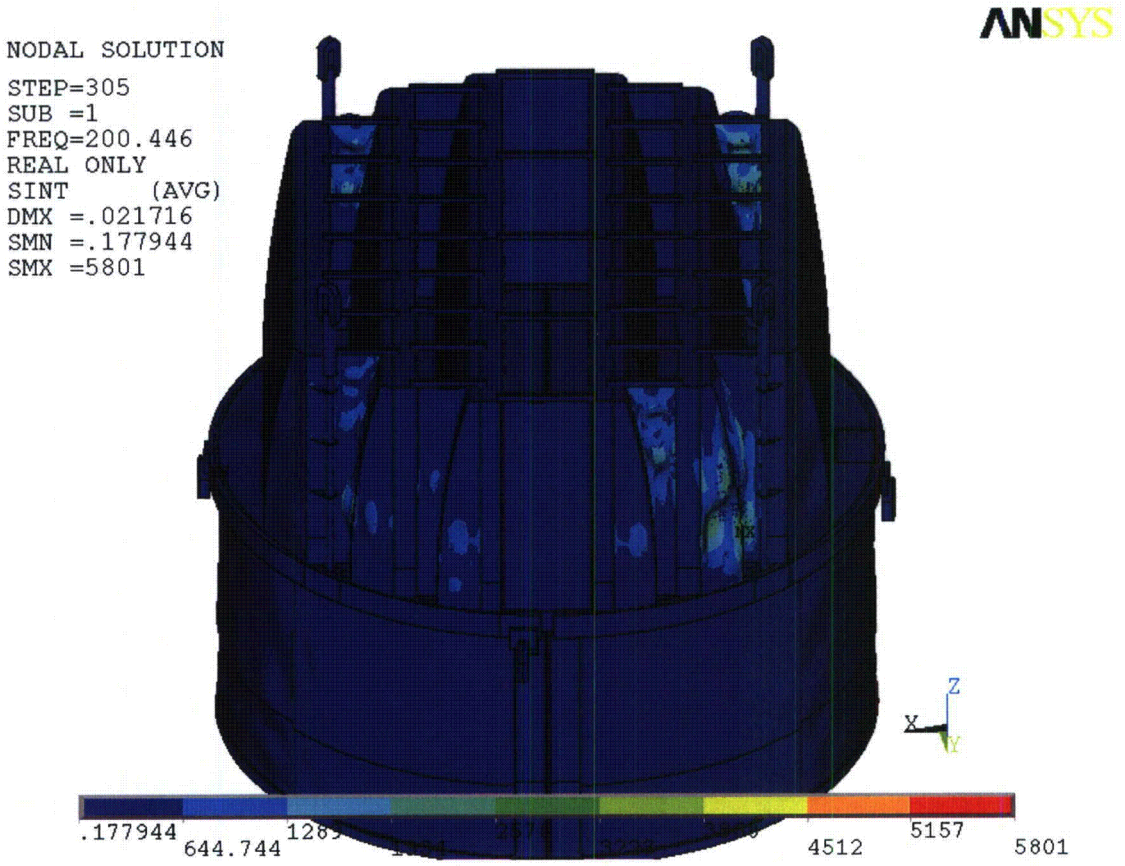

Figure 14b. Overview of harmonic calculations showing real part of stress intensities (in psi) along with displacements. Unit loading MSL A at 200.5 Hz.

4.3 Post-Processing

The static and transient stresses computed at every node with ANSYS were exported into files for subsequent post-processing. These files were then read into separate customized software to compute the maximum and alternating stresses at every node. The maximum stress was defined for each node as the largest stress intensity occurring during the time history. Alternating stresses were calculated according to the ASME standard described above. For shell elements the maximum stresses were calculated separately at the mid-plane, where only membrane stress is present, and at top/bottom of the shell, where bending stresses are also present.

For nodes that are shared between several structural components or lie on junctions, the maximum and alternating stress intensities are calculated as follows. First, the nodal stress tensor is computed separately for each individual component by averaging over all finite elements meeting at the node and belonging to the same structural component. The time histories of these stress tensors are then processed to deduce the maximum and alternating stress intensities for each structural component. Finally for nodes shared across multiple components the highest of the component-wise maximum and alternating stresses is recorded as the "nodal" stress. This approach prevents averaging of stresses across components and thus yields conservative estimates for nodal stresses at the weld locations where several components are joined together.

The maximum stresses are compared against allowable values which depend upon the stress type (membrane, membrane+bending, alternating – Pm, Pm+Pb, S_{alt}) and location (at a weld or away from welds). These allowables are specified in the following section. For solid elements the most conservative allowable for membrane stress, Pm, is used, although bending stresses are nearly always present also. The structure is then assessed in terms of stress ratios formed by dividing allowables by the computed stresses at every node. Stress ratios less than unity imply that the associated maximum and/or alternating stress intensities exceed the allowable levels. Post-processing tools calculate the stress ratios, identifying the nodes with low stress ratios and generating files formatted for input to the 3D graphics program, TecPlot, which provides more general and sophisticated plotting options than currently available in ANSYS.

4.4 Computation of Stress Ratios for Structural Assessment

The ASME B&PV Code, Section III, subsection NG provides different allowable stresses for different load combinations and plant conditions. The stress levels of interest in this analysis are for the normal operating condition, which is the Level A service condition. The load combination for this condition is:

Normal Operating Load Combination = Weight + Pressure + Thermal

The weight and fluctuating pressure contributions have been calculated in this analysis and are included in the stress results. The static pressure differences and thermal expansion stresses are small, since the entire steam dryer is suspended inside the reactor vessel and all surfaces are exposed to the same conditions. Seismic loads only occur in Level B and C cases, and are not considered in this analysis.

Allowable Stress Intensities

The ASME B&PV Code, Section III, subsection NG shows the following (Table 6) for the maximum allowable stress intensity (Sm) and alternating stress intensity (Sa) for the Level A service condition. The allowable stress intensity values for type 304 stainless steel at operating temperature 550°F are taken from Table I-1.2 and Fig. I-9.2.2 of Appendix I of Section III, in the ASME B&PV Code. The calculation for different stress categories is performed in accordance with Fig. NG-3221-1 of Division I, Section III, subsection NG. The allowable value for alternating stress is taken from curve C of Fig. I-9.2.2 in Appendix I in Section III of the ASME B&PV Code.

Table 6. Maximum Allowable Stress Intensity and Alternating Stress Intensity for all areas other than welds. The notation Pm represents membrane stress; Pb represents stress due to bending; Q represents secondary stresses (from thermal effects and gross structural discontinuities, for example); and F represents additional stress increments (due to local structural discontinuities, for example).

Type	Notation	Service Limit	Allowable Value (ksi)
Maximum Stress Allowables:			
General Membrane	Pm	Sm	16.9
Membrane + Bending	Pm + Pb	1.5 Sm	25.35
Primary + Secondary	Pm + Pb + Q	3.0 Sm	50.7
Alternating Stress Allowable:			
Peak = Primary + Secondary + F	S_{alt}	Sa	13.6

When evaluating welds, either the calculated or allowable stress was adjusted, to account for stress concentration factor and weld quality. Specifically:

- For maximum allowable stress intensity, the allowable value is decreased by multiplying its value in Table 6 by 0.55.

- For alternating stress intensity, the calculated weld stress intensity is multiplied by a weld stress intensity (fatigue) factor of 1.8 for a fillet weld and 1.4 for a full penetration weld, before comparison to the Sa value given above.

The weld factors of 0.55 and 1.4 (full penetration weld) or 1.8 (fillet weld) were selected based on the observable quality of the shop welds and liquid penetrant NDE testing of all welds (excluding tack and intermittent welds, which were subject to 5X visual inspection) during fabrication. These factors are consistent with fatigue strength reduction factors recommended by the Welding Research Council, [25], and stress concentration factors at welds, provided in [26] and [27]. In addition, critical welds are subject to periodical visual inspections in accordance with the requirements of GE SIL 644 SIL and BWR VIP-139 [28]. Therefore, for weld stress intensities, the allowable values are shown in Table 7. These factors (0.55 and 1.4 or 1.8) also conservatively presume that the structure is joined using fillet welds unless specified otherwise. Since fillet welds correspond to larger stress concentration factors than other types of welds, this assumption is a conservative one.

Table 7. Weld Stress Intensities.

Type	Notation	Service Limit	Allowable Value (ksi)
Maximum Stress Allowables:			
General Membrane	Pm	0.55 Sm	9.30
Membrane + Bending	Pm + Pb	0.825 Sm	13.94
Primary + Secondary	Pm + Pb + Q	1.65 Sm	27.89
Alternating Stress Allowables:			
Peak = Primary + Secondary + F	S_{alt}	Sa	13.6

Comparison of Calculated and Allowable Stress Intensities

The classification of stresses into general membrane or membrane + bending types was made according to the exact location, where the stress intensity was calculated; namely, general membrane, Pm, for middle surface of shell element, and membrane + bending, Pm + Pb, for other locations. For solid elements the most conservative, general membrane, Pm, allowable is used.

The structural assessment is carried out by computing stress ratios between the computed maximum and alternating stress intensities, and the allowable levels. Locations where any of the stresses exceed allowable levels will have stress ratios less than unity. Since computation of stress ratios and related quantities within ANSYS is time-consuming and awkward, a separate FORTRAN code was developed to compute the necessary maximum and alternating stress intensities, Pm, Pm+Pb, and S_{alt}, and then compare it to allowables. Specifically, the following quantities were computed at every node:

1. The maximum membrane stress intensity, Pm (evaluated at the mid-thickness location for shells),
2. The maximum membrane+bending stress intensity, Pm+Pb, (taken as the largest of the maximum stress intensity values at the bottom, top, and mid thickness locations, for shells),
3. The alternating stress, S_{alt}, (the maximum value over the three thickness locations is taken).
4. The stress ratio due to a maximum stress intensity assuming the node lies at a non-weld location (note that this is the minimum ratio obtained considering both membrane stresses and membrane+bending stresses):
   SR-P(nw) = min{ Sm/Pm, 1.5 * Sm/(Pm+Pb) }.
5. The alternating stress ratio assuming the node lies at a non-weld location,
   SR-a(nw) = Sa / (1.1 * S_{alt}),
6. The same as 4, but assuming the node lies on a weld,
   SR-P(w)=SR-P(nw) * 0.55
7. The same as 5, but assuming the node lies on a weld,
   SR-a(w)=SR-a(nw) / f_{sw}.

Note that in steps 4 and 6, the minimum of the stress ratios based on Pm and Pm+Pb, is taken. The allowables listed in Table 7, Sm=16,900 psi and Sa=13,600 psi. The factors, 0.55 and f_{sw}, are the weld factors discussed above with f_{sw}=1.8 being appropriate for a fillet weld and f_{sw}=1.4 for a full penetration weld. The factor of 1.1 accounts for the differences in Young's moduli for the steel used in the steam dryer and the values assumed in alternating stress allowable. According to NG-3222.4 in subsection NG of Section III of the ASME Code [3], the effect of elastic modulus upon alternating stresses is taken into account by multiplying alternating stress S_{alt} at all locations by the ratio, E/E_{model}=1.1, where:

E = 28.3 10^6 psi, as shown on Fig. I-9.2.2. ASME BP&V Code
E_{model} = 25.55 10^6 psi (Table 2)

The appropriate maximum and alternating stress ratios, SR-P and SR-a, are thus determined and a final listing of nodes having the smallest stress ratios is generated. The nodes with stress ratios lower than 4 are plotted in TecPlot (a 3D graphics plotting program widely used in engineering communities [29]). These nodes are tabulated and depicted in the following Results Section.

[[4.5 **(3)]]**

[[

(3)]]

[[

(3)]]

5. Modifications Implemented to Meet EPU Stress Margins

The dryer analyzed in Section 5 [10] identified several locations with alternating stress ratios below the EPU target of 2.0 when subjected to the ACM Rev. 4.1 acoustic loads. To achieve the desired EPU stress margins several modification were proposed and analyzed in Section 6 of the same report. These evaluations were carried out using [[(3)]]. The present section provides definitive specifications of the required modifications that were implemented in the NMP2 dryer for EPU operation. The collection of modifications organized into the following distinct groups:

Group 1: The lifting rod bracket/side plate welds. The upper and middle brackets already have weld reinforcement, but this does not reduce stresses sufficiently under the new loads.
Group 2: The middle hood reinforcement strip incurs a high stress due to vibration of the outboard section of the middle hood.
Group 3: The inner hood/hood support welds that experience high stresses due to the inner hood vibrations.
Group 4: The remaining points which are readily modified to achieve SR-a>2.0 at EPU.
Group 5: Closure plate welds which are addressed by adding reinforcement strips to these plates.

Below, these groups are discussed in further detail. In this discussion the "pre-modified" state of steam dryer is taken to be its configuration before the Group 1-5 modifications were implemented (i.e., the NMP2 configuration prior to the Spring 2012 outage).

5.1 Lifting Rod Support Brackets (Group 1)

Without any modification other than an increase in the existing weld size from ¼" to ½" which, [[(3)]] it was determined on the basis of CLTP loads that the limiting alternating stress locations would occur on the lifting rod support brackets (see Figure 15) with an alternating stress ratio below 2.76 at CLTP, which, using a velocity square-based scaling would indicate an alternating stress ratio below 2.0 at EPU. The stresses were highly localized (only one node on each such bracket is affected) which is indicative of development of stress singularities at this re-entrant corner. It was further established that with the weld reinforcement, the lower-most brackets had sufficient stress margin and only the middle and upper brackets did not meet the target stress ratios. For these brackets further weld reinforcement appeared unlikely by itself to achieve the necessary stress reductions. Instead a more substantial structural reinforcement was developed.

The localized nature of the stress concentration called for a corresponding localized reinforcement. Several such concepts were proposed in [10]. There it was shown that increasing the local thickness – specifically that of all elements with at least one node on the vertical plate/brace weld line – from 0.375" to 0.75" satisfactorily reduced the stress and did not

significantly impact the modal properties or stresses elsewhere on the steam dryer. Of the various concepts considered, Concept 2 was recommended as it provided substantial stress reduction while requiring less severing, grinding and re-welding than some of the other concepts. This configuration shown in Figure 16 consists of a 2" radius, 0.375" thick circular disk welded to the vertical plate and a small reinforcement plate, shaped to match the re-entrant corner contour as shown, is welded onto the support bracket to increase the effective thickness and thereby reduce the membrane stress. By examining the maximum stress in the unit solution stresses over the 128–145 Hz frequency range (which brackets the dominant frequencies for this location in the global solution) it was shown that this reinforcement reduces the maximum stress by a factor of 0.18 (Table 11 of [10]).

The design finalized here builds upon the semi-circular disc concept 2 but is modified to eliminate any cutting of existing welds. It consists of a 2.5" wide by 3" high 3/8" thick rectangular plate with a 1.5" long and 1" wide slot cut out as indicated in Figure 17. The dimensions are selected so that the plate can slide over the existing 0.25" brace attachment weld (W1). Note that the total width of the existing 0.25" double sided fillet weld is 2x0.25" (two fillets) plus 0.375" (brace plate thickness) or 0.875". The larger 1" slot accommodates possible irregularities in the actual weld. The length of the slot is sized so that the plate can slide up to the existing weld (again accounting for possible irregularities in the wrap around portion of the existing weld) and leave sufficient room for a 0.375 fillet weld (W2) around its perimeter. The plate and slot has ¼" rounded fillets. The installation process begins by sliding this plate over the brace and attaching it to the vertical plate by a 3/8" fillet weld as indicated in Figure 17. Next a ½" weld (W4) is created as shown in Figure 18 to attach the 3/8" brace reinforcement plates. These welds are continued to the right along the entire length of the vertical plate/brace joint wrapping around the end. This allows continued used of the SRF=0.64 for this reinforced weld line. The attachment is completed by adding a ¼" weld W5 to attach the brace reinforcement plates to the brace. A top view of the brace reinforcement plate is shown in Figure 19. The plate is 5" long by 1.25" wide and trimmed at a 47.5 deg. angle as indicated so that the edge is parallel to the existing weld joining the two plates comprising the lifting rod brace.

This reinforcement is used for the middle and top lifting rod braces. For the lowest braces adequate stress margin is achieved by increasing the existing weld size to ½" allowing application of [[

$^{(3)}$]] to this weld as shown in [30].

Prior to final design and installation it was required that available photographs of the as-built lifting rod brace installations be reviewed to ensure that there is adequate clearance relative to existing welds and to ensure proper fitting of the new components. For example, reference to the photograph in Figure 20 suggests that proper fitting of the vertical plate will entail milling out a step on the face adjacent to the vertical plate to accommodate the closure plate and its attachment weld.

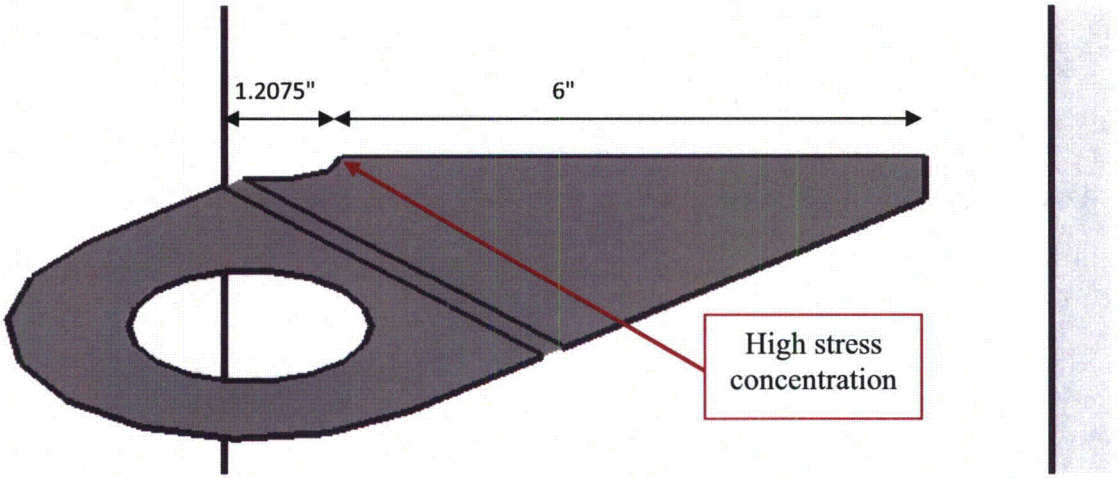

Figure 15. Basic geometry of lifting rod brace. The lifting rod slides through the circular hole and the brace is attached to the vane bank vertical plate.

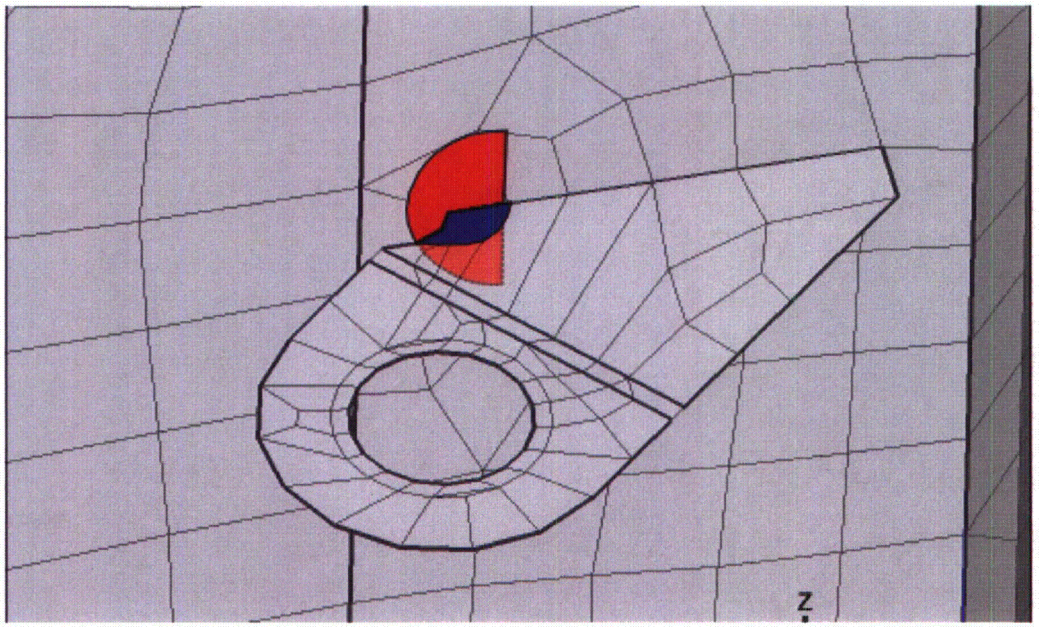

Figure 16. Reinforcement concept 2: Partial reinforcement – semi-circular plate one side plate (red) and reinforcement of re-entrant corner on support bracket (blue)

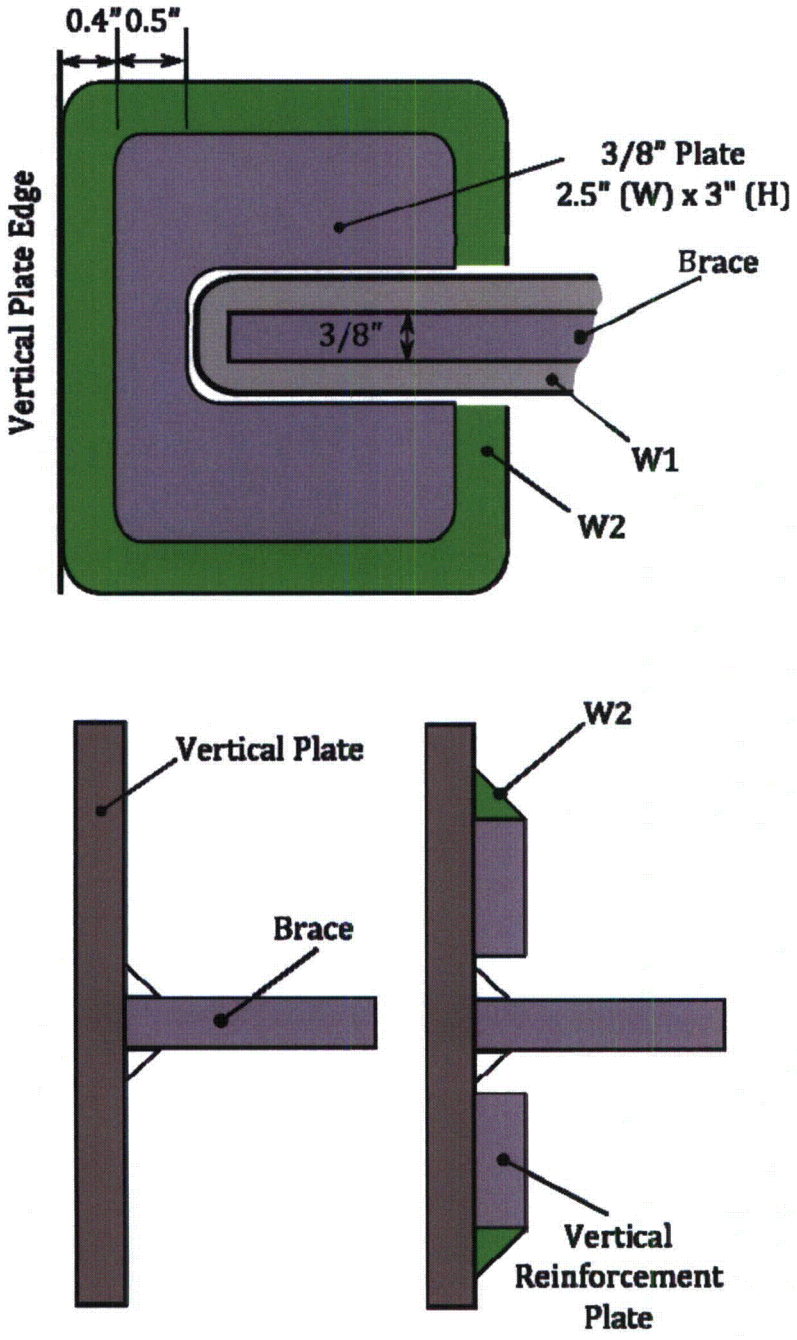

Figure 17. Schematic of reinforcement. W1 is the existing 0.25" weld; W2 is the new 0.375" weld for attaching the vertical reinforcement plate.

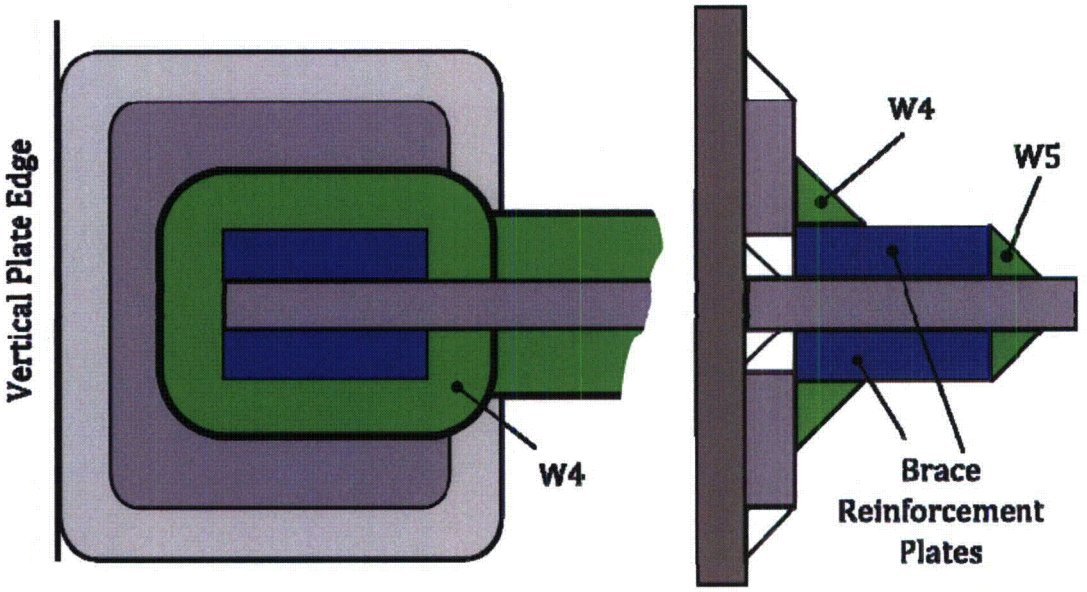

Figure 18. Additional welds. The 0.5" fillet weld, W4, attaches the 3/8" brace reinforcement plates to the vertical reinforcement plate. The weld continues on over the existing brace attachment weld. W5 attaches the brace reinforcement plates to the existing brace.

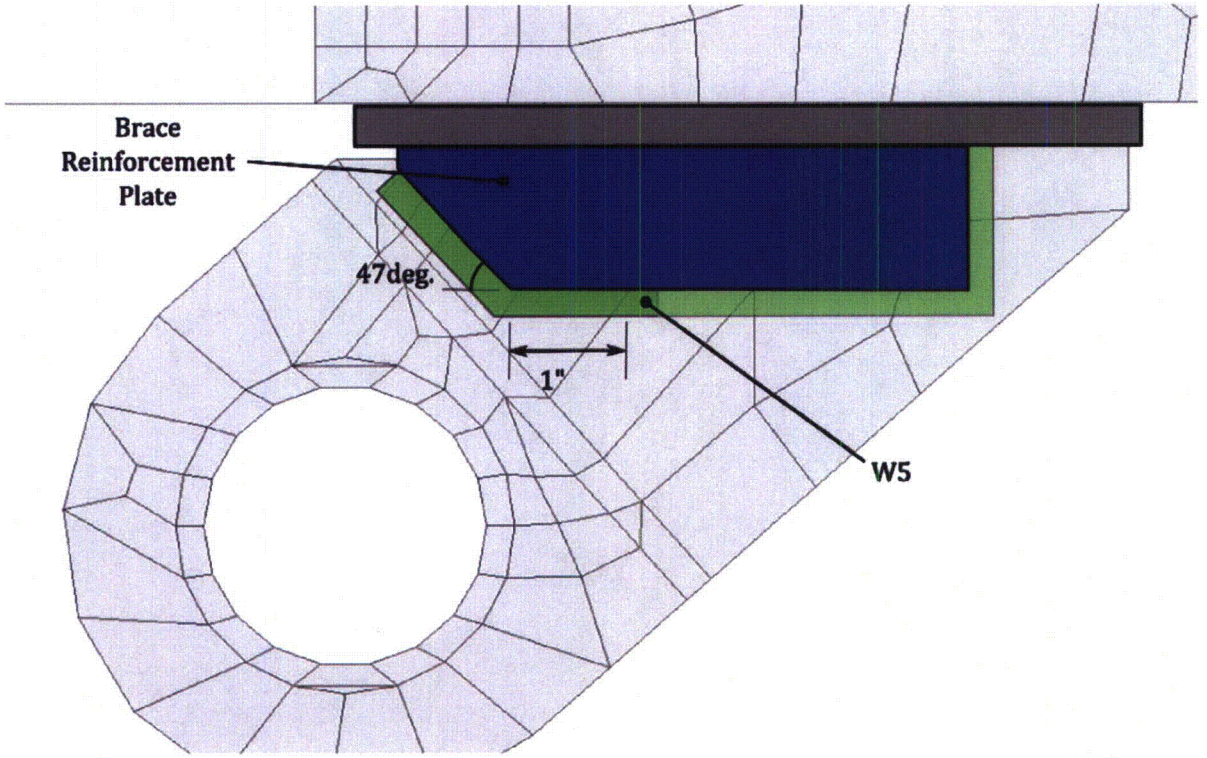

Figure 19. Depiction of brace reinforcement plate.

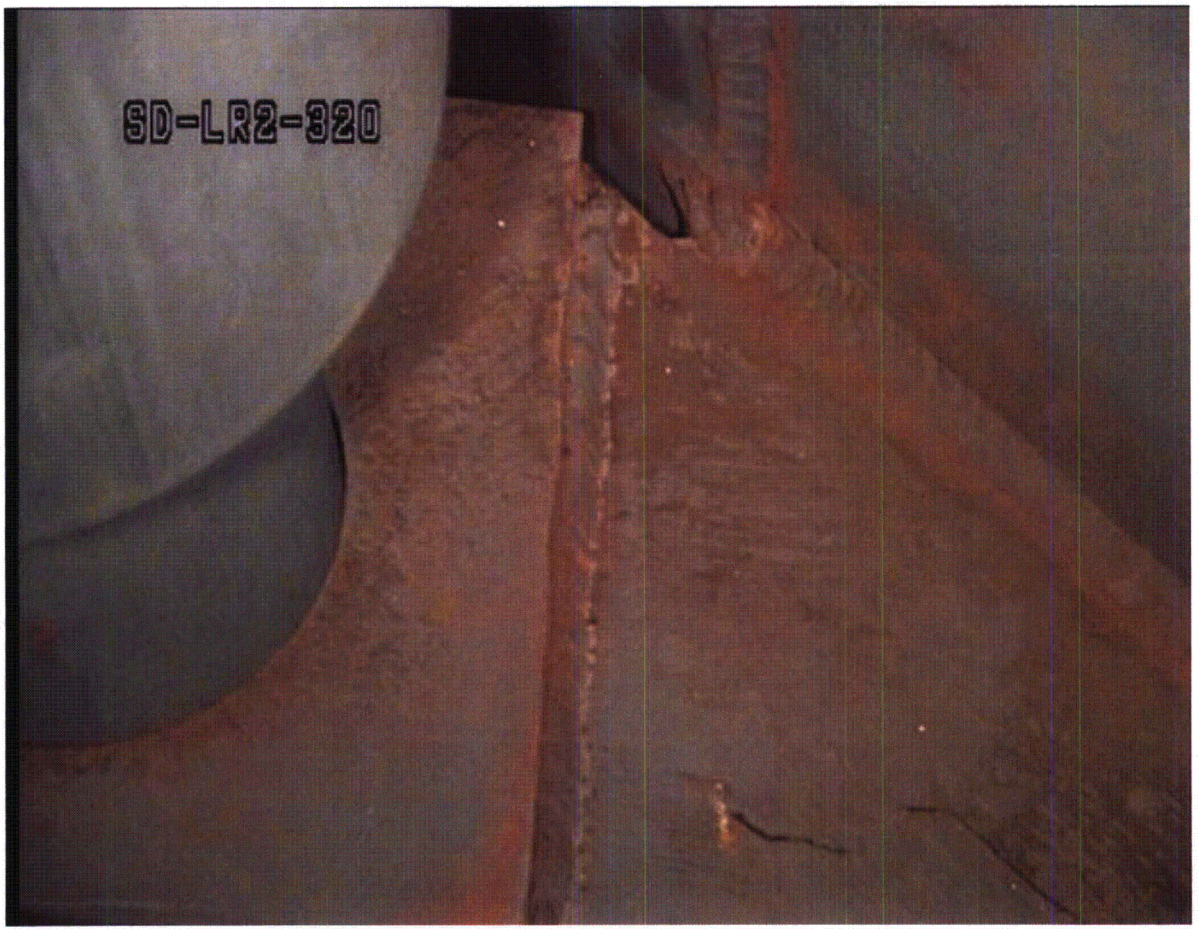

Figure 20. As built lifting rod brace.

5.2 Middle Hood/Reinforcement Strip (Group 2)

Application of the Rev. 4.1 CLTP acoustic loads to the pre-modified steam dryer induced a strong response on the section of the middle hood lying between the closure plate and the vertical reinforcement strip (see Figure 21), and produced stresses along this strip that exceeded target levels. This strip was originally added to address indications on the outboard section of the middle hood. The high stresses occur on the 1/8" middle hood rather than within the much thicker strip (additional 3/8") and are dominated by a 109.0 Hz signal which, at the +10% shift, excites a structural response at 119.9 Hz.

In Section 6 of [10] it was reasoned that a local modification was unlikely to rectify the high stress, but merely shift its location slightly. Therefore, to reduce the stress it was proposed to suppress the active oscillation by covering this section of the middle hood with a 3/8" curved plate welded about its perimeter to the hood and closure plate. Manufacture of the plate is straightforward and creating the attachment weld does not pose accessibility challenges. However, since each such plate would weigh approximately 90 lbs and stress evaluations showed that all previously limiting locations on the hood acquired very high alternating stress ratios (SR-a>20) after the modification it was surmised that adequate stress reduction could easily be achieved using thinner reinforcement plates.

Therefore the steam dryer stress evaluation was repeated by replacing the previous 3/8" curved reinforcement plate by one that is 1/8" thick thus increasing the effective thickness of the hood section to ¼". Unit solution stresses of the complete steam dryer with this modified middle hood section (and also the other planned reinforcements – reinforced closure plate and added masses on the inner and middle hoods as discussed below) were developed in the 30-250 Hz frequency range. This range: (i) encompasses the frequency where stresses are highest and (ii) ensures that any higher order modes occurring at higher frequencies are fully accounted for. Recalculation of the stresses at the Group 2 locations results in CLTP stresses that are below 1300 psi which maintains ample margin for EPU operation.

It was recommended that the panels be trimmed to size such that the plate edges reach to within 1/8" of the existing welds on the closure plate and the reinforcement strip. A 3/16" inch fillet weld is then applied around the perimeter of the reinforcement plate.

Table 8. Group 2 CLTP stresses after adding 1/8th reinforcement plate over the middle hood section lying between the existing reinforcement strip and closure plate.

Location	node	Pm	Pm+Pb	Sa	SR-P	SR-a	% Freq. Shift	Dom. Freq. [Hz]
2. Hood Reinforcement/Middle Hood	98275	200	497	362	28.07	18.96	0	135.4
8. Hood Reinforcement/Middle Hood	90126	981	1462	381	9.47	18.05	5	51.2
9. Hood Reinforcement/Middle Hood	98268	352	597	377	23.34	18.24	2.5	135.4
10. Hood Reinforcement/Middle Hood	90949	993	1112	321	9.36	21.36	-5	140.9

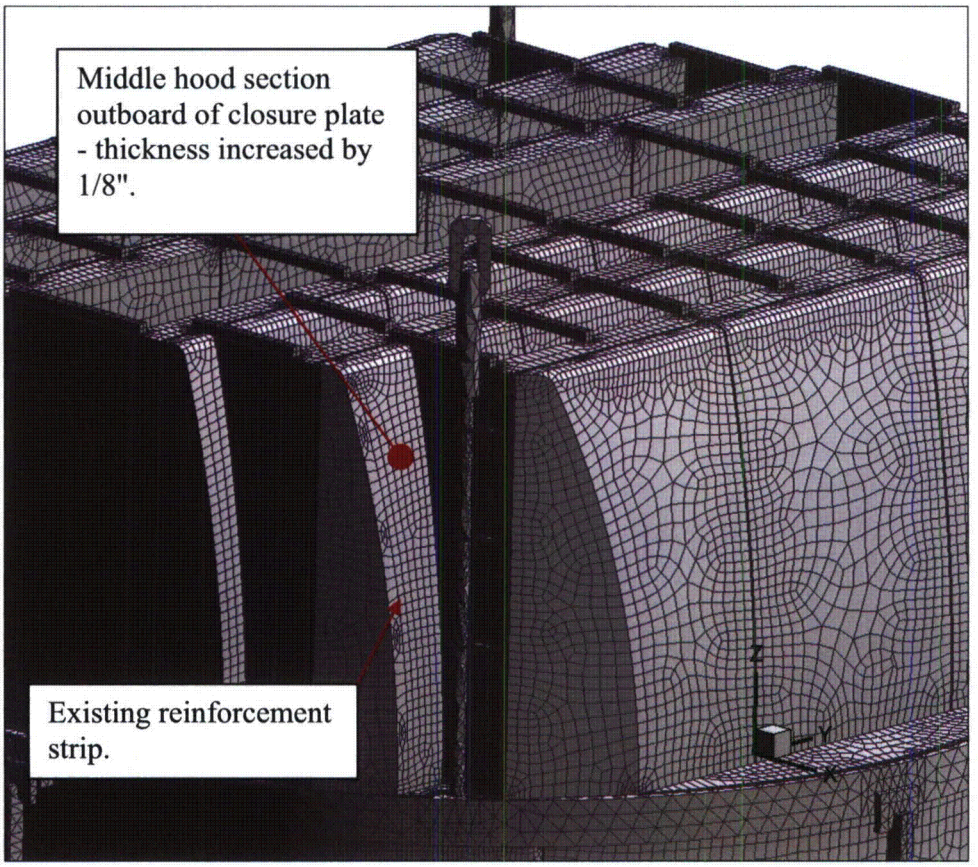

Figure 21. Middle hood section subject to modification and existing reinforcement strip.

5.3 Inner Hoods/Hood Support (Group 3)

In the pre-modified steam dryer configuration the inner hoods and to a lesser extent also the middle hoods, showed a strong stress response on the hood/hood support welds in the 45-60 Hz range. The stresses resulted from strong vibrations of the central sections of the inner and middle hoods and did not meet the required margin for EPU operation. Since the acoustic loads on these hoods are relatively low, these vibrations are caused by transmission of loads from other steam dryer components such as the directly forced outer hoods. Since the welds, particularly at higher elevations, are difficult to access and reinforce it was necessary to pursue alternate modifications. One option was to stiffen the hood panels and suppress vibrations by adding reinforcement strips at the modal displacement response peaks. This would generally result in similar response modes occurring at upward-shifted natural frequencies. However, examination of the MSL signals indicates that these signals increase with frequency so that an upward shift in the hood frequencies would place these frequencies into a range with stronger MSL signals.

Therefore the option pursued was to add small 15 lb masses on the inner hoods. Specifically one such mass was added to each of four central inner hood sections as indicated in Figure 22. Each mass is located 18" below the top of the vane bank surface since this is approximately the reach length of a submerged diver welding the masses to the inner hoods. The addition of the masses lowers the natural response frequencies and reduces the modal amplitudes (since the generalized masses of the participating modes are reduced). These masses were added into the global model and unit solutions regenerated over the 30-250 Hz frequency range (in conjunction with the other modifications to the dryer including the thickened closure plates, middle hood masses and middle hood reinforcement described for Group 2). As shown in Section 6.2, with these masses in place all locations meet the required margins.

Using a density of 0.284 lb/in^3 for stainless steel it follows that the volume of the 15 lb mass is 52.8 in^3. It was originally proposed to employ a rounded 8"x8" 1" thick rectangular mass with two interior slits – a lower 6" slit and an upper 3" slit - added for additional weld support (see **Error! Reference source not found.**). The mass would be attached with a ¼" weld around the top and side edges (the bottom edge is considered inaccessible to diver reach) and the same sized weld around the interior perimeters of the two slits. The bottom face of the mass would be located at 18" below the top of the vane bank. The upper and lower slots were added to allow for additional attachment welds. Due to additional manufacturing requirements and installation constraints these masses were modified while maintaining the total mass and CG location constant. Stress evaluations of the redesigned masses and their attachment welds confirmed that adequate stress margin was maintained.

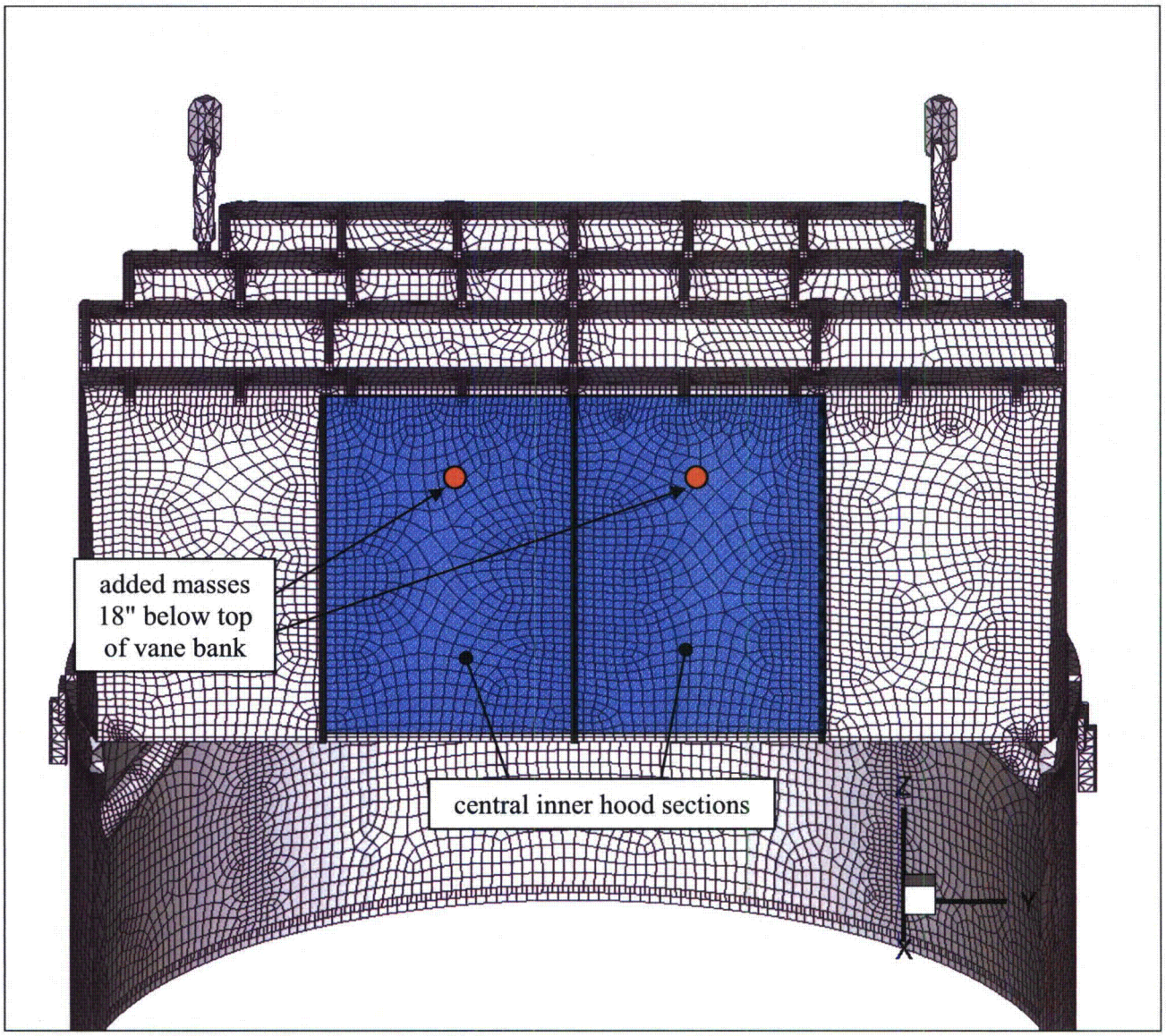

Figure 22. The inner hood sections (blue) whose response contributes to the high stresses on the central hood support/inner hood weld. Middle and outer hoods excluded from view to expose inner hood surfaces. Proposed masses are added 18" below the top of the vane bank.

[[

(3)]]

5.4 Group 4 Locations

Under a previous load definition three families of locations were identified as having alternating stress ratios between 2.65 and 2.76 before modifications [10]. Because these locations were close to, but did not meet the target margin it was natural to collect these locations into a single fourth group. To meet EPU margin, modifications were developed for the group 4 members and assessed on the basis of the older loads. The modifications identified for these locations are described below. Assessment of the modifications for the hood/hood support/base plate junction and of the bottom of the drain channel/skirt weld is [[

(3)]].

The following locations were addressed under group 4.

(a) *Outer hood/hood support/cover plate junctions.* These points lie on the common intersection between the hood, hood support and base plate. To alleviate the stress a stress relief cut-out hole in the hood support was incorporated. A detailed evaluation of this modification was developed in Section 3.4 and Appendix A.11 of [7] showing that the stress reduction factor achieved with [[

(3)]]. The semi-circular stress relief cut-out hole can be generated using electrical discharge machining (EDM) that can be implemented remotely thus reducing diver dose to at most the period required to attach the device to the hood support.

(b) *Bottoms of the drain channel/skirt welds.* These locations are easily accessible and can be reinforced by adding a wrap-around reinforcement weld to alleviate the stress. Specifically, it was proposed to increase the existing bottom 4" of weld to a thickness of 0.25" and wrap the weld around the bottom of the drain channel and 1" up on the interior side of the junction. In Section 3.1 of [7] a stress reduction factor of [[

(3)]]. Without application of the SRF, the limiting alternating stress ratio at CLTP was shown to be SR-a=3.06. Therefore, using the up-to-date CLTP load definition this location met the required stress margin without any modification needed. When the stress reduction factor is invoked the limiting stress ratio at CLTP for this weld increased to SR-a=4.84 and occurred on a point that is 1" above the bottom of the drain channel/skirt junction where the SRF is in fact not applied.

(c) Middle hood/hood support welds. High stresses occur on the middle hood/hood support welds due to vibrations of the middle hoods. The stresses at these locations have been addressed by adding a total of four 10 lb masses on the central sections of the middle hoods. These function in a manner similar to the masses employed for the inner hoods. However, because a lesser reduction is needed the masses are smaller than those installed on the inner hoods. Other than a reduction in the lower ledge height to achieve the required mass, all other details of the mass design are identical to that attached to the inner hood. The middle hood masses are placed at the same 18" depth measured from the top of the vane bank as the inner hood masses. The impact on stress of adding these masses in and also the other reinforcements including the reinforced closure plates, inner hood masses and reinforced middle hood section outboard of the closure plate was quantified by generating unit solutions with all modifications implemented over the 30-250 Hz frequency range and applying the ACM Rev. 4.1 loads. With these modifications the limiting alternating stress ratio at this location SR-a=3.71 at CLTP.

The resulting changes in the stress ratios for the Group 4 locations when implementing all steam dryer modifications are summarized in Table 9.

Table 9. Alternating stress ratios for group 4 locations before and after modifications.

Location	Modification	SR-a (at CLTP)	
		Pre-Modification	Post-Modification
(a) Hood Support/Outer Base Plate/Middle Backing Bar	Cut-out in hood support (SRF=0.80, Section 3.4 and Appendix A.11 in [7])	2.29	2.83
(b) Submerged Drain Channel/Submerged Skirt	Wrap around weld (SRF=0.56, Section 3.1 in [7]))	3.06	4.84
(c) Hood Support/Middle Hood	Added 10 lb mass	2.94 (1)	3.71

Note: (1). Pre-modification value is estimated as follows. In [2] it was shown that the limiting alternating stress ratios on the middle hood/hood support weld were 2.68 before modification (Table 6 in [2]) and 3.38 after modification (Entry 16 in Table 10 of [2]). This implies a stress increase of 26% when removing the middle hood masses. The pre-modification value is thus estimated as SR-a=3.71/1.26.

5.5 Group 5 Locations - Modification of Closure Plates

The pre-modification closure plates are 1/8 in thick and contained a structural mode near 128 Hz. This mode is a second order mode in the vertical direction and first order in the horizontal direction. In preliminary analyses of the dryer these plates were found to respond strongly to a 135.7 Hz component in the acoustic signal which when shifted by -10% during frequency shifting, couples closely to the closure plate frequency. The response mode induced high stresses along the lateral welds connecting the closure plate to the vane bank (a straight vertical weld) and to the adjacent hood (a mostly vertical weld, but curved to accommodate the hood geometry). The highest stresses generally occurred at the top of this weld. However, significant stresses also developed on these weld lines between 10-20 inches below the top of the weld. This corresponds to the weld locations nearest the maximum displacement of this mode. In preliminary stress assessments made for the dryer where noise was filtered from the signal on the basis of low power measurements, several locations on the closure plate welds emerged as having stress ratios that do not meet target levels at EPU. These locations were addressed by performing a [[

(3)]]. In some cases, addition of an interior weld or thickening of the existing weld (see Section 2.2) was required to achieve acceptable stress ratios.

With updated acoustic loads processed with the ACM Rev. 4.1 (and where low power subtraction is <u>not</u> performed) the closure plate weld reinforcements were found insufficient to achieve the target EPU stress margin. Rather than pursue further weld reinforcement, which is limited in regard to both access (finite arm reach limits the length of weld that can be produced on the interior side of the closure plate) and prospect for improvement (making weld legs significantly larger than the plate thickness does not necessarily improve the stresses), it was

decided to reinforce the closure plate itself to simultaneously reduce stresses and separate structural mode and peak acoustic frequencies.

[[

(3)]]

With the closure plate reinforcement and other steam dryer modifications it is determined that the previous closure plate attachment weld reinforcements are no longer needed and the existing welds are sufficient to meet the EPU stress margins. [[

(3)]]

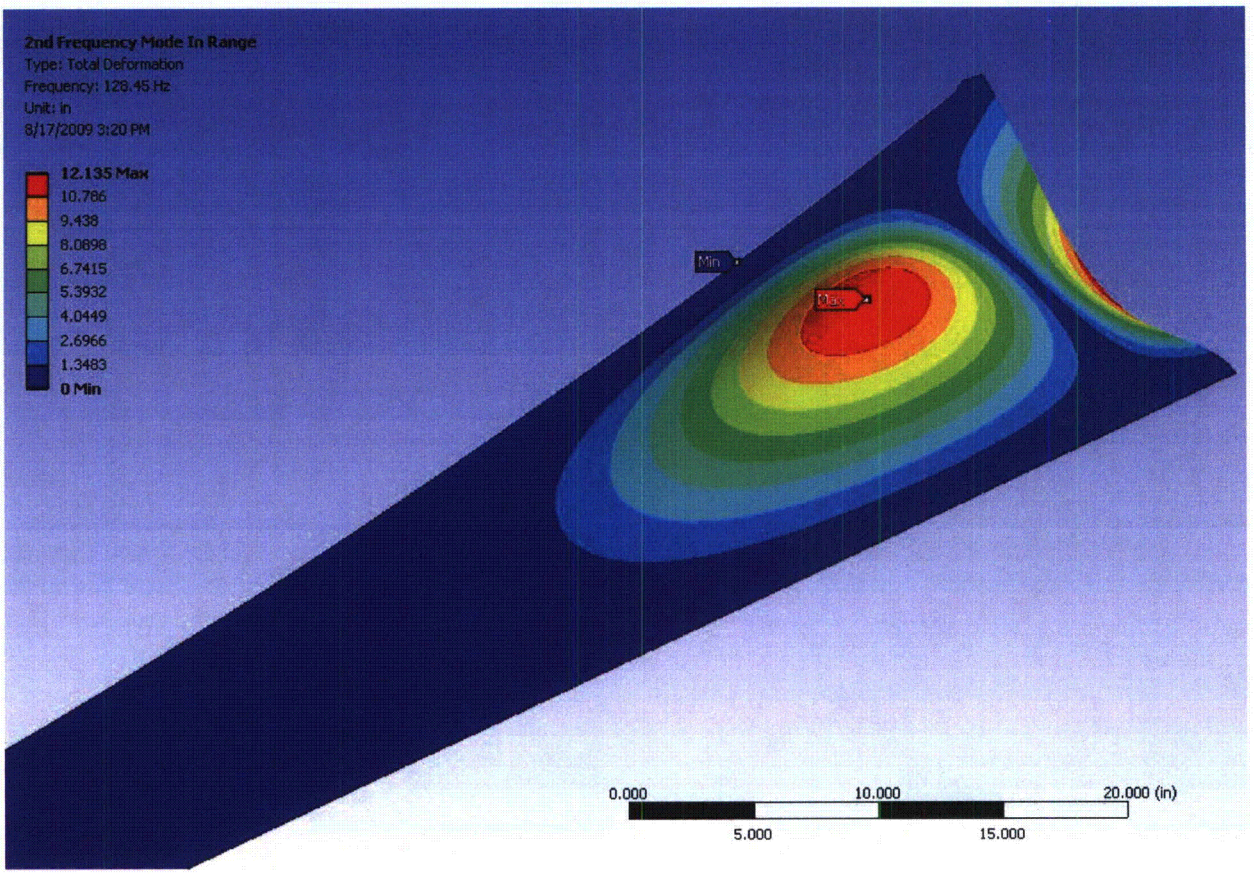

Figure 23: Second mode shape (f=128.45 Hz) of unmodified closure plates

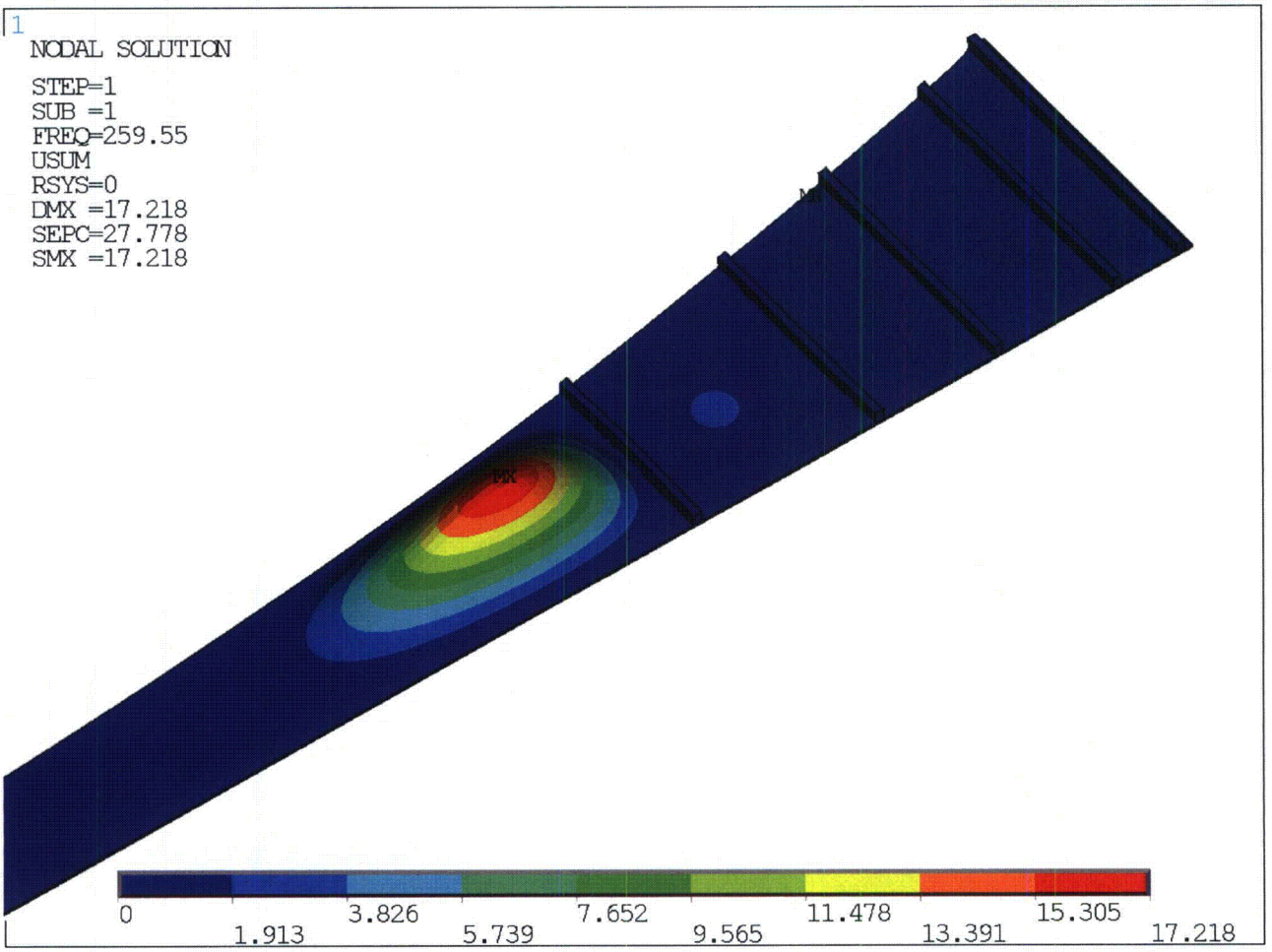

Figure 24: Fundamental mode shape (f=259.6 Hz) of modified closure plate.

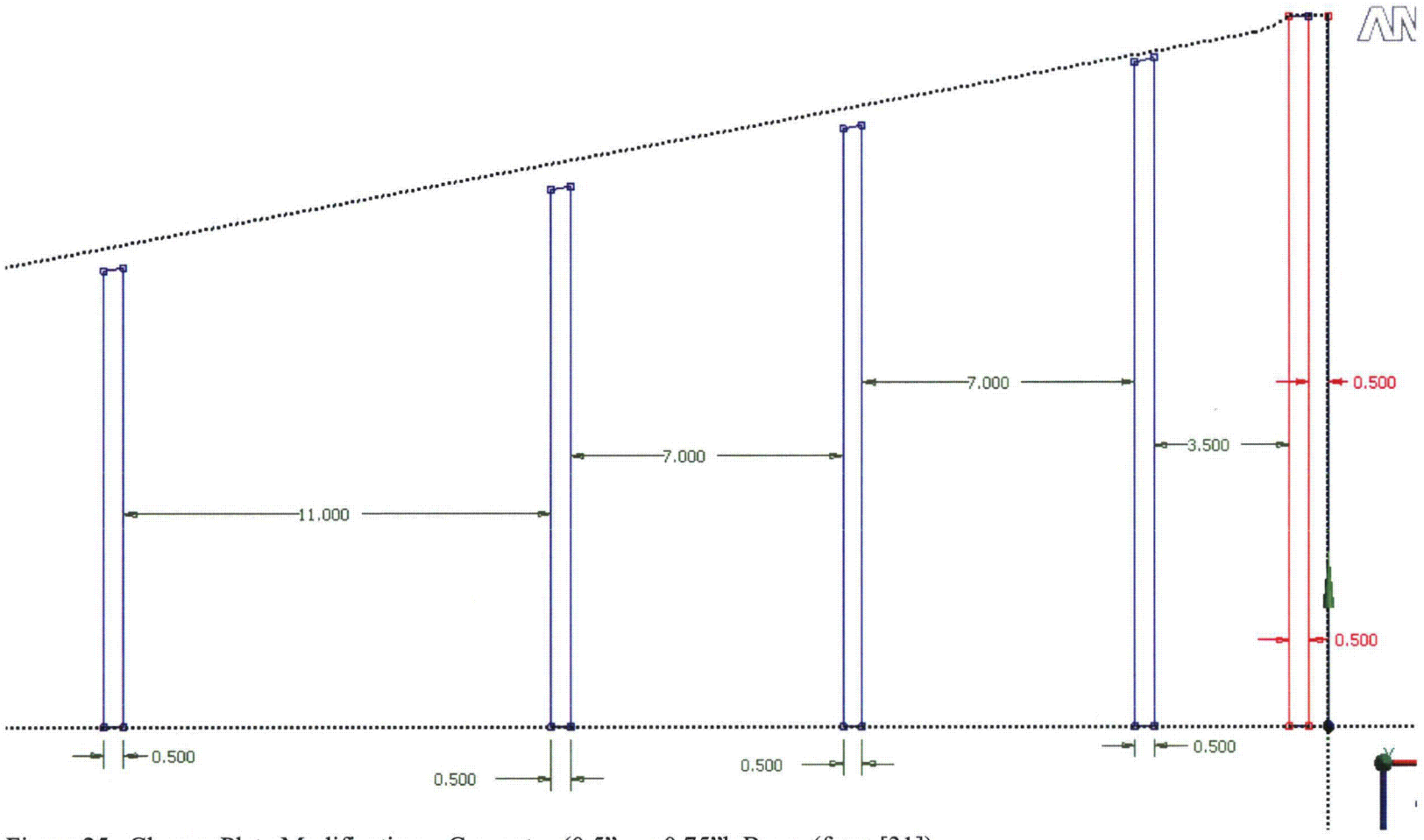

Figure 25. Closure Plate Modification – Geometry (0.5"w x 0.75"h Beam (from [31])

5.6 Summary of Modifications

The dryer modifications are summarized in Table 10. To implement the modifications 1, 4, 5 and 8 unit solutions were regenerated over the 30-250 Hz frequency range with these modifications in place. Below 30 Hz the unit solutions for the original unmodified dryer were used. Since the original dryer had no significant stress response below 30 Hz, the splitting of the unit solutions in this manner is acceptable. For the remaining locations [[(3)]]. The unit solutions are combined with the MSL signals in the manner described in Section 2 to obtain the results in Section 6.

Table 10. Summary of modifications made to the NMP2 steam dryer.

Reinforcement / Modification	Details	FEA Implementation
1. Add reinforcement ribs to all (8) closure plates.	Section 5.5	Closure plates are thickened to obtain dynamically equivalent structure a described in Section 3.5
2. Increase weld of the lowest lifting rod brace/vertical plate welds to 0.5"	Section 5.4; Section 3.5 in [7]	[[(3)]]
3. Reinforce middle and upper lifting rod braces to eliminate stress concentration on weld to vertical plate.	Section 5.1	Reduce stresses by 0.18 at this location based on FEA reductions shown for Concept 2 in Table 11 of [10])
4. Add 1/8" thick plate over the middle hood section lying between the closure plate and existing reinforcement strip.	Section 5.2	Thicken the existing plate by 1/8".
5. Add total of four 15 lb masses to the central sections of the inner hoods.	Section 5.3	Place 15 lb point masses on the inner hoods at the mass centers.
6. Add stress relief cut-out at the bottom edge of the outer hood supports.	Section 5.4; Section 3.4 in [7]	[[(3)]]
7. Reinforce the bottom of the drain channel/skirt weld with thickened wrap-around weld.	Section 5.4; Section 3.1 in [7]	[[(3)]]
8. Add total of four 10 lb masses to the central sections of the middle hoods.	Section 5.4	Place 10 lb point masses on the middle hoods at the mass centers.

5.7 Final (As-Built) Modifications and Installation

In order to facilitate installation and access during underwater welding operations the modification designs described above were refined and analyzed in more detail prior to installation. The adjustments made were negligible with regard to the global analysis since: (i) integral properties such as added mass and overall stiffness of the structure were unchanged so that deviations in mode shapes and natural frequencies from those analyzed in the full steam dryer model would be negligible; and (ii) the modifications generally occurred on a level of detail that was finer than considered in the global model. An example of the latter involves a weld used to attach a 15 lb mass to the inner hood. This weld was extended by 1" relative to the design and the extension analyzed in detail to show it reduced the maximum weld stress by a 1.5%. Such details are not resolved on the global model with a 2.5 in mesh spacing but are instead conservatively compensated for by imposing an overall bias (9.53%) on the stress predictions to account for finite mesh size. In addition to these adjustments, additional information, such as tolerances for the outer hood support cut-outs and closure plate reinforcement rib installations, was developed to provide appropriate manufacturing and installation constraints.

The refinements to the modification groups are summarized below:

Group 1: The lifting rod bracket/side plate welds are essentially unchanged from the designed configurations.

Group 2: The original design of the reinforcement plate attached to the middle hood located outboard of the closure plate did not include an adequate standoff between the perimeter of the reinforcement plate and adjacent structural elements thus posing welding difficulties. Consequently a 2.25 in standoff and beveling of the reinforcement plate perimeter were incorporated. This configuration was reanalyzed to ensure that stresses remain acceptable and determined that at CLTP the limiting conservative alternating stress ratio on the plate reduced from SR-a=3.47 to 3.02 which remains well above margin.

Group 3: The 15 lb masses attached to the inner hoods were modified to facilitate welding and installation without altering the mass and center of gravity. As shown in Figure 26 the added mass structure has evolved into a thinner plate with an upper rounded edge and the mass concentrated on the lower part. The rounded upper edge allows for a longer weld length while concentrating the mass towards the bottom shortens the required reach of the welder to the attachment welds. Dynamic stress analyses of the masses added to the global steam dryer model (see Figure 27) confirmed that stresses near and on the attachment welds remain acceptable [6] for more detail).

Group 4: The 10 lb masses added to the central panels of the middle hoods were modified to match the final 15 lb inner hood mass designs except for the thickness and height of the lower ledge where the mass is concentrated – this ledge is modified so that the correct mass and center of gravity location are maintained. The 10 lb mass geometry is shown in Figure 28. Other than providing tolerances for the outer hood support cutouts near the outer hood/cover plate junction, there were no other adjustments to the Group 4 designs.

Group 5: Tolerances on the vertical positioning of the reinforcement ribs were developed. The rib cross-section was modified by incorporating a chamfer to improve weld access, ensure good weld quality and minimize heat transfer to the closure plate. The resulting cross-section was analyzed to ensure adequate bending stiffness and fundamental frequency (i.e., >250 Hz) of the closure plate are maintained. Finally, due to clearance requirements it was necessary to reposition the lower-most rib by 2.5" relative to the original design. This configuration was evaluated and determined to acceptable.

Complete details of the design adjustments and associated stress evaluations are provided in [6].

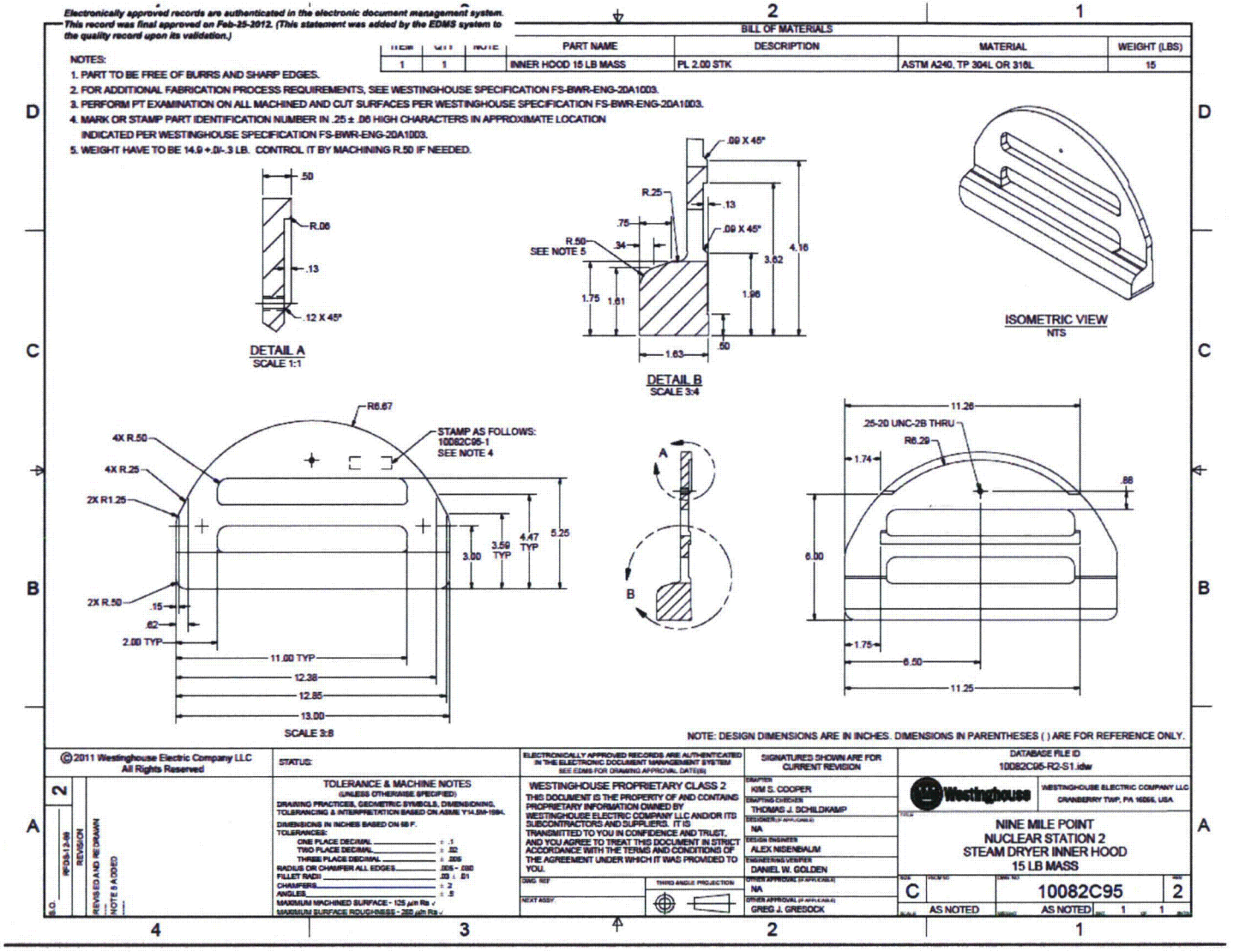

Figure 26. Drawing of 15 lb added mass from Appendix E in [32].

Figure 27. 15 lb masses embedded into the global model. Top – overview; bottom - close up of mesh near added masses.

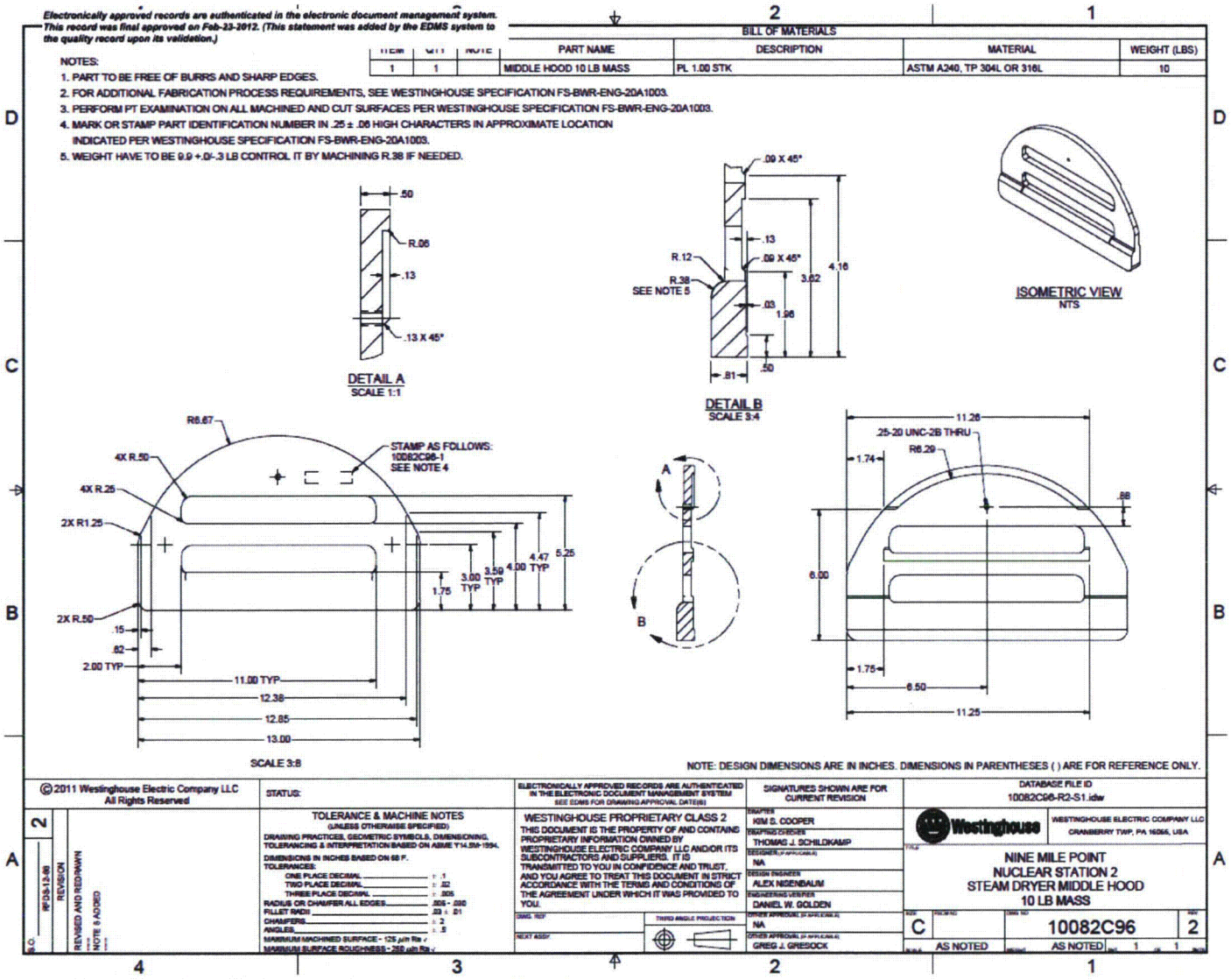

Figure 28. Drawing of 10 lb added mass from Appendix E in [32].

6. Results

The stress intensities and associated stress ratios resulting from the Rev. 4.1 acoustic/hydrodynamic loads [4, 5] with associated biases and uncertainties factored in, are presented below. The bias due to finite frequency discretization and uncertainty associated with the finite element model itself, are also factored in. In the following sections the highest maximum and alternating stress intensities are presented to indicate which points on the dryer experience significant stress concentration and/or modal response (Section 6.1). The lowest stress ratios obtained by comparing the stresses against allowable values, accounting for stress type (maximum and alternating) and location (on or away from a weld), are also reported (Section 6.2). Finally the frequency dependence of the stresses at nodes experiencing the lowest stress ratios is depicted in the form of accumulative PSDs (Section 6.3).

In each section results are presented both at nominal conditions (no frequency shift) and with frequency shift included. Unless specified otherwise, frequency shifts are generally performed at 2.5% increments. The tabulated stresses and stress ratios are obtained using a 'blanking' procedure that is designed to prevent reporting a large number of high stress nodes from essentially the same location on the structure. In the case of stress intensities this procedure is as follows. The relevant stress intensities are first computed at every node and then nodes sorted according to stress level. The highest stress node is noted and all neighboring nodes within 10 inches of the highest stress node and its symmetric images (i.e., reflections across the x=0 and y=0 planes) are "blanked" (i.e., excluded from the search for subsequent high stress locations). Of the remaining nodes, the next highest stress node is identified and its neighbors (closer than 10 inches) blanked. The third highest stress node is similarly located and the search continued in this fashion until all nodes are either blanked or have stresses less than half the highest value on the structure. For stress ratios, an analogous blanking procedure is applied. Thus the lowest stress ratio of a particular type in a 10" neighborhood and its symmetric images is identified and all other nodes in these regions excluded from listing in the table. Of the remaining nodes, the one with the lowest stress ratio is reported and its neighboring points similarly excluded, and so on until all nodes are either blanked or have a stress ratio higher than 5.

The acoustic loads applied to the steam dryer are obtained using the most recent and complete strain gage signals [5] and processed using the ACM Rev. 4.1 analysis with associated biases and uncertainties updated to reflect the new revision as described in [4]. For the FEM structural model there are three main contributors to the bias and uncertainty. The first is an uncertainty (21.5%) that accounts for modeling idealizations (e.g., vane bank mass model), geometrical approximations and other discrepancies between the modeled and actual dryer such as neglecting of weld mass and stiffness in the FEA. The second contributor is a bias of 9.53% accounting for discretization errors associated with using a finite size mesh, upon computed stresses. The third contributor is also a bias and compensates for the use of a finite discretization schedule in the construction of the unit solutions. The frequencies are spaced such that at 1% damping the maximum (worst case) error in a resonance peak is 5%. The average error for this frequency schedule is 1.72%.

6.1 General Stress Distribution and High Stress Locations

The maximum stress intensities obtained by post-processing the ANSYS stress histories for EPU at nominal frequency and with frequency shift operating conditions are listed in Table 11. Contour plots of the maximum stress intensities with all frequency shifts included are shown in Figure 29. The figures are oriented to emphasize the high stress regions. Note that these stress intensities *do not* account for weld factors but do include end-to-end bias and uncertainty. Further, it should be noted that since the allowable stresses vary with location, stress intensities do not necessarily correspond to regions of primary structural concern. Instead, structural evaluation is more accurately made in terms of the stress ratios which compare the computed stresses to allowable levels with due account made for stress type and weld. Comparisons on the basis of stress ratios are made in Section 6.2.

The maximum stress intensities in most areas are low (less than 1000 psi). For the membrane stresses (Pm) the high stress regions tend to occur at: (i) the bottom of the central vertical side plate that joins the innermost vane banks (stress concentrations occur where this plate is welded to the inner base plates resting on the upper support ring); (ii) the welds joining the tie bars to the top cover plates on the vane banks; (iii) the seismic blocks that rest on the steam dryer supports; (iv) the bottoms of the inner vane bank side plates where they connect to the USR; and (v) the closure plate welds. For these locations the stresses are dominated by the static contribution as can be inferred from the small alternating stress intensities (Salt) tabulated in Table 11 for the high Pm locations. From Figure 29a higher Pm regions are seen to be in the vicinity of the supports where all of the dryer deadweight is transmitted, the closure plates connecting the inner hoods to the middle vane banks, and various localized concentrations such those along the bottom of the outer hood.

The membrane + bending stress (Pm+Pb) distributions evidence a more pronounced modal response especially on the inner and middle hood structures. High stress concentrations are recorded on the bottom edge of the central vertical plate where it joins to the USR (immediately above the support blocks) and the inner vane bank. Other areas with high Pm+Pb stress concentrations include: (i) the tops of the closure plates where they are welded to a hood or vane bank end plates; (ii) the skirt/drain channel welds; (iii) the outer cover plates connecting to the upper support ring and bottom of the outer hoods; (iv) the common junction between each hood, its hood support (or stiffener), and (v) the central panels of the inner and (to a lesser extent) middle hoods (see Figure 29b-c).

The alternating stress, S_{alt}, distributions are most pronounced on the inner and middle hoods. The highest stress intensity at any frequency shift at a non-weld location occurs on the inner hood. Though not exposed directly to the MSL acoustic sources, these hoods are thinner than the outer ones and their response is driven mainly by structural coupling rather than direct forcing. Significant response is also observed on the outer hoods nearest the MSL inlet acoustics. Numerous weld locations also show significant stress including the bottoms of drain channels and the junctions between the hoods, hood supports and base plates. These locations are characterized by localized stress concentrations as indicated in Figure 29e and have emerged as high stress locations in other steam-dryers also. Other locations with high alternating stress intensities include the tie bar/top cover plate weld, the weld joining the lifting rod braces to the vertical vane bank end plate and welds involving the closure plate.

Comparing the nominal results (Table 11a) and results with frequency shifting (Table 11b) it can be seen that maximum stress intensities, Pm and Pm+Pb, do not differ significantly. The highest alternating stress is approximately 25.0% higher when frequency shifts are considered.

Table 11a. Locations with highest predicted stress intensities for EPU conditions with no frequency shift.

Stress Category	Location	Weld	SRF(a)	Location (in)			node	Stress Intensities (psi)			Dom. Freq. (Hz)
				x	y	z		Pm	Pm+Pb	S_{alt}	
Pm	Inner Side Plate	No		3.1	119	0.5	37229	7545	8933	570	73.9
"	Upper Support Ring (USR)/Support/Seismic Block	Yes		-6.9	-122.3	-9.5	113554	7271	7271	945	15.5
"	Side Plate Ext/Inner Base Plate	Yes		16.3	119	0	94143	6985	9878	544	44.9
"	Tie Bar	Yes		49.3	108.1	88	141275	6228	6228	1182	97.4
"	Side Plate/Closure Plate/Top Plate	Yes		-47.1	-108.6	88	91558	5674	6267	1009	199.0
Pm+Pb	Side Plate Ext/Inner Base Plate	Yes		16.3	119	0	94143	6985	9878	544	44.9
"	Inner Side Plate	No		3.1	119	0.5	37229	7545	8933	570	73.9
"	Side Plate/Top Plate	Yes		49.6	108.6	88	93256	2584	8882	1637	97.4
"	Side Plate/Top Plate	Yes		17.6	119	88	91215	964	7654	1732	69.4
"	Middle Base Plate/Inner Hood/Backing Bar	Yes		-39.9	-108.6	0	84197	532	7381	1451	71.3
S_{alt}	Inner Hood	No		-32.4	27	72.4	81316	1350	4052	3799	44.9
"	Brace	No		79.6	85.5	75.8	37811	3580	3617	3529	136.7
"	Middle Hood	No		63.6	-30	73.3	34302	1267	3483	3324	61.2
"	Inner Hood	No		31.4	-36.1	77.1	70582	1053	3027	2848	44.5
"	Middle Hood	No		63.2	-18.3	75.4	34769	816	2883	2755	61.2

Notes: (a) [[(3)]] Entry is empty if no SRF is applied.
(b) Full penetration weld so that weld factor, WF=1.4.
(1-5) Number referring to the [[(3)]]

Table 11b. Locations with highest predicted stress intensities taken over all frequency shifts at EPU conditions.

Stress Category	Location	Weld	SRF(a)	Location (in)			node	Stress Intensities (psi)			% Freq. Shift	Dom. Freq. (Hz)
				x	y	z		Pm	Pm+Pb	S_{alt}		
Pm	Inner Side Plate	No		3.1	119	0.5	37229	7600	9091	737	-10	70.8
"	USR/Support/Seismic Block	Yes		-6.9	-122.3	-9.5	113554	7460	7460	1118	-10	14.2
"	Side Plate Ext/Inner Base Plate	Yes		16.3	119	0	94143	7092	10071	712	7.5	101.0
"	Tie Bar	Yes		49.3	108.1	88	141275	6391	6391	1273	10	91.1
"	Top Plate/Side Plate/Closure Plate	Yes		-47.1	-108.6	88	91558	5940	6670	1290	7.5	195.5
Pm+Pb	Side Plate Ext/Inner Base Plate	Yes		16.3	119	0	94143	7092	10071	712	7.5	101.0
"	Side Plate/Top Plate	Yes		49.6	108.6	88	93256	2610	9167	1790	10	91.1
"	Inner Side Plate	No		3.1	119	0.5	37229	7600	9091	737	5	70.8
"	Side Plate/Top Plate	Yes		17.6	119	88	91215	994	7829	1986	5	69.8
"	Middle Base Plate/Inner Backing Bar/Inner Hood	Yes		-39.9	-108.6	0	84197	586	7729	1854	7.5	52.1
S_{alt}	Inner Hood	No		-32.4	27	72.4	81316	1632	5221	4778	-7.5	60.8
"	Brace	No		79.6	85.5	75.8	37811	3624	3854	3722	-2.5	134.3
"	Inner Hood	No		31.4	-36.1	77.1	70582	1165	3773	3660	-7.5	60.6
"	Middle Hood	No		-64.8	24.8	67.6	30488	923	3488	3361	5	59.5
"	Inner Hood	No		31.8	-16.2	75.4	70627	907	3202	3162	-7.5	60.6

Notes: (a) [[(3)]] Entry is empty if no SRF is applied.
(b) Full penetration weld so that weld factor, WF=1.4.
(1-5) Number referring to the [[(3)]]

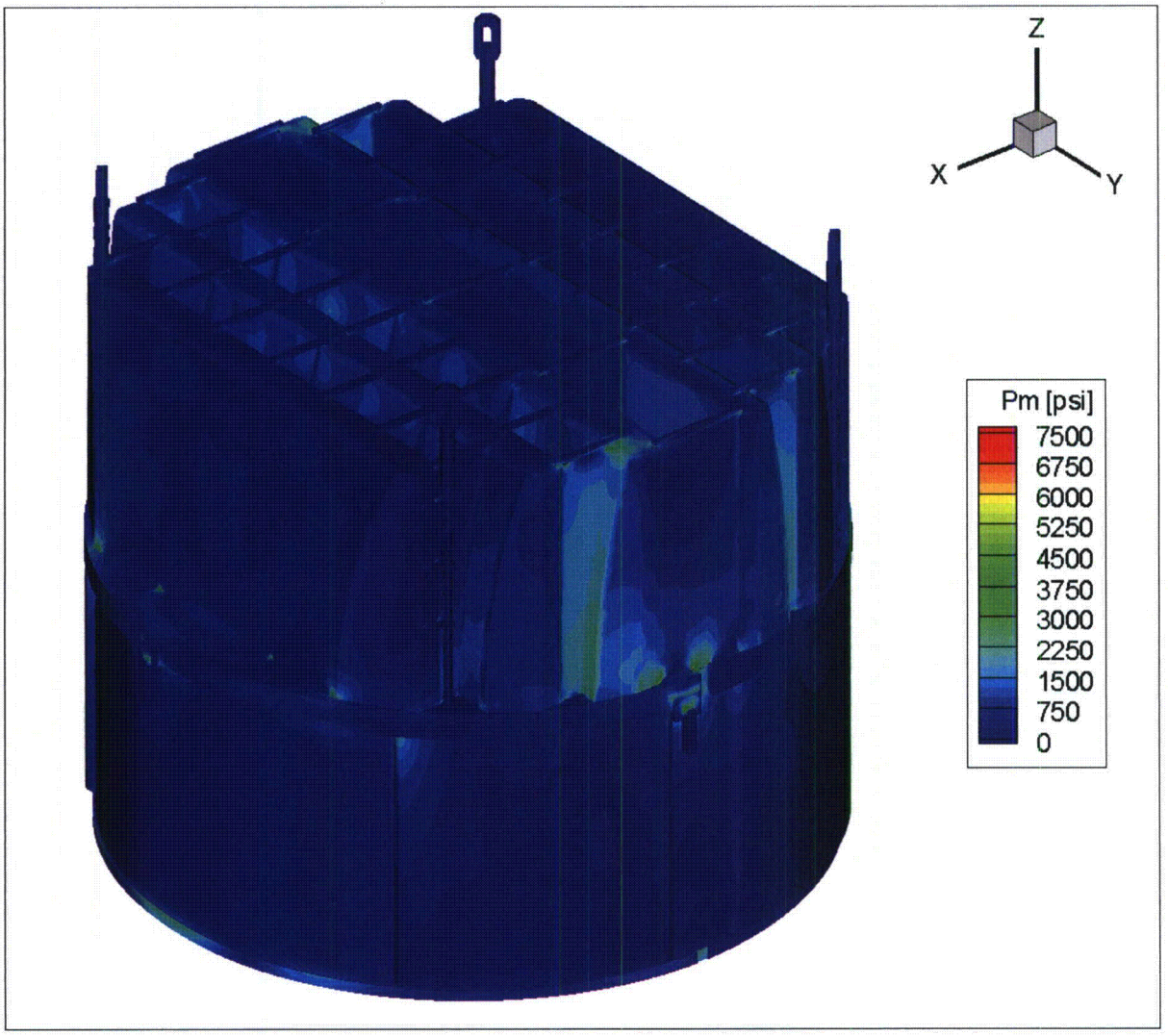

Figure 29a. Contour plot of maximum membrane stress intensity, Pm, for EPU operation with frequency shifts. The recorded stress at a node is the maximum value taken over all frequency shifts. The maximum stress intensity is 7600 psi.

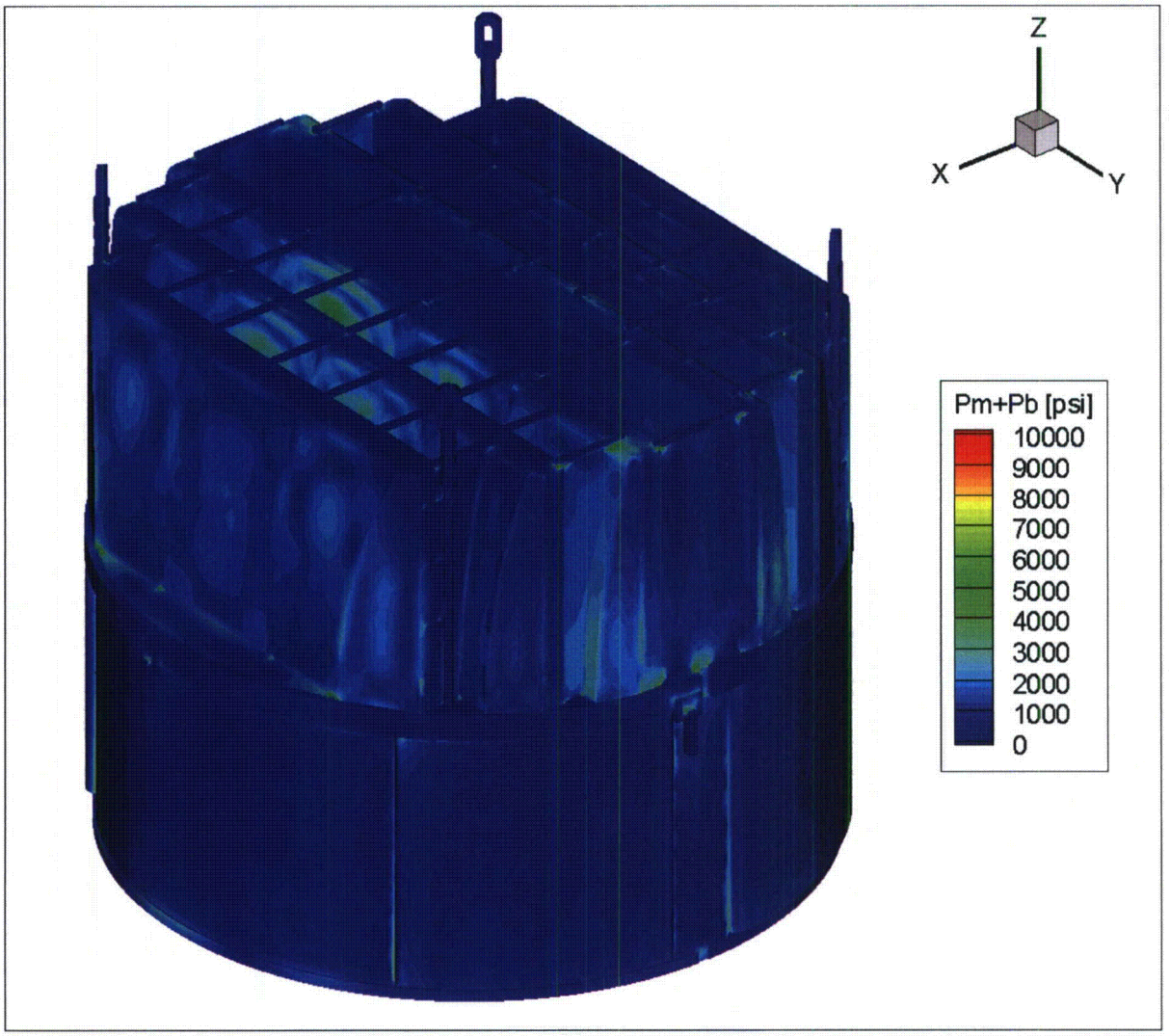

Figure 29b. Contour plot of maximum membrane+bending stress intensity, Pm+Pb, for EPU operation with frequency shifts. The recorded stress at a node is the maximum value taken over all frequency shifts. The maximum stress intensity is 10071 psi. First view.

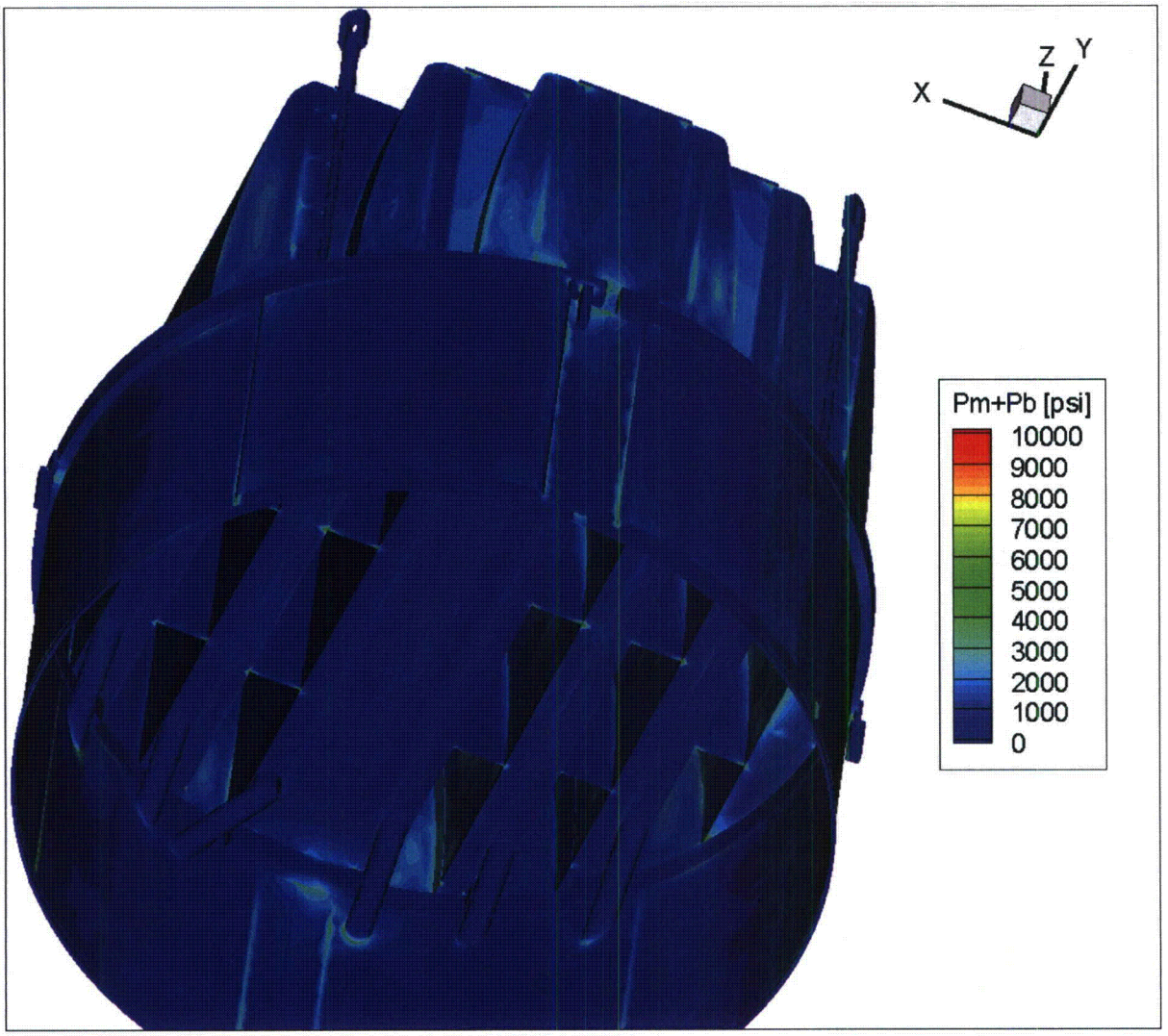

Figure 29c. Contour plot of maximum membrane+bending stress intensity, Pm+Pb, for EPU operation with frequency shifts. Second view from beneath.

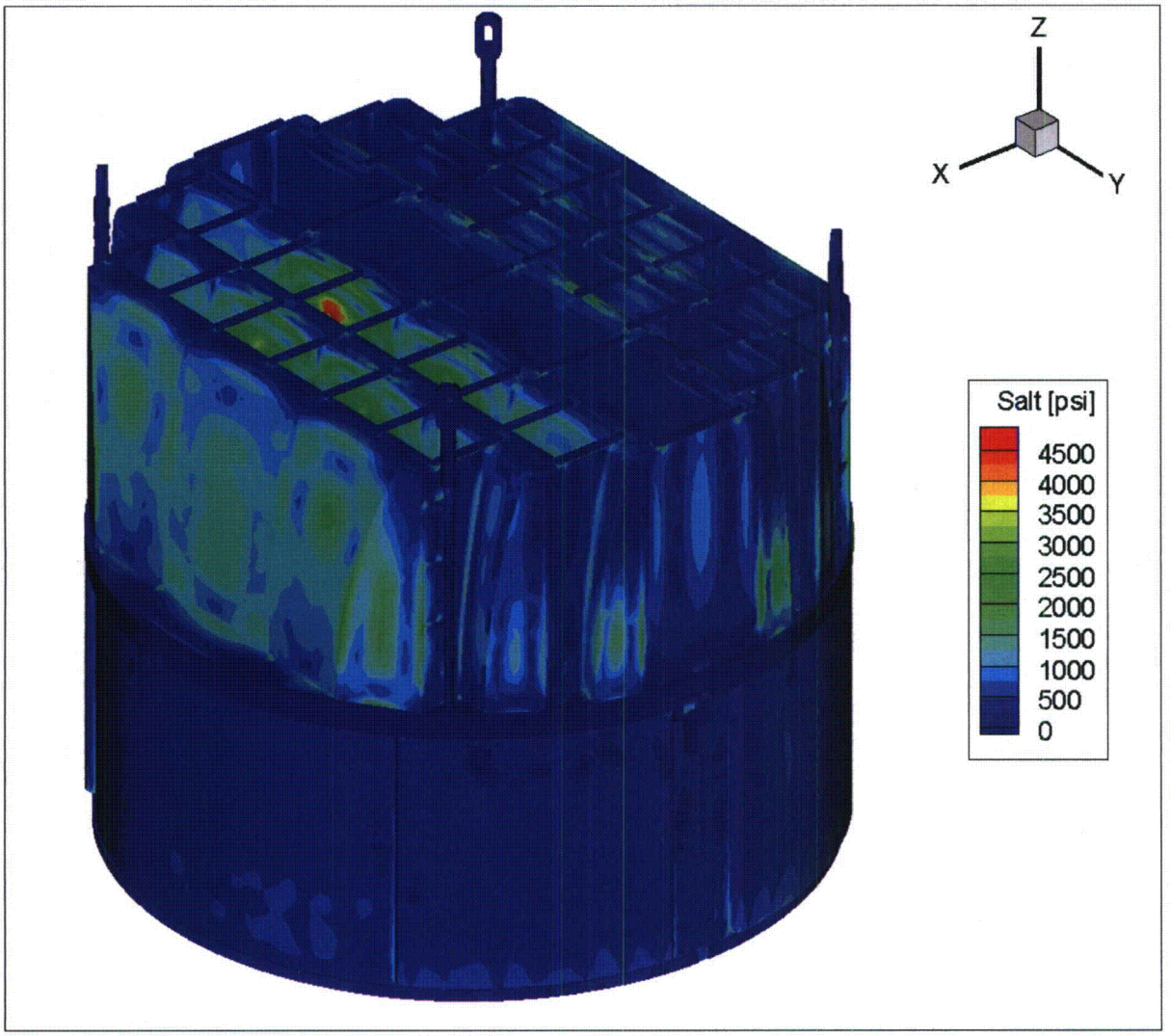

Figure 29d. Contour plot of alternating stress intensity, S_{alt}, for EPU operation with frequency shifts. The recorded stress at a node is the maximum value taken over all frequency shifts. The maximum alternating stress intensity is 4778 psi. First view.

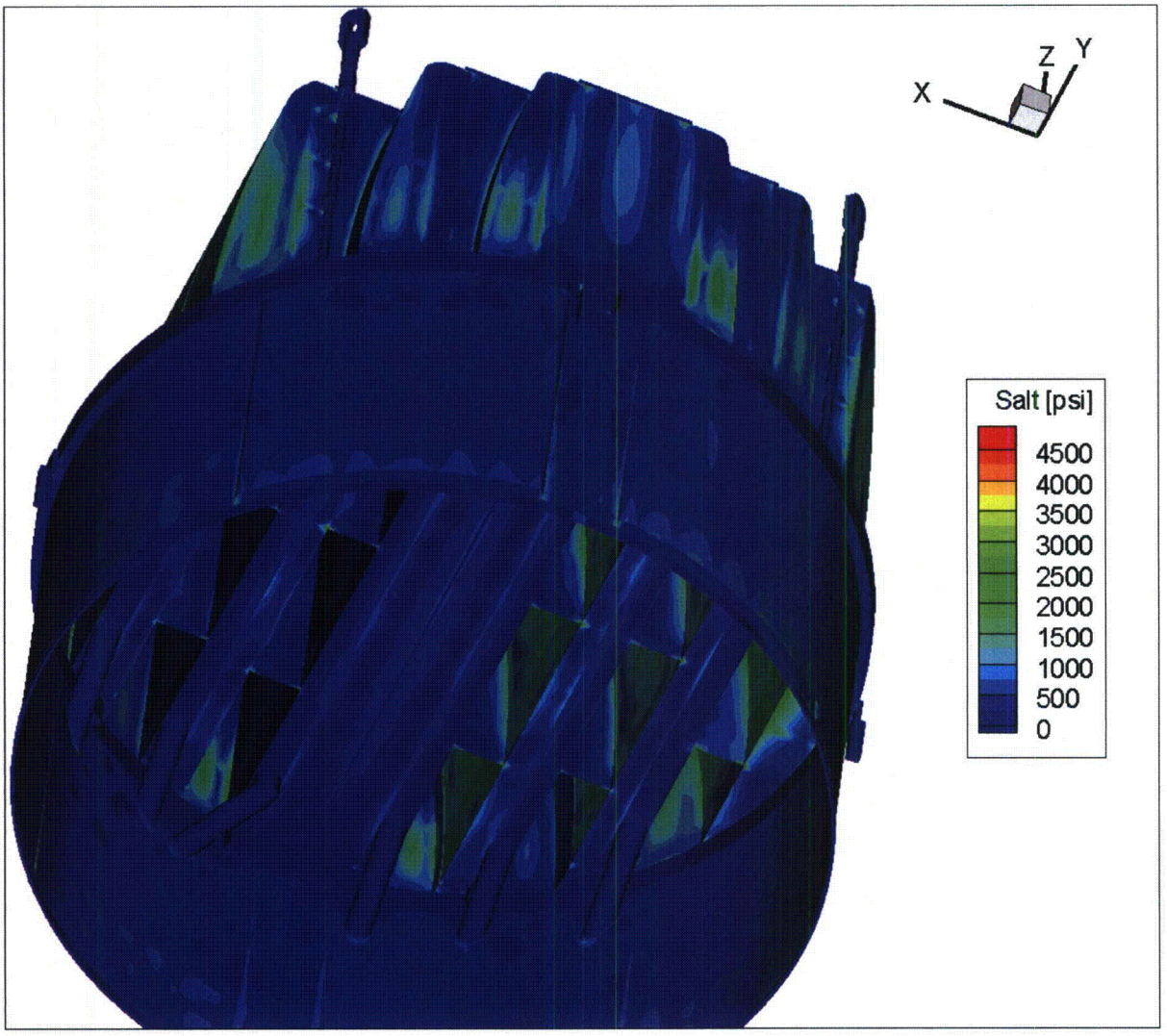

Figure 29e. Contour plot of alternating stress intensity, S_{alt}, for EPU operation with frequency shifts. The recorded stress at a node is the maximum value taken over all frequency shifts. Second view from below.

6.2 Load Combinations and Allowable Stress Intensities

The stress ratios computed for EPU at nominal frequency and with frequency shifting are listed in Table 12 (without frequency shifting) and Table 13 (with frequency shifting). The stress ratios are grouped according to type (SR-P for maximum membrane and membrane+bending stress, SR-a for alternating stress) and location (away from welds or on a weld). The tabulated nodes with frequency shifting in Table 13 are also depicted in Figure 30. The plots corresponding to maximum stress intensities depict all nodes with stress ratios SR-P≤5 or SR-P≤4 as indicated, and the plots of alternating stress ratios display all nodes with SR-a≤5.

For EPU operation at nominal frequency (no frequency shift) the minimum stress ratio is identified as a maximum stress, SR-P=1.28, and is recorded on upper support ring where it rests on the support block. This stress at this location is dominated by the static stress due to deadweight and is only weakly responsive to acoustic loads as can be seen from the high alternating stress ratio at this location (SR-a>6.15 at all frequency shifts). This is true for all four nodes having the lowest values of SR-P, all having SR-a>5.32 at all frequency shifts. The minimum alternating stress ratio at zero frequency shift, SR-a=3.09, occurs on the weld connecting the middle hood, hood support and outer base plate.

The effects of frequency shifts are conservatively accounted for by identifying the minimum stress ratio at every node, where the minimum is taken over all the frequency shifts considered (including the nominal or 0% shift case). The resulting stress ratios are then processed as before to identify the smallest stress ratios anywhere on the structure, categorized by stress type (maximum or alternating) and location (on or away from a weld). The results are summarized in Table 13 and show that the lowest stress ratio, SR-P=1.25, occurs at the same location as in the nominal case and is only slightly lower. Moreover, the limiting value closely matches that predicted in [1] at CLTP. Again this is due to the dominance of static contributions and comparatively weak dependence on acoustic loads. The next three lowest SR-P locations in Table 13b are the same as in Table 12b. With frequency shifting the lowest alternating stress ratio occurs at a different location, the side plate/end plate weld of the inner vane bank (see location 1 in Figure 30h) and assumes a value of SR-a=2.49. Based on the largest Fourier coefficient, the dominant frequency contributing to this stress is 142 Hz. In addition to this weld the first several limiting nodes involve the bottom of a hood/hood support weld (locations 2, 9 and 10, with dominant frequencies 51-52 Hz and 66 Hz), the end of a tie bar (locations 4, 5, 7, 8 and 13, with dominant frequencies 69 Hz and 61 Hz), or a closure plate (location 6, dominant frequency 70 Hz). More details of the stress response spectra are provided in the following section. In the CLTP-based stress evaluation [1] the limiting node location was node 95267. This is a mirror node of 99337 (the sign of y is reversed) which is the second entry in Table 13c.

It is noted that in Table 13c the application of an SRF is only required for entry 12 (node 87633) which corresponds to the both lifting rod brace. The other locations achieve an alternating stress ratio, SR-a>2 even when the SRF is set to unity.

In the most recent previous stress evaluation [1] using loads obtained at CLTP the limiting alternating stress ratio was SR-a=2.83 which, using a velocity squared scaling corresponds to an alternating stress ratio of SR-a=2.83/1.382=2.05 at EPU. This prediction is conservative relative to the value of SR-a=2.49 obtained using actual EPU loads which can be attributed to the

confluence of one or more of the following explanations. First, the measured steam flow at EPU was 115.5% [5] rather than the analysis assumption of 117.56%. This reduces the velocity squared scaling factor from 1.38 to 1.33 so that the alternating stress ratio at EPU obtained by scaling the CLTP value would be SR-a=2.83/1.33=2.13. Furthermore, NMP2 has indicated the potential that an additional 1% to 1.5% measurement + bias exists reducing the actual flow to 114.5%. The velocity square scaling factor in that case would be 1.31 and the corresponding alternating stress ration inferred using this factor would be SR-a=2.16.

Second, it is known that the measured signals are contaminated with noise associated with structural vibrations, sensor noise (contributing to a noise floor) and other possible non-acoustic sources such as MSL turbulence. Except for coherence filtering, no attempt to remove this noise is made so that for the purposes of stress evaluation it is effectively treated as acoustic. A power is increased the noise contributions generally remain approximately constant or scale at a rate that is slower than the velocity-square scaling associated with acoustic sources. Thus when power is increased one expects that a signal combining an acoustic contribution (which scales with velocity squared) and a non-acoustic part (which grows more slowly or remains constant) will scale at a rate somewhat less than velocity squared. Thus one expects that the alternating stress ratios obtained from actual plant measurements at EPU will be larger (stresses will be lower) than those obtained by scaling the values measured at CLTP.

Another contributing explanation is that the [[

$^{(3)}$]].

Finally, when the CLTP data used to calculate the stresses in [1] was collected, a strain gage channel was dropped on both the upper and lower MSL D measurement locations. This means that there was a higher degree of contamination by structural vibration resulting in higher estimates of acoustic loads. Note that since structural vibrations are coherent the coherence filter would not be effective in removing these non-acoustic signals. In the data collected at 115% CLTP and used to prepare the results in Table 12 and Table 13 all data channels were operative at the upper station in MSL D. At the lower MSL D station one channel was again absent, but since the structural contributions to the signals at the upper and lower MSL D locations are less likely to be coherent (because they are essentially absent at the upper location) the coherence filter removes them from the final signal. Removal of these non-acoustic structural contributions to the signals results in lower and more accurate stress estimates.

Table 12a. Limiting non-weld locations with at EPU conditions with no frequency shift. Stress ratios are grouped according to stress type (maximum – SR-P; or alternating – SR-a).

Stress Ratio	Location	Location (in.)			node	Stress Intensity (psi)			Stress Ratio		Dom. Freq. (Hz)
		x	y	z		Pm	Pm+Pb	S_{alt}	SR-P	SR-a	
SR-P	1. Inner Side Plate	3.1	119	0.5	37229	7545	8933	570	2.24	21.71	73.9
"	2. Thin Vane Bank Plate	-15.6	-118.4	0.6	2558	4841	5253	281	3.49	> 40	44.9
"	3. Support/Seismic Block	10.2	123.8	-9.5	113286	4566	4566	1485	3.70	8.33	15.5
SR-a	1. Inner Hood	-32.4	27	72.4	81316	1350	4052	3799	6.26	3.25	44.9
"	2. Brace	79.6	85.5	75.8	37811	3580	3617	3529	4.72	3.50	136.7
"	3. Middle Hood	63.6	-30	73.3	34302	1267	3483	3324	7.28	3.72	61.2

Table 12b. Limiting peak stress ratios, SR-P, on welds at EPU conditions with no frequency shift. Bold text indicates minimum stress ratio on the structure.

Location	SRF(a)	Location (in.)			node	Stress Intensity (psi)			Stress Ratio		Dom. Freq. (Hz)
		x	y	z		Pm	Pm+Pb	S_{alt}	SR-P	SR-a	
1. USR/Support/Seismic Block		**-6.9**	**-122.3**	**-9.5**	**113554**	**7271**	**7271**	**945**	**1.28**	**7.27**	**15.5**
2. Side Plate Ext/Inner Base Plate		16.3	119	0	94143	6985	9878	544	1.33	12.62	44.9
3. Tie Bar		49.3	108.1	88	141275	6228	6228	1182	1.49	5.81	97.4
4. Side Plate/Closure Plate/Top Plate		-47.1	-108.6	88	91558	5674	6267	1009	1.64	6.80	199.0
5. Inner Side Plate/Inner Base Plate		2.3	119	0	98446	4653	7968	681	1.75	10.08	73.9
6. Side Plate/Top Plate		17.6	119	88	91215	964	7654	1732	1.82	3.97	69.4
7. Hood Support/Outer Base Plate/Middle Backing Bar		-71.3	0	0	95428	5079	5388	2178	1.83	3.15	53.6
8. Closure Plate/Backing Bar/Inner Hood		39.9	108.6	0.5	93062	5060	5121	801	1.84	8.58	70.8
9. Hood Support/Middle Base Plate/Backing Bar/Inner Hood(b)		39.9	0	0	88639	4884	5031	1976	1.90	3.48	70.8
10. Vane Bank Plate/Hood Support/Inner Base Plate		24.1	-59.5	0	85191	4859	4940	1237	1.91	5.55	54.4
11. Hood Support/Outer Cover Plate/Outer Hood(4)	0.8	-102.8	28.4	0	95267	4800	4915	2192	1.94	3.13	54.4
12. Outer Cover Plate/Outer Hood		102.8	-58.1	0	94498	1039	7166	901	1.95	7.63	11.5
13. Hood Support/Middle Base Plate/Backing Bar/Inner Hood(b)		39.9	-59.5	0	101435	4442	4738	1562	2.09	4.40	44.1

Notes: (a) [[(3)]] Entry is empty if no SRF is applied.

(b) Full penetration weld so that weld factor, WF=1.4.

(1-5) Number referring to the [[(3)]]

Table 12c. Limiting alternating stress ratios, SR-a, on welds at EPU conditions with no frequency shift.

Location	SRF(a)	Location (in.)			node	Stress Intensity (psi)			Stress Ratio		Dom. Freq. (Hz)
		x	y	z		Pm	Pm+Pb	S_{alt}	SR-P	SR-a	
1. Hood Support/Outer Base Plate/Backing Bar		71.3	0	0	98067	4669	5074	2219	1.99	3.09	44.1
2. Side Plate/Top Plate		-80.2	-85.2	88	93031	522	2779	2217	5.02	3.10	71.3
3. Closure Plate/Middle Hood		60.2	-85.2	87	89317	1216	5186	2203	2.69	3.12	71.0
4. Hood Support/Inner Hood(b)		-36.8	0	46.9	95644	836	2384	2198	5.85	3.12	44.4
5. Hood Support/Inner Hood(b)		32.4	0	72.5	99540	577	2472	2194	5.64	3.13	55.4
6. Hood Support/Outer Cover Plate/Outer Hood(4)	0.80	-102.8	28.4	0	95267	4800	4915	2192	1.94	3.13	54.4
7. Top Plate/Middle Hood/Top Plate		55.6	-28.4	88	90955	899	2600	2093	5.36	3.28	61.2
8. Double Side Plate/Top Plate		49.3	0	88	93197	1200	2884	2091	4.83	3.29	70.8
9. Hood Support/Middle Hood(b)		63.8	0	72.5	98462	500	2281	2062	6.11	3.33	61.2
10. Hood Support/Inner Hood(b)		-38.2	0	34.9	95638	801	2033	2028	6.86	3.39	44.1
11. Tie Bar/Top Plate(2)	0.77	-81.1	85.2	88	99456	914	4324	2026	3.22	3.39	71.3
12. Inner Hood/Top Plate		24.1	-30.6	88	85512	773	2228	1991	6.26	3.45	55.4
13. Hood Support/Middle Base Plate/Backing Bar/Inner Hood(b)		39.9	0	0	88639	4884	5031	1976	1.90	3.48	70.8
14. Side Plate/Top Plate		17.6	0	88	95617	1144	2709	1962	5.15	3.50	71.3

Notes: (a) [[(3)]] Entry is empty if no SRF is applied.
(b) Full penetration weld so that weld factor, WF=1.4.
(1-5) Number referring to the [[(3)]]

Table 13a. Limiting non-weld locations with at EPU conditions with frequency shifts. Stress ratios are grouped according to stress type (maximum – SR-P; or alternating – SR-a). Locations are depicted in Figure 30.

Stress Ratio	Location	Location (in.)			node	Stress Intensity (psi)			Stress Ratio		% Freq. Shift	Dom. Freq. (Hz)
		x	y	z		Pm	Pm+Pb	S_{alt}	SR-P	SR-a		
SR-P	1. Inner Side Plate	3.1	119	0.5	37229	7600	9091	737	2.22	16.78	-10	70.8
"	2. Thin Vane Bank Plate	-15.6	-118.4	0.6	2558	4898	5321	318	3.45	38.92	5	14.4
"	3. Support/Seismic Block	10.2	123.8	-9.5	113286	4618	4618	1574	3.66	7.86	10	13.9
SR-a	1. Inner Hood	-32.4	27	72.4	81316	1632	5221	4778	4.86	2.59	-7.5	60.8
"	2. Brace	79.6	85.5	75.8	37811	3624	3854	3722	4.66	3.32	-2.5	134.3
"	3. Inner Hood	31.4	-36.1	77.1	70582	1165	3773	3660	6.72	3.38	-7.5	60.6
"	4. Middle Hood	-64.8	24.8	67.6	30488	923	3488	3361	7.27	3.68	5	59.5

Table 13b. Limiting peak stress ratios, SR-P, on welds at EPU conditions with frequency shifts. Bold text indicates minimum stress ratio on the structure. Locations are depicted in Figure 30.

Location	SRF[a]	Location (in.)			node	Stress Intensity (psi)			Stress Ratio		% Freq. Shift	Dom. Freq. (Hz)
		x	y	z		Pm	Pm+Pb	S_{alt}	SR-P	SR-a		
1. USR/Support/Seismic Block		**-6.9**	**-122.3**	**-9.5**	**113554**	**7460**	**7460**	**1118**	**1.25**	**6.15**	**-10**	**14.2**
2. Side Plate Ext/Inner Base Plate		16.3	119	0	94143	7092	10071	712	1.31	9.65	7.5	101.0
3. Tie Bar		49.3	108.1	88	141275	6391	6391	1273	1.45	5.40	10	91.1
4. Side Plate/Closure Plate/Top Plate		-47.1	-108.6	88	91558	5940	6670	1290	1.56	5.32	7.5	195.5
5. Inner Side Plate/Inner Base Plate		-2.3	-119	0	99200	4533	8367	896	1.67	7.67	7.5	69.8
6. Hood Support/Outer Base Plate/Middle Backing Bar		-71.3	0	0	95428	5297	5388	2454	1.75	2.80	5	51.2
7. Side Plate/Top Plate		17.6	119	88	91215	994	7829	1986	1.78	3.46	5	69.8
8. Hood Support/ Cover Plate/Outer Hood[4]	0.8	-102.8	28.4	0	95267	5181	5343	2695	1.79	2.55	5	52.1
9. Hood Support/Middle Base Plate/Inner Backing Bar/Inner Hood[b]		39.9	0	0	88639	5181	5193	2010	1.79	3.42	10	40.5
10. Middle Base Plate/Backing Bar/Inner Hood		-39.9	-108.6	0	84197	586	7729	1854	1.80	3.71	7.5	52.1
11. Vane Bank Plate/Hood Support/Base Plate		-24.1	59.5	0	99487	5126	5232	1569	1.81	4.38	7.5	44.9
12. Outer Cover Plate/Outer Hood		102.8	-58.1	0	94498	1078	7303	1072	1.91	6.41	10	10.5
13. Hood Support/Middle Base Plate/Backing Bar/Inner Hood[b]		-39.9	59.5	0	90468	4569	4674	1822	2.03	3.77	-5	69.8

Notes: (a) [[[3]]] Entry is empty if no SRF is applied.

(b) Full penetration weld so that weld factor, WF=1.4.

(1-5) Number referring to the [[[3]]]

Table 13c. Limiting alternating stress ratios, SR-a, on welds at EPU conditions with frequency shifts. Locations are depicted in Figure 30.

Location	SRF(a)	Location (in.)			node	Stress Intensity (psi)			Stress Ratio		% Freq. Shift	Dom. Freq. (Hz)
		x	y	z		Pm	Pm+Pb	S_{alt}	SR-P	SR-a		
1. Vane Bank Plate/Side Plate/End Plate		-24.1	119	11.6	90170	842	3084	2757	4.52	2.49	7.5	142.0
2. Hood Support/Outer Cover Plate/Outer Hood(4)	0.8	-102.8	-28.4	0	99337	3681	4009	2704	2.53	2.54	5	52.1
3. Side Plate/End Plate		-24.1	119	21.9	90232	912	2905	2687	4.80	2.56	5	146.1
4. Side Plate/Top Plate		17.6	0	88	95617	1381	3359	2644	4.15	2.60	5	69.4
5. Side Plate/Top Plate		-49.3	0	88	97693	1220	3420	2641	4.08	2.60	2.5	69.8
6. Closure Plate/Middle Hood		60.2	-85.2	87	89317	1341	5726	2638	2.43	2.60	2.5	70.1
7. Side Plate/Top Plate		-80.2	-85.2	88	93031	556	3048	2617	4.57	2.62	5	69.4
8. Top Plate/Inner Hood		24.1	-30.6	88	85512	785	2698	2575	5.17	2.67	-7.5	60.6
9. Hood Support/Outer Base Plate/Backing Bar		-71.3	0	0	95428	5297	5388	2454	1.75	2.8	5	51.2
10. Hood Support/Middle Base Plate/Backing Bar/Inner Hood(b)		-39.9	0	0	85723	5130	5381	2418	1.81	2.84	7.5	66.4
11. Side Plate/Top Plate		-54	-54.3	88	85117	607	2641	2410	5.28	2.85	5	69.4
12. Side Plate/Brace(5)	0.64	79.7	-85.2	31.2	87633	2735	2901	2404	3.40	2.86	7.5	123.5
13. Top Plate/Side plate/Inner Hood(3)	0.83	24.1	-27.8	88	90897	889	2702	2367	5.16	2.90	-7.5	60.6
14. Outer Cover Plate/Outer Hood		-102.8	-1	0	95236	1302	2741	2359	5.09	2.91	-10	60.6
15. Hood Support/Inner Hood(b)		32.4	0	72.5	99540	631	2627	2347	5.31	2.93	-10	61.3
16. End Plate/Inner Hood		-39.3	115.1	20.5	95777	1941	2787	2306	4.79	2.98	5	146.1
17. Tie Bar		17.6	59.8	88	137575	3258	3258	2301	2.85	2.98	10	65.5
18. Outer End Plate/Outer Hood		-97.9	-69.4	58.4	99213	856	2427	2273	5.74	3.02	2.5	69.8

Notes: (a) [[(3)]] Entry is empty if no SRF is applied.
(b) Full penetration weld so that weld factor, WF=1.4.
(1-5) Number referring to the [[(3)]]

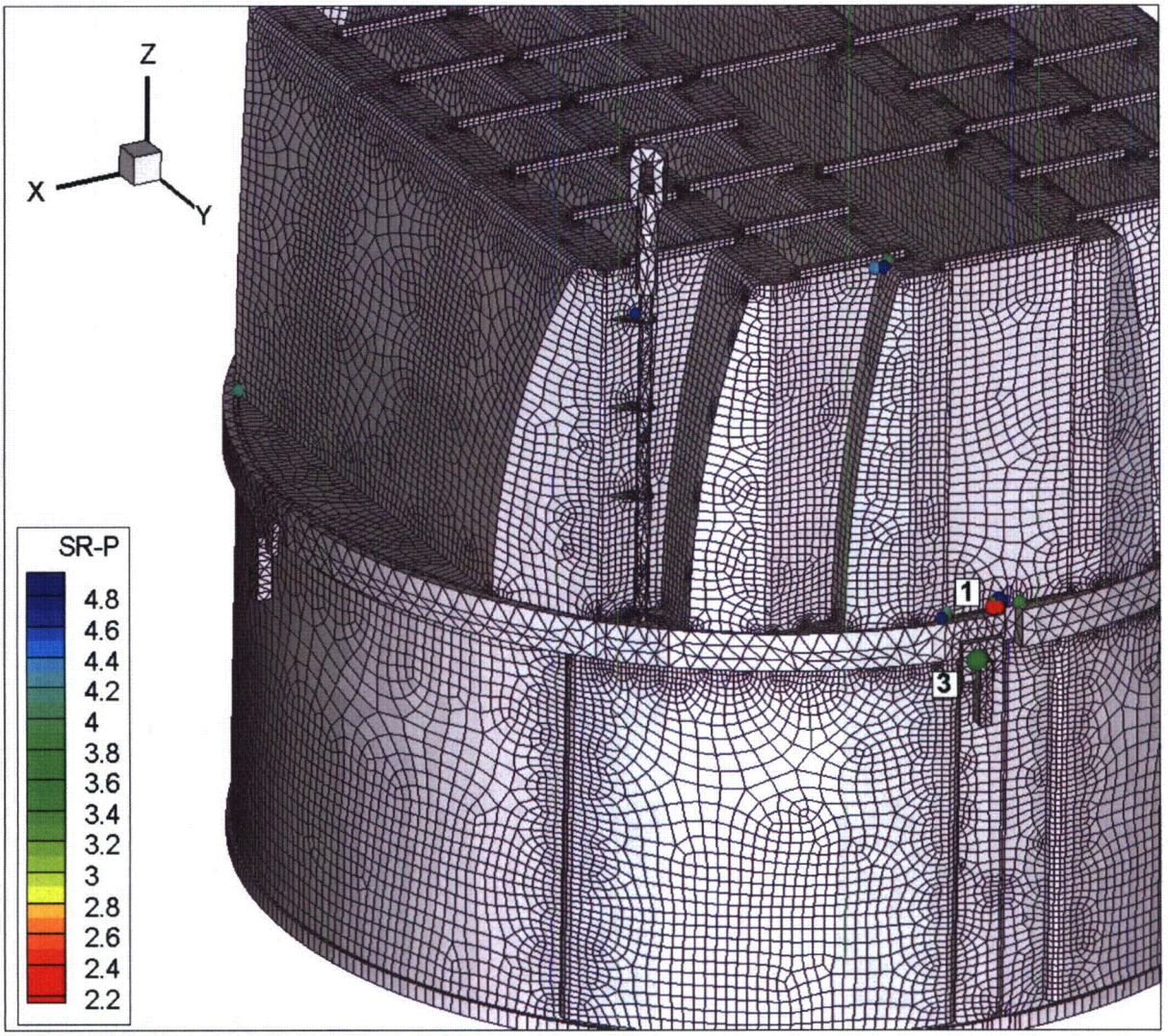

Figure 30a. Locations of minimum stress ratios, SR-P≤5, associated with maximum stresses at non-welds for EPU operation with frequency shifts. The recorded stress ratio is the minimum value taken over all frequency shifts. The numbers refers to the enumerated location for SR-P values at non-welds in Table 13a. This view shows locations 1 and 3.

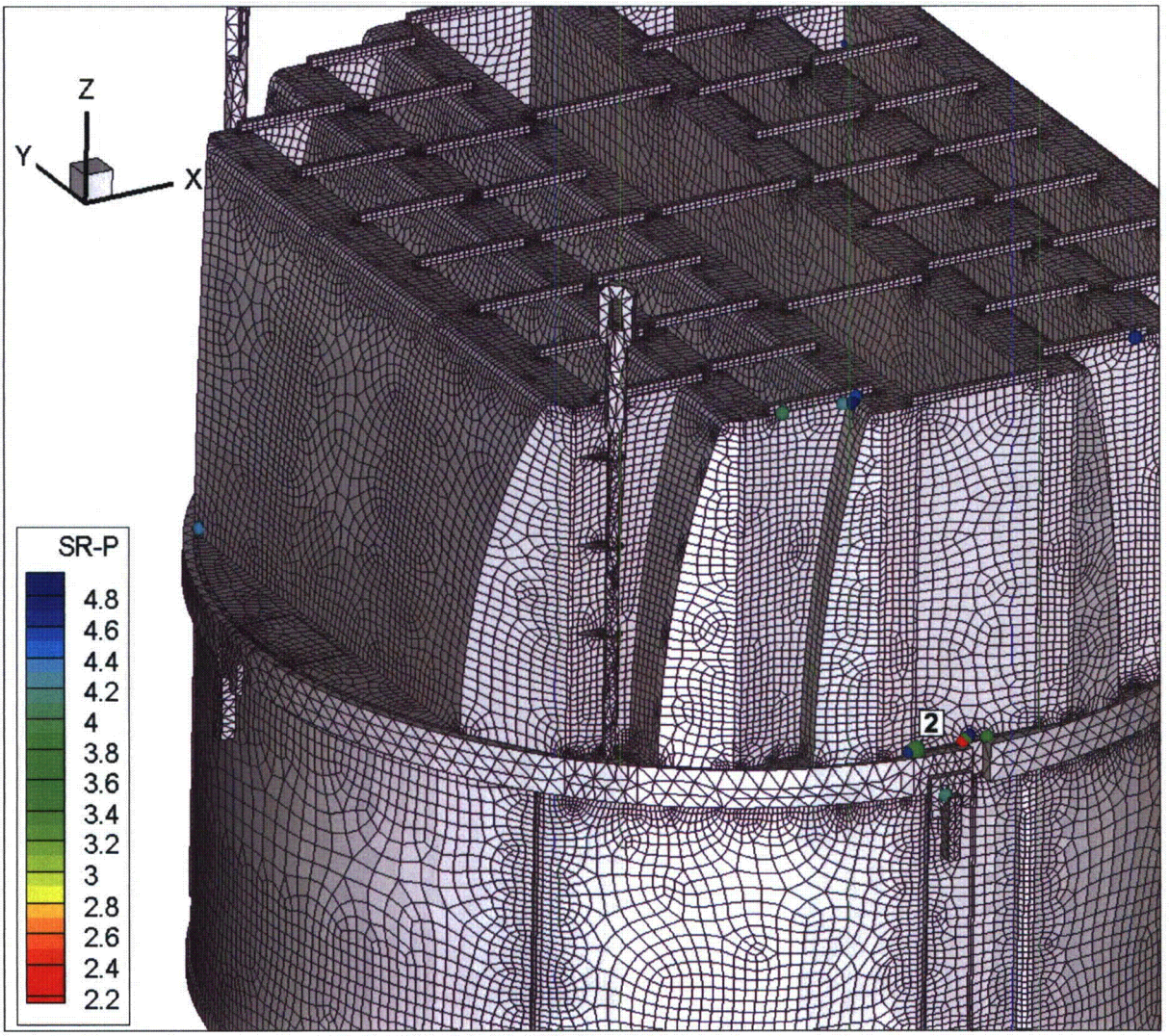

Figure 30b. Locations of minimum stress ratios, SR-P≤5, associated with maximum stresses at non-welds for EPU operation with frequency shifts. The recorded stress ratio is the minimum value taken over all frequency shifts. The numbers refers to the enumerated location for SR-P values at non-welds in Table 13a. This view shows location 2.

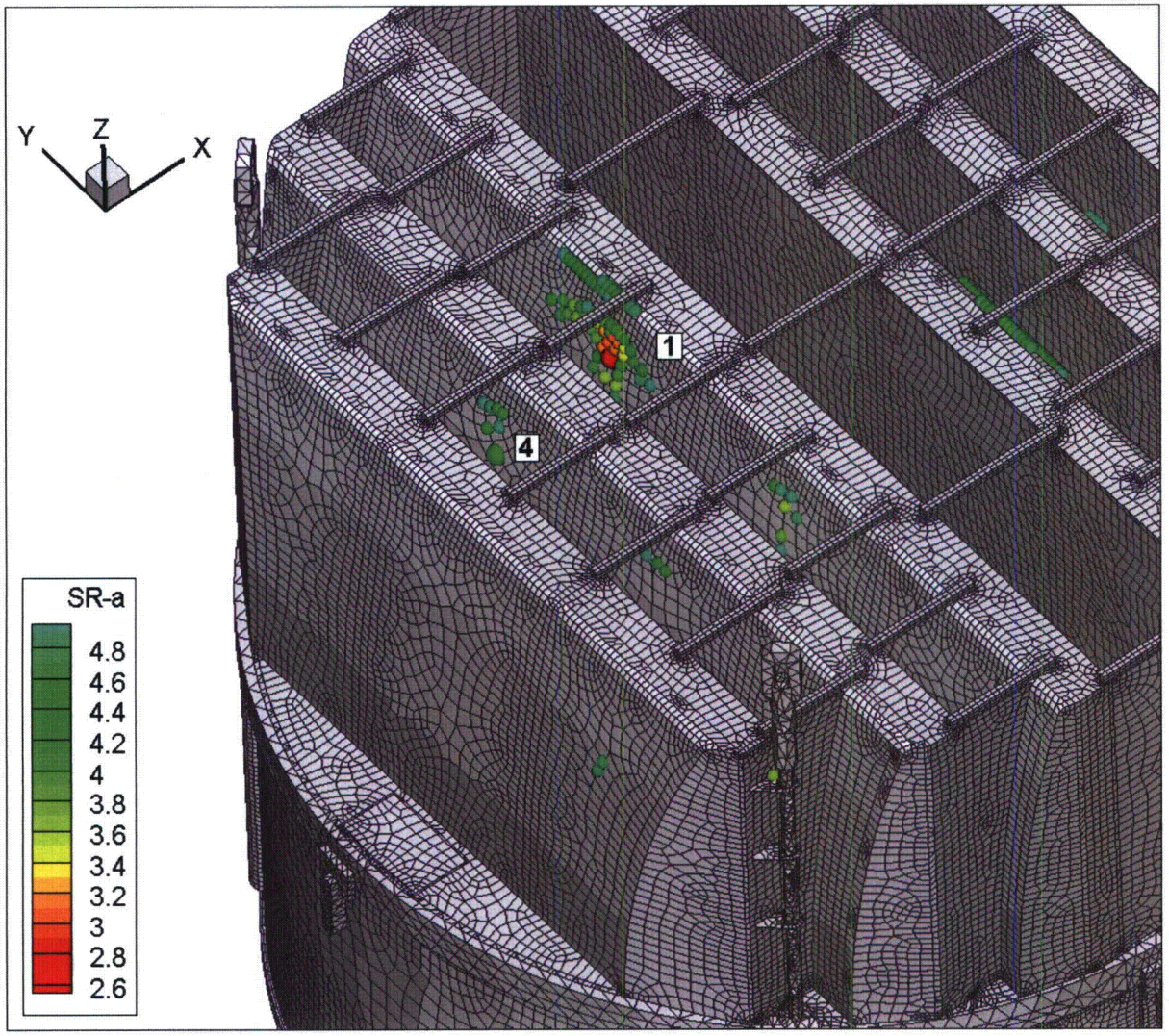

Figure 30c. Locations of minimum alternating stress ratios, SR-a≤5, at non-welds for EPU operation with frequency shifts. The recorded stress ratio at a node is the minimum value taken over all frequency shifts. Numbers refer to the enumerated locations for SR-a values at non-welds in Table 13a. View showing locations 1 and 4.

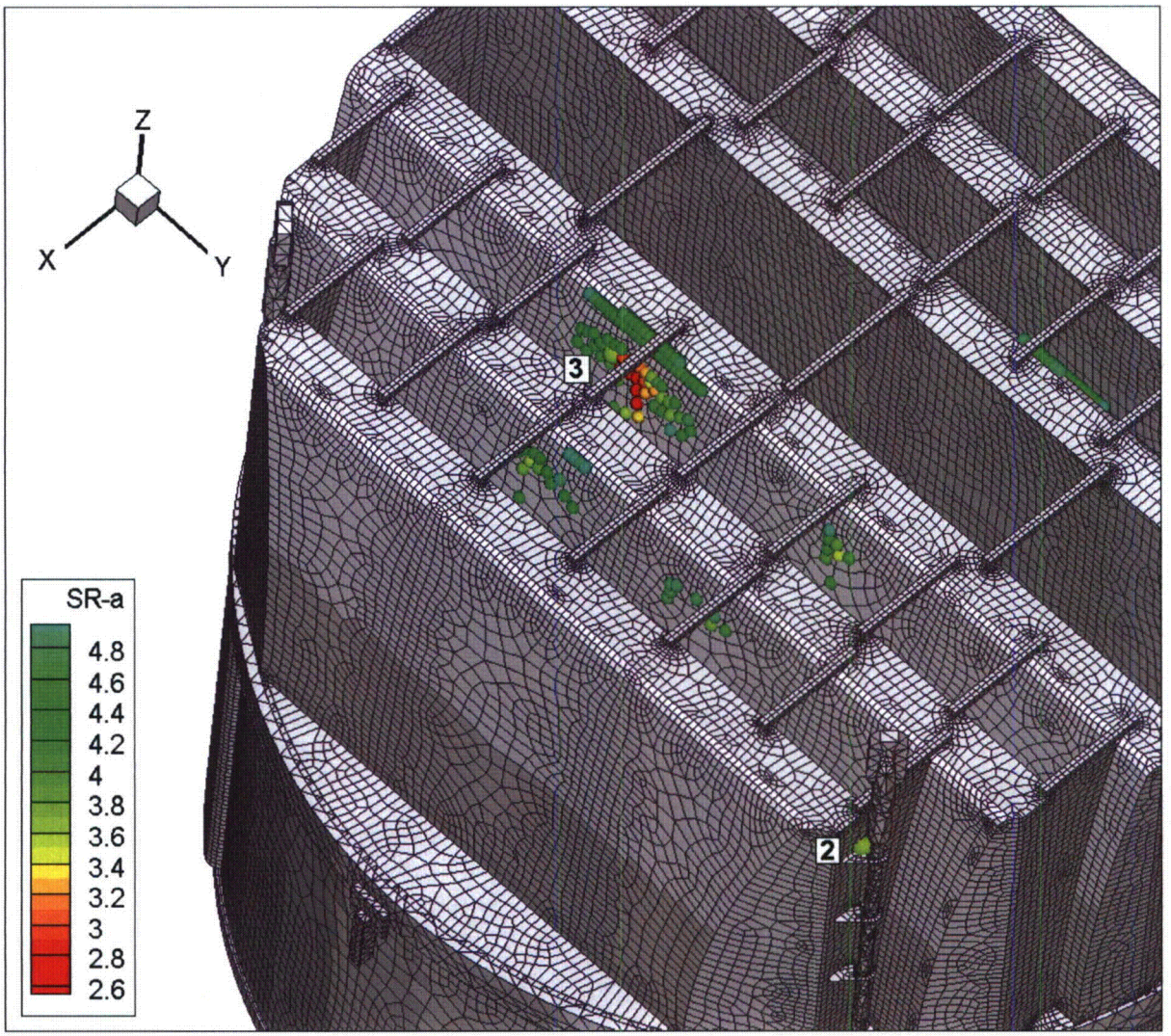

Figure 30d. Locations of minimum alternating stress ratios, SR-a≤5, at non-welds for EPU operation with frequency shifts. The recorded stress ratio at a node is the minimum value taken over all frequency shifts. Numbers refer to the enumerated locations for SR-a values at non-welds in Table 13a. View showing locations 2 and 3.

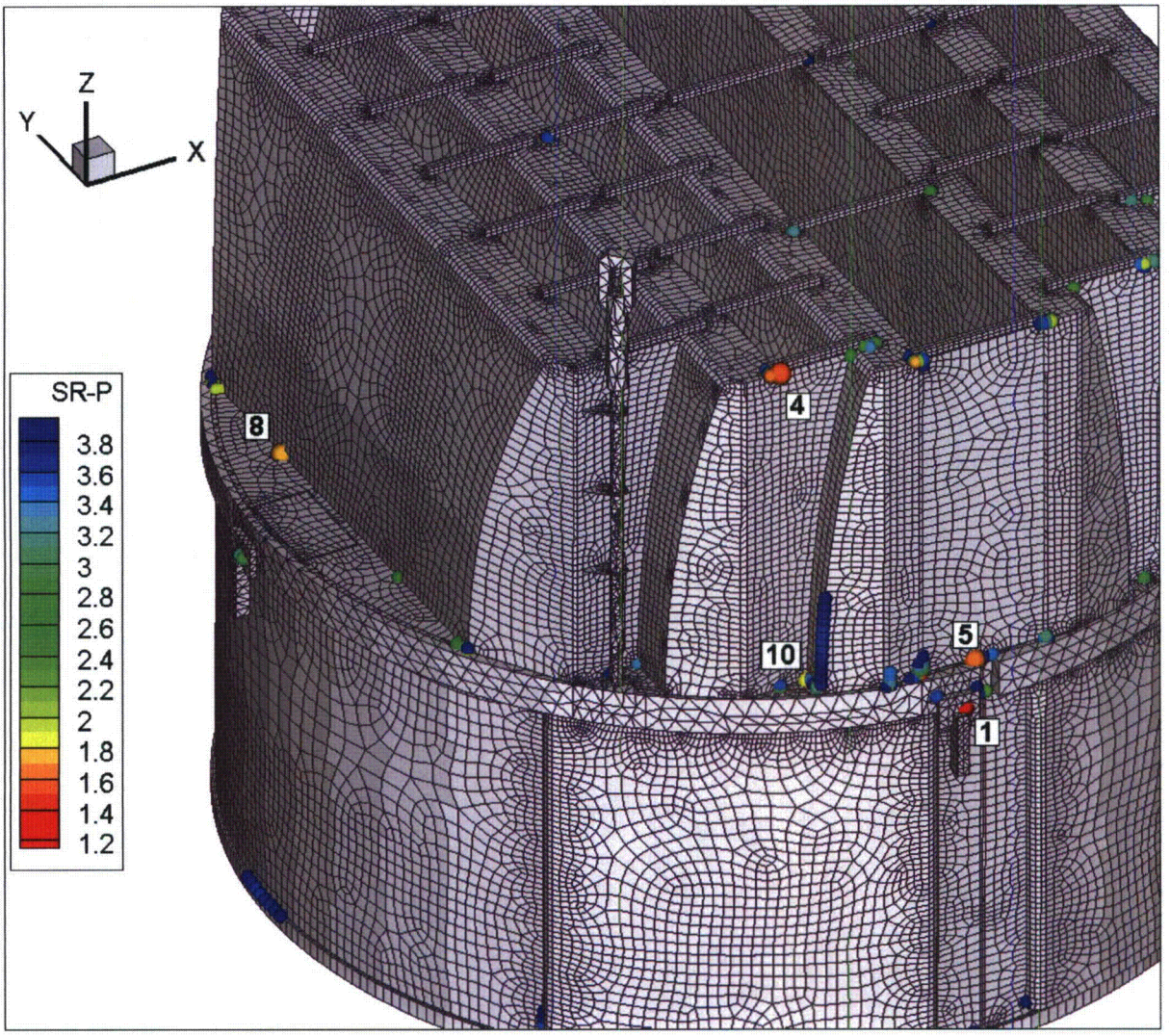

Figure 30e. Locations of minimum stress ratios, SR-P≤4, associated with maximum stresses at welds for EPU operation with frequency shifts. The recorded stress ratio at a node is the minimum value taken over all frequency shifts. Numbers refer to the enumerated locations for SR-P values at welds in Table 13b. This view shows locations 1, 4, 5, 8 and 10.

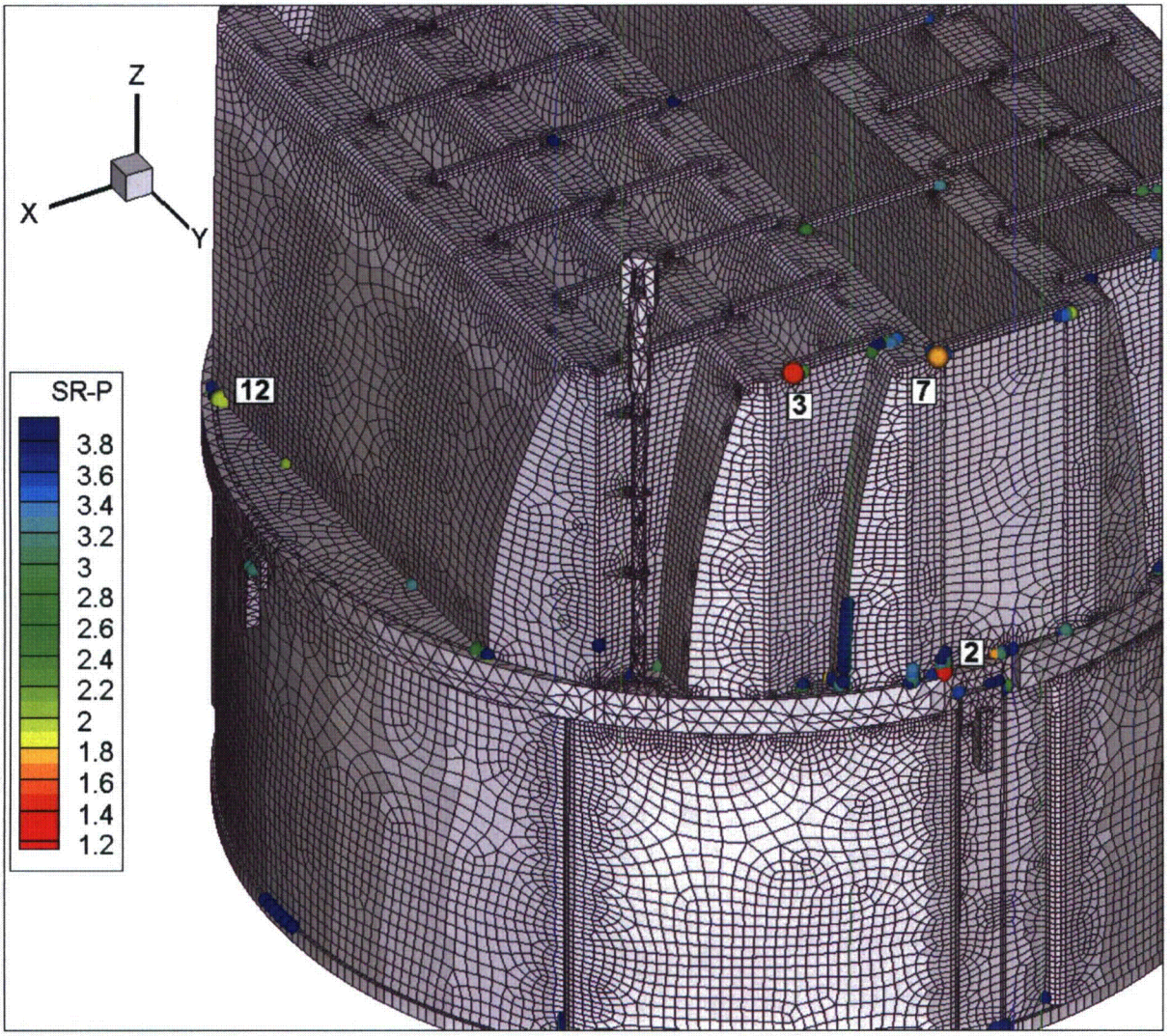

Figure 30f. Locations of minimum stress ratios, SR-P≤4, associated with maximum stresses at welds for EPU operation with frequency shifts. The recorded stress ratio at a node is the minimum value taken over all frequency shifts. Numbers refer to the enumerated locations for SR-P values at welds in Table 13b. This view shows locations 2, 3, 7 and 12.

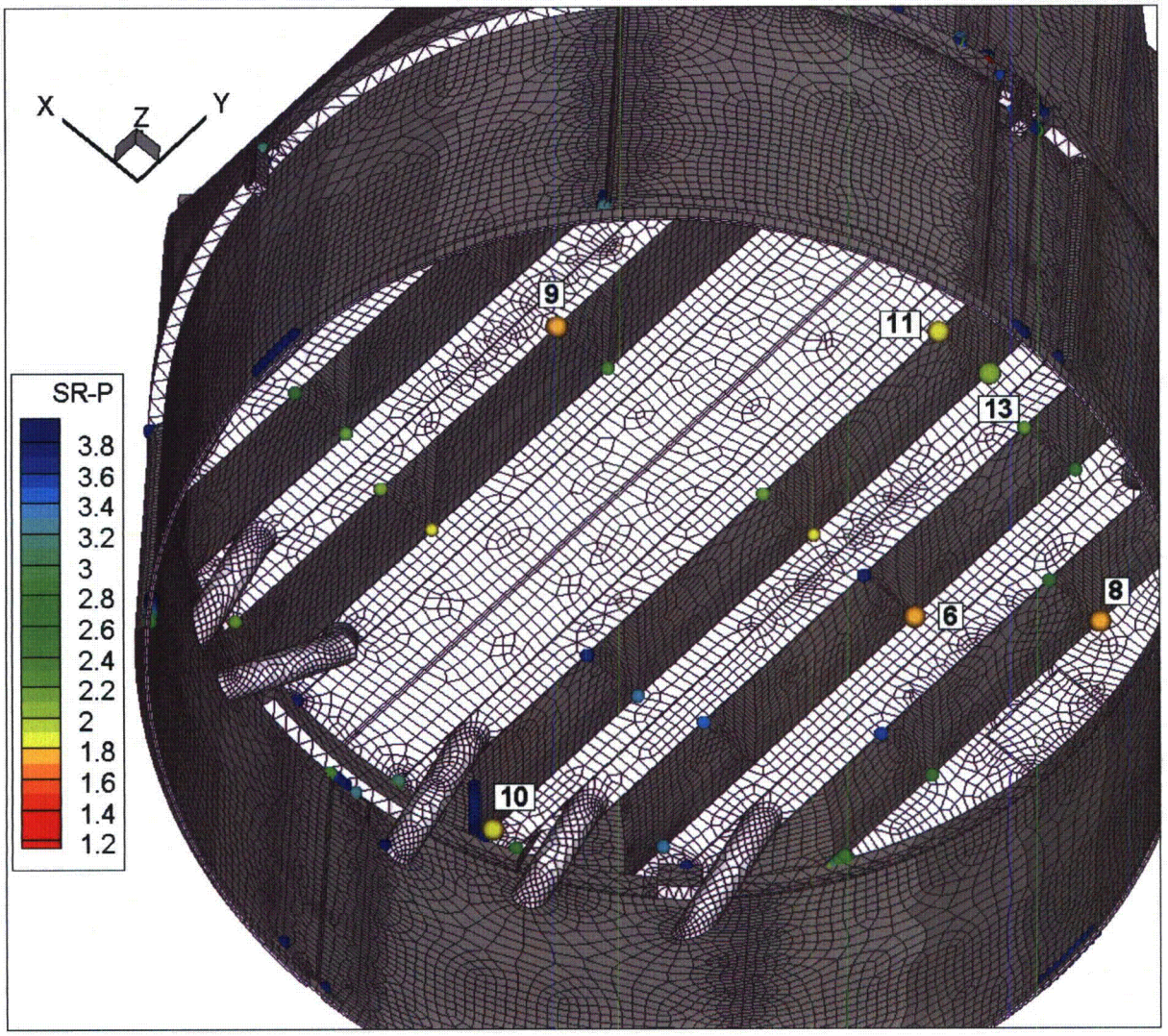

Figure 30g. Locations of minimum stress ratios, SR-P≤4, at welds for EPU operation with frequency shifts. The recorded stress ratio at a node is the minimum value taken over all frequency shifts. Numbers refer to the enumerated locations for SR-P values at welds in Table 13b. This view from below shows locations 6, 8-11 and 13.

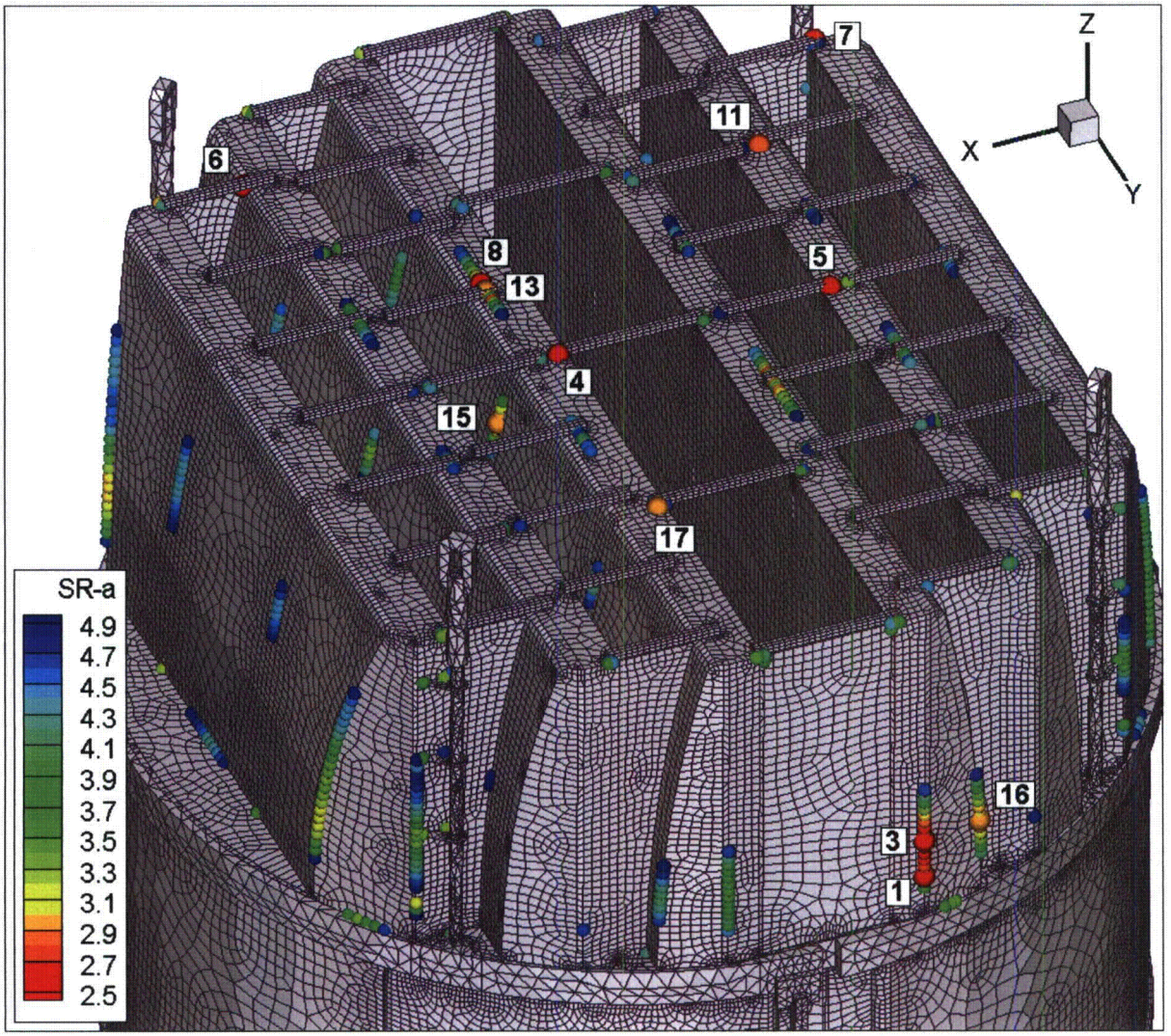

Figure 30h. Locations of minimum alternating stress ratios, SR-a≤5, at welds for EPU operation with frequency shifts. The recorded stress ratio at a node is the minimum value taken over all frequency shifts. Numbers refer to the enumerated locations for SR-a values at welds in Table 13c. This view shows locations 1, 3-8, 11, 13 and 15-17.

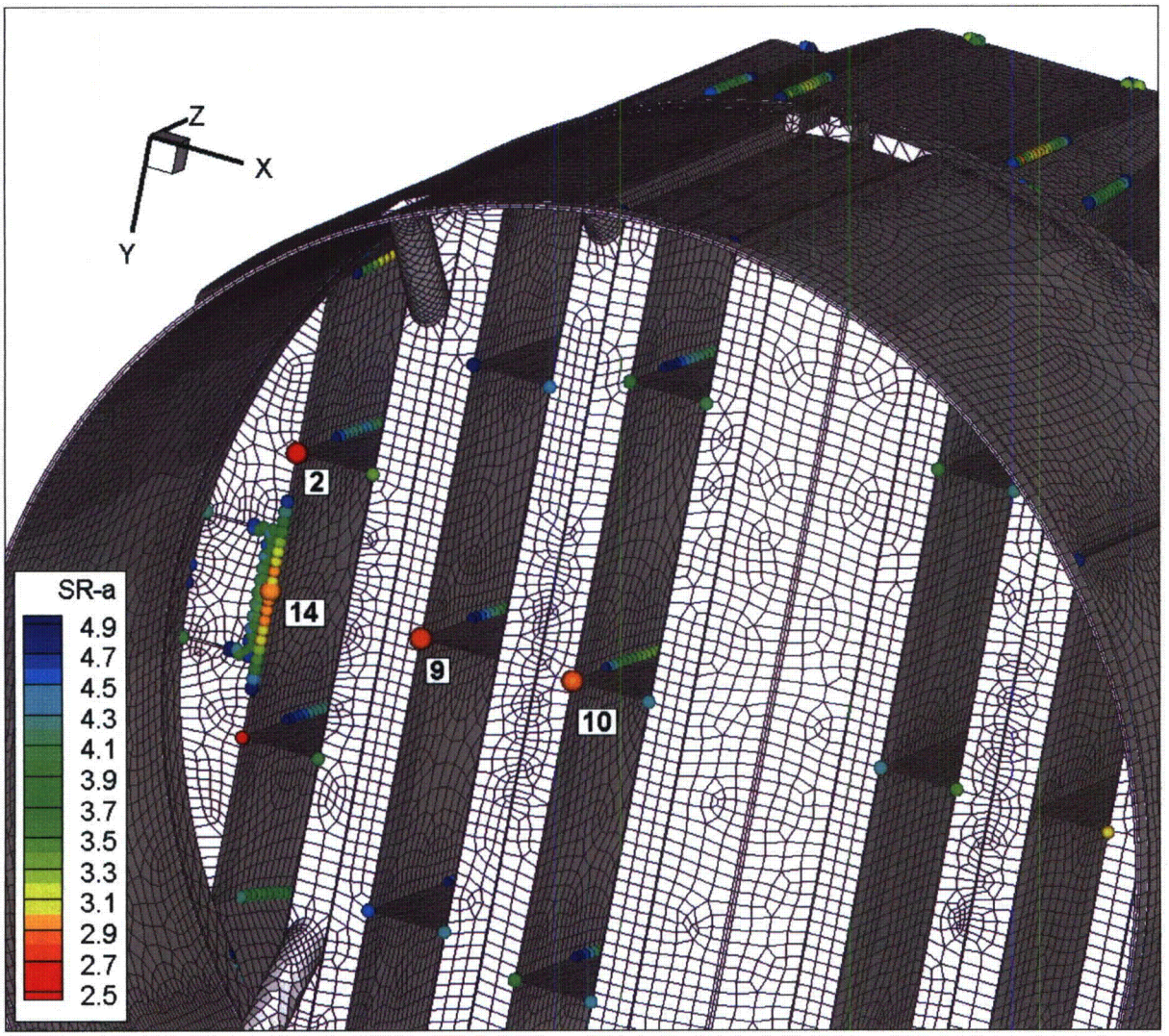

Figure 30i. Locations of minimum alternating stress ratios, SR-a≤5, at welds for EPU operation with frequency shifts. The recorded stress ratio at a node is the minimum value taken over all frequency shifts. Numbers refer to the enumerated locations for SR-a values at welds in Table 13c. View showing locations 2, 9, 10 and 14.

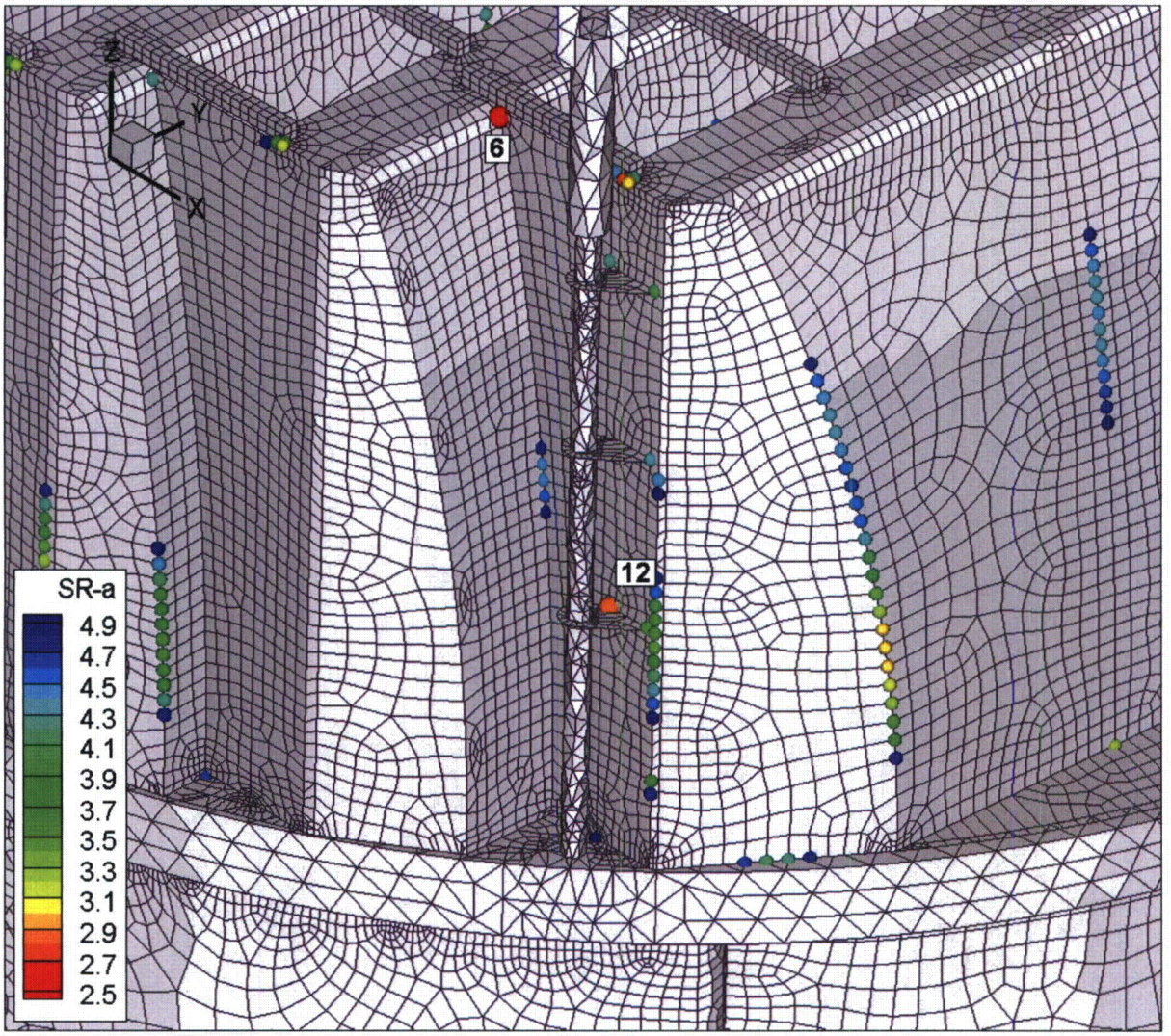

Figure 30j. Locations of minimum alternating stress ratios, SR-a≤5, at welds for EPU operation with frequency shifts. The recorded stress ratio at a node is the minimum value taken over all frequency shifts. Numbers refer to the enumerated locations for SR-a values at welds in Table 13c. View around locations 6 and 12.

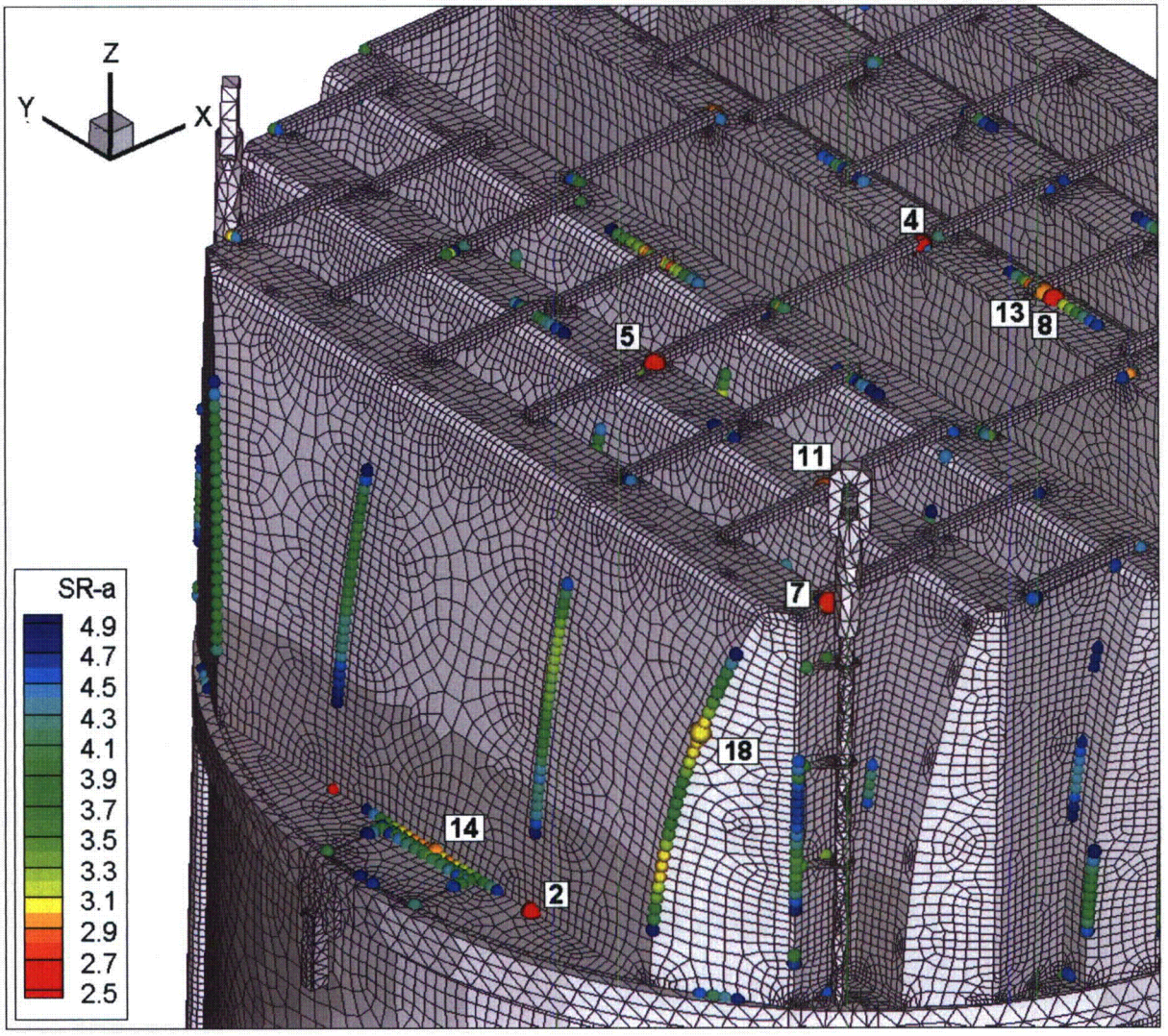

Figure 30k. Locations of minimum alternating stress ratios, SR-a≤5, at welds for EPU operation with frequency shifts. The recorded stress ratio at a node is the minimum value taken over all frequency shifts. Numbers refer to the enumerated locations for SR-a values at welds in Table 13c. View around locations 2, 4, 5, 7, 8, 11, 13, 14 and 18.

6.3 Frequency Content and Filtering of the Stress Signals

The frequency contribution to the stresses can be investigated by examining the power spectral density (PSD) curves and accumulative PSDs for selected nodes having low alternating stress ratios. The accumulative PSDs are computed directly from the Fourier coefficients as

$$\Sigma(\omega_n) = \sqrt{\sum_{k=1}^{n} |\tilde{\sigma}(\omega_k)|^2}$$

where $\tilde{\sigma}(\omega_k)$ is the complex stress harmonic at frequency, ω_k. Accumulative PSD plots are useful for determining the frequency components and frequency ranges that make the largest contributions to the fluctuating stress. Unlike PSD plots, no "binning" or smoothing of frequency components is needed to obtain smooth curves. Steep step-like rises in $\Sigma(\omega)$ indicate the presence of a strong component at a discrete frequency whereas gradual increases in the curve imply significant content over a broader frequency range. From Parsival's theorem, equality between $\Sigma(\omega_N)$ (where N is the total number of frequency components) and the RMS of the stress signal in the time domain is established.

The selected nodes are the ones having the lowest alternating stress ratios (at a weld) in Table 13c. These are:

Node 90170 – located on the inner vane band side plate/end plate weld. This is the limiting alternating stress location. The associated PSDs are shown in Figure 31a.

Node 99337 – located on the welded common junction between the outer hood, hood support and outer cover plate. This node is a mirror image of the limiting alternating stress location (node 95267) at CLTP. The associated PSDs are shown in Figure 31b.

Node 95617 – located on the weld joining the tie bar and inner vane bank top plate. The associated PSDs are shown in Figure 31c.

Node 89317 – located on the weld joining the closure plate and middle hood. The associated PSDs are shown in Figure 31d.

Node 87633 – located on the lifting rod brace/vane bank end plate connection. The associated PSDs are shown in Figure 31e.

These are the nodes labeled 1, 2, 4, 6 and 12 in Table 13c for alternating stresses on a weld and accompanying Figure 30h-k.

In each case, since there are six stress components and up to three different section locations for shells (the top, mid and bottom surfaces), there is a total of 18 stress histories per component. Moreover, at junctions there are at least two components that meet at the junction. The particular stress component that is plotted is chosen as follows. First, the component and section location (top/mid/bottom) is taken as the one that has the highest alternating stress. This narrows the selection to six components. Of these, the component having the highest Root Mean Square (RMS) is selected. For comparison the PSDs and cumulative PSDs are also shown for the CLTP load examined in [1] at the shifts producing the highest stress intensity at that load.

The first node (90170) is dominated by a peak centered at near 152 Hz for the +7.5% shifted case (this corresponds to a 142 Hz peak shifted upward by the frequency shift). From the accumulative PSD it is evident that frequency shifting increases this peak, but does not shift its frequency. This is indicative of a peak in the signal moving closer to a structural resonance. A very similar behavior is observed for node 99337 which has a dominant frequency about 52.1 Hz (this was a significant frequency for the CLTP loads also). At the limiting +5% frequency shift this peak grows with frequency shift. The third node (95617) follows a similar behavior (Peak frequency about 69 Hz) whereas the fourth node (89317) exhibits two distinct peaks. Finally for node 87633, several peaks are present. In all cases the CLTP curves are qualitatively very similar to the EPU results after the expected adjustment for gross amplitude is made. This indicates that, as anticipated, neither the acoustic loads nor resulting stress response have developed any significant new peaks.

Another way to characterize the dominant frequencies is to plot the dominant frequency over the dryer surface. For each finite element node the frequency associated with the largest stress harmonic (at any frequency shift) is recorded. A contour map of this dominant frequency is shown in Figure 32. This map is useful in a qualitative sense for identifying what dryer components appear most responsive to particular frequencies. For most of the dryer, including the central section of the outer hoods, the inner hoods and most of the skirt the dominant frequencies are in the 50-60 Hz range as indicated in Figure 32b. From Figure 32b the outer sections of the outer hoods show peak frequencies near 65-75 Hz. The middle hoods respond in the ranges 58-62 Hz whereas the inner hoods respond in the range 45-60 Hz.

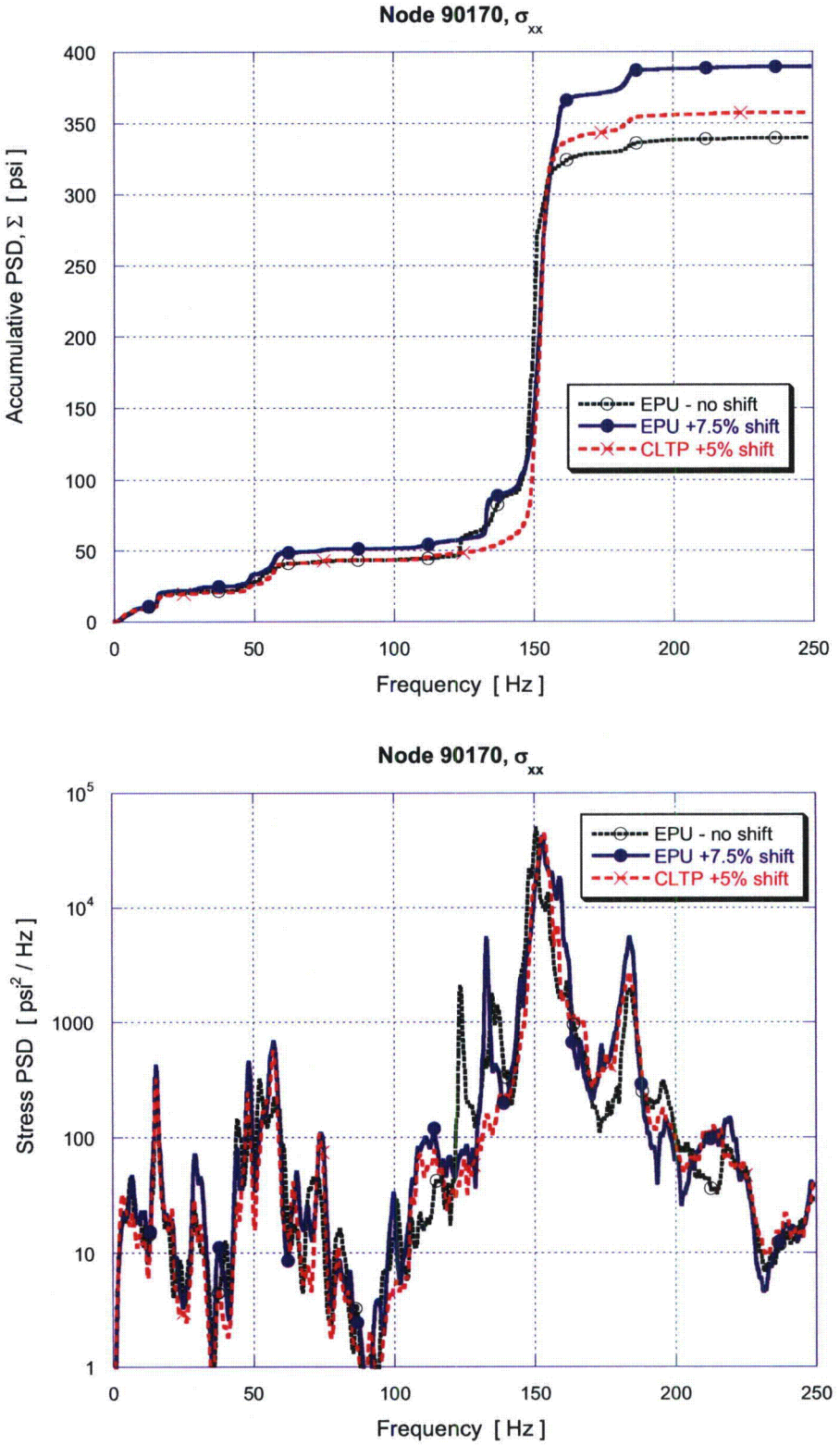

Figure 31a. Accumulative PSD and PSD curves of the σ_{xx} stress response at node 90170.

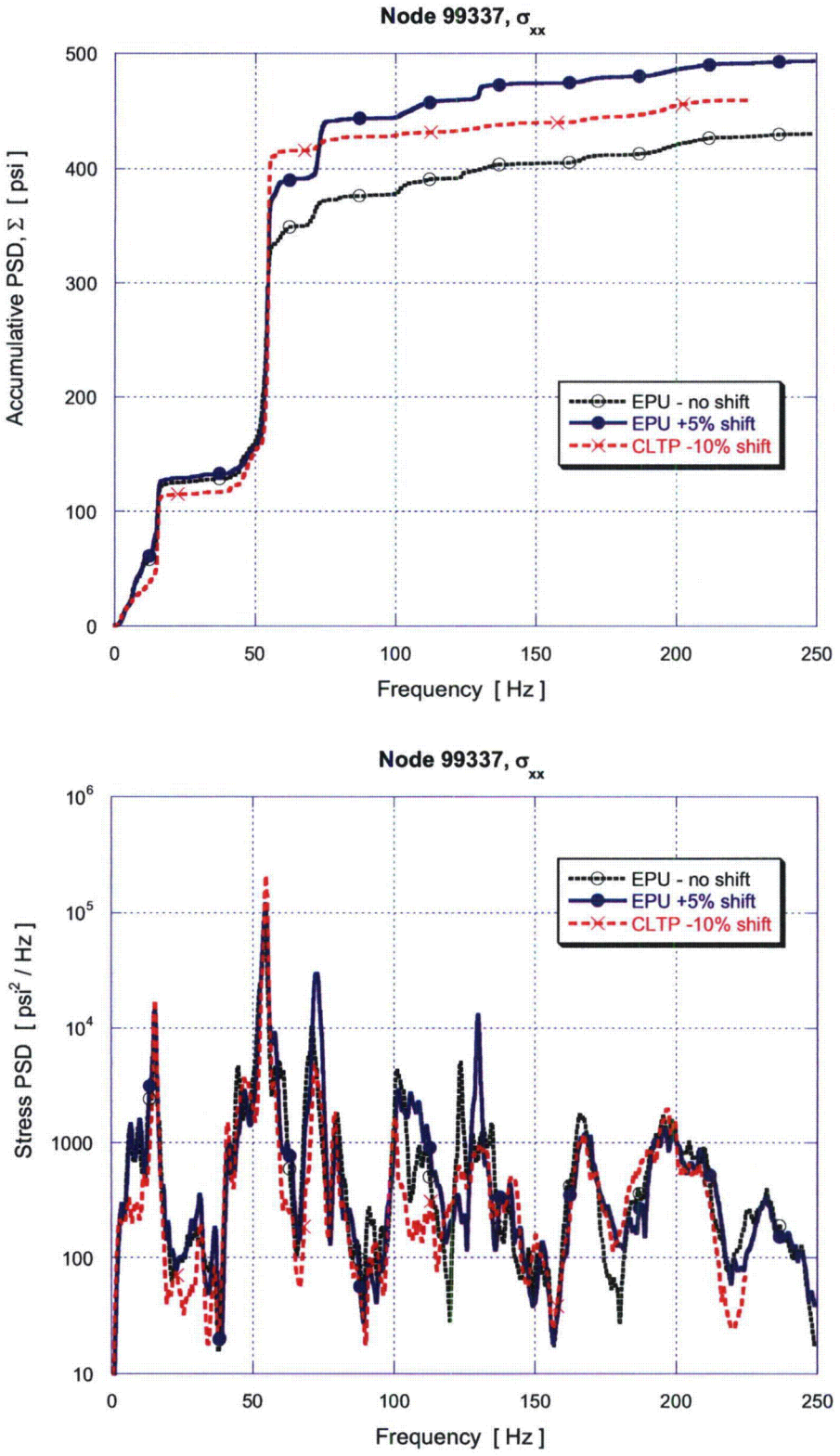

Figure 31b. Accumulative PSD and PSD of the σ_{xx} stress response at node 99337.

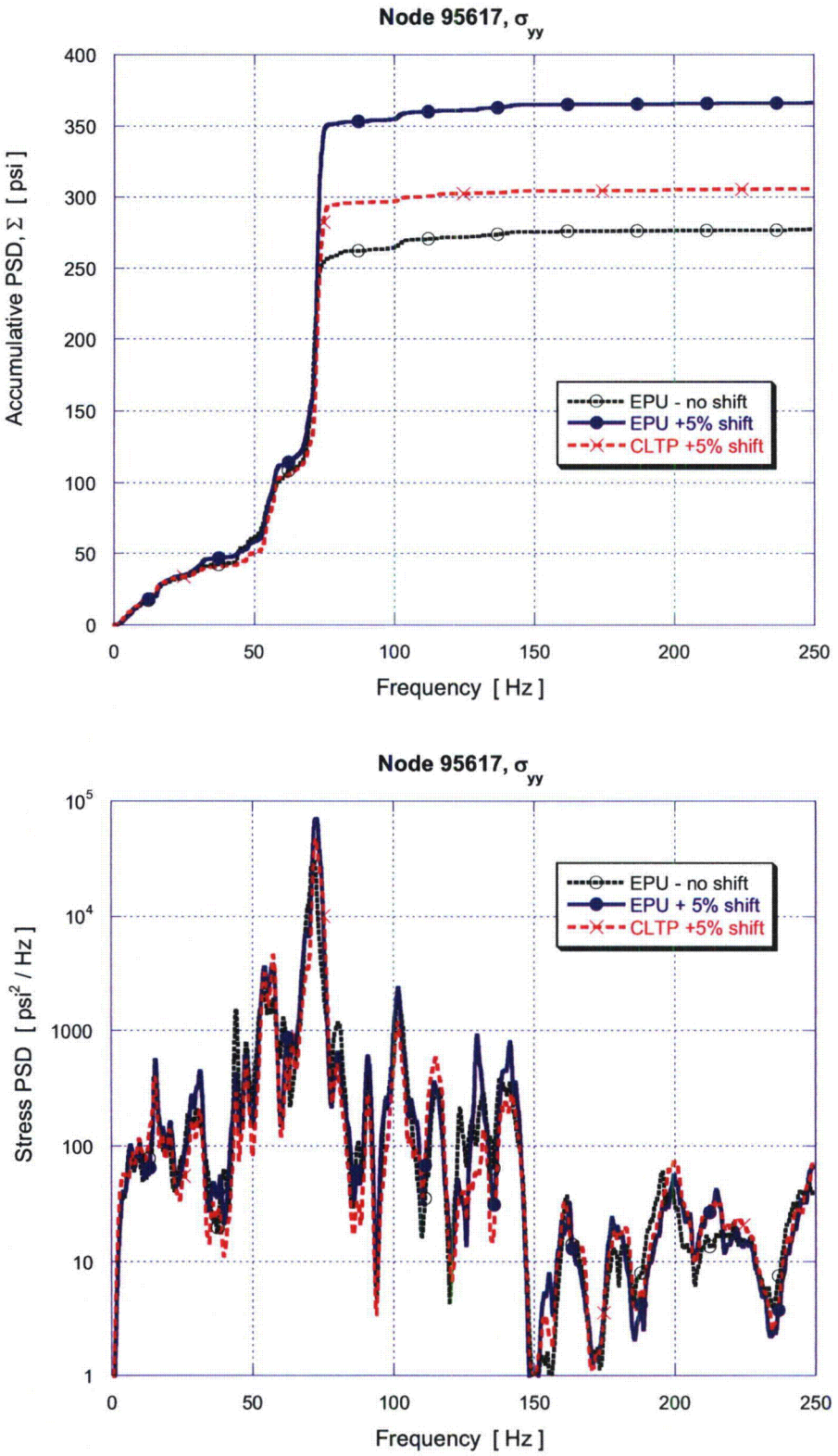

Figure 31c. Accumulative PSD and PSD of the σ_{yy} stress response at node 95617.

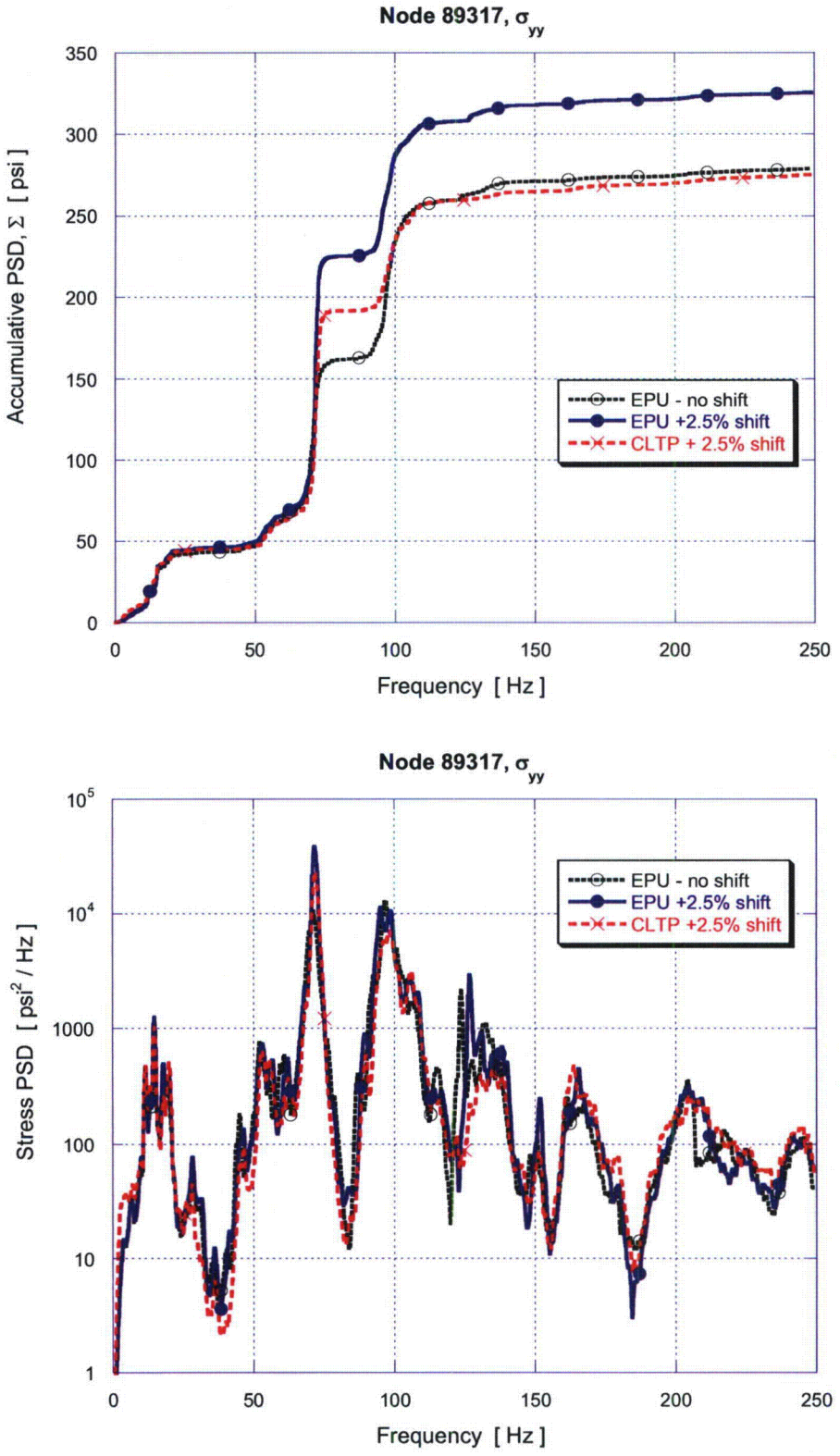

Figure 31d. Accumulative PSD and PSD of the σ_{yy} stress response at node 89317.

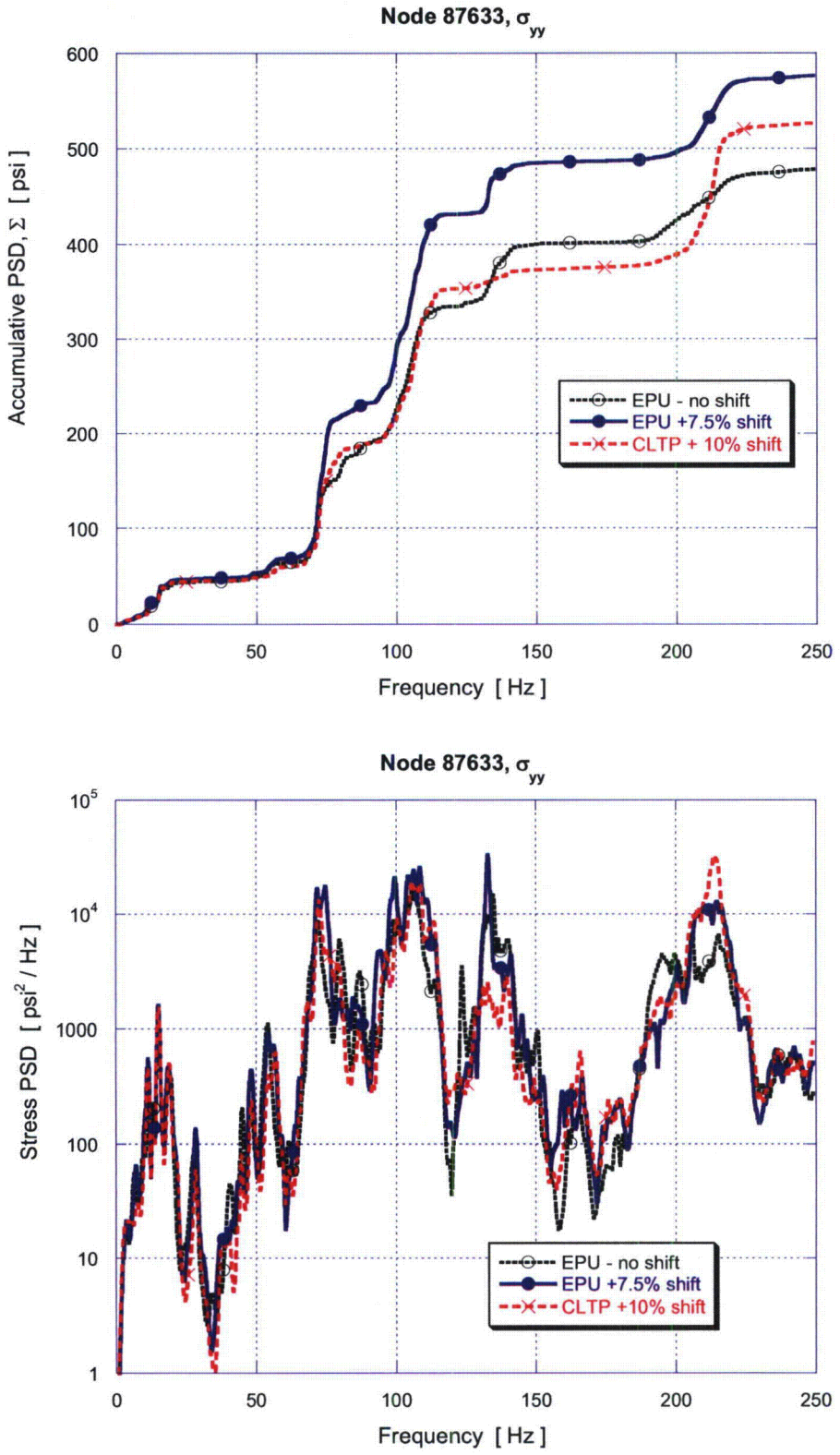

Figure 31e. Accumulative PSD and PSD of the σ_{yy} stress response at node 87633.

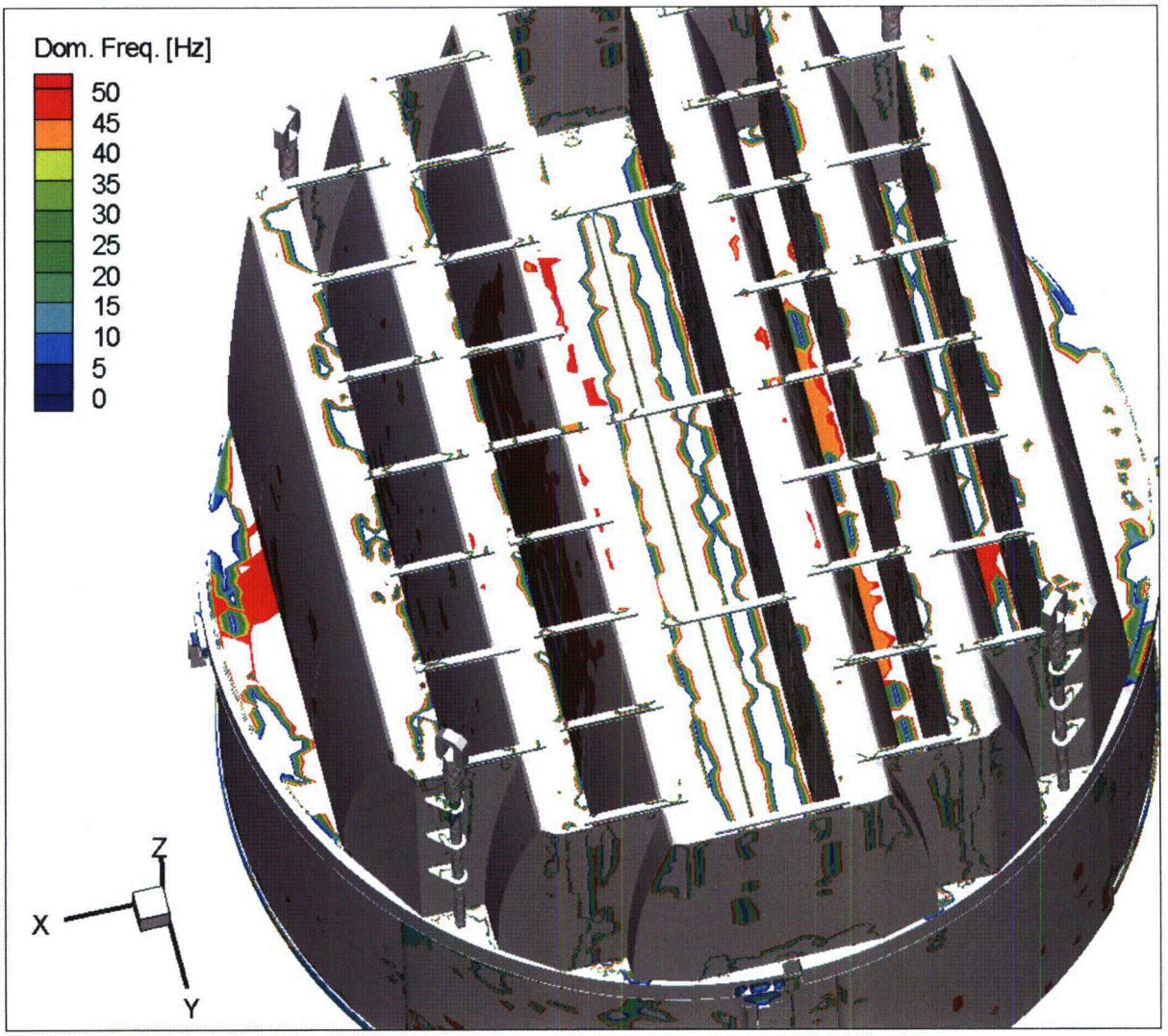

Figure 32a. Contour map showing the dominant frequencies (i.e., the frequency with the largest stress harmonic). This shows locations with dominant frequencies in the range 0-50 Hz.

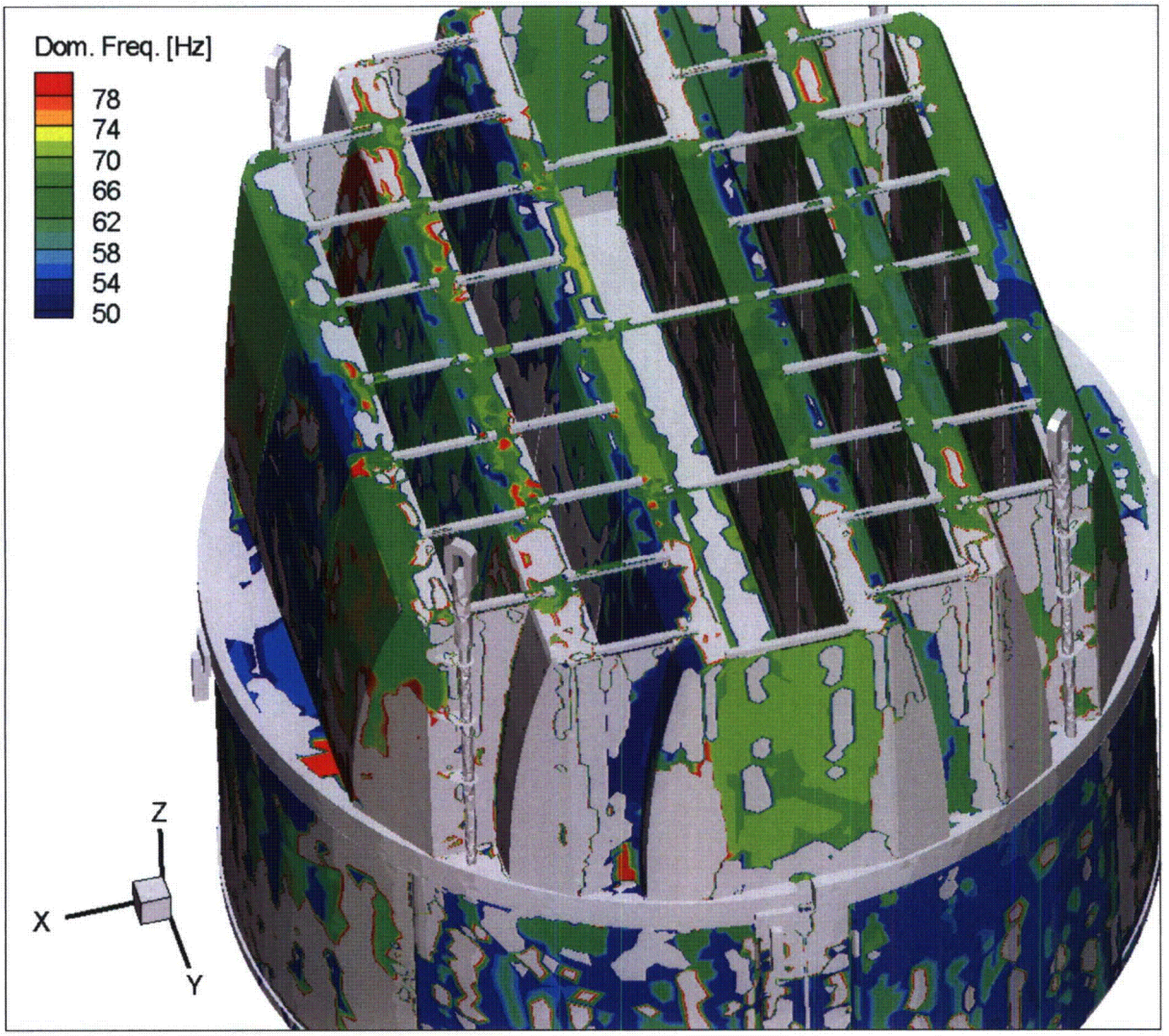

Figure 32b. Contour map showing the dominant frequencies (i.e., the frequency with the largest stress harmonic). This shows locations with dominant frequencies in the range 50-80 Hz.

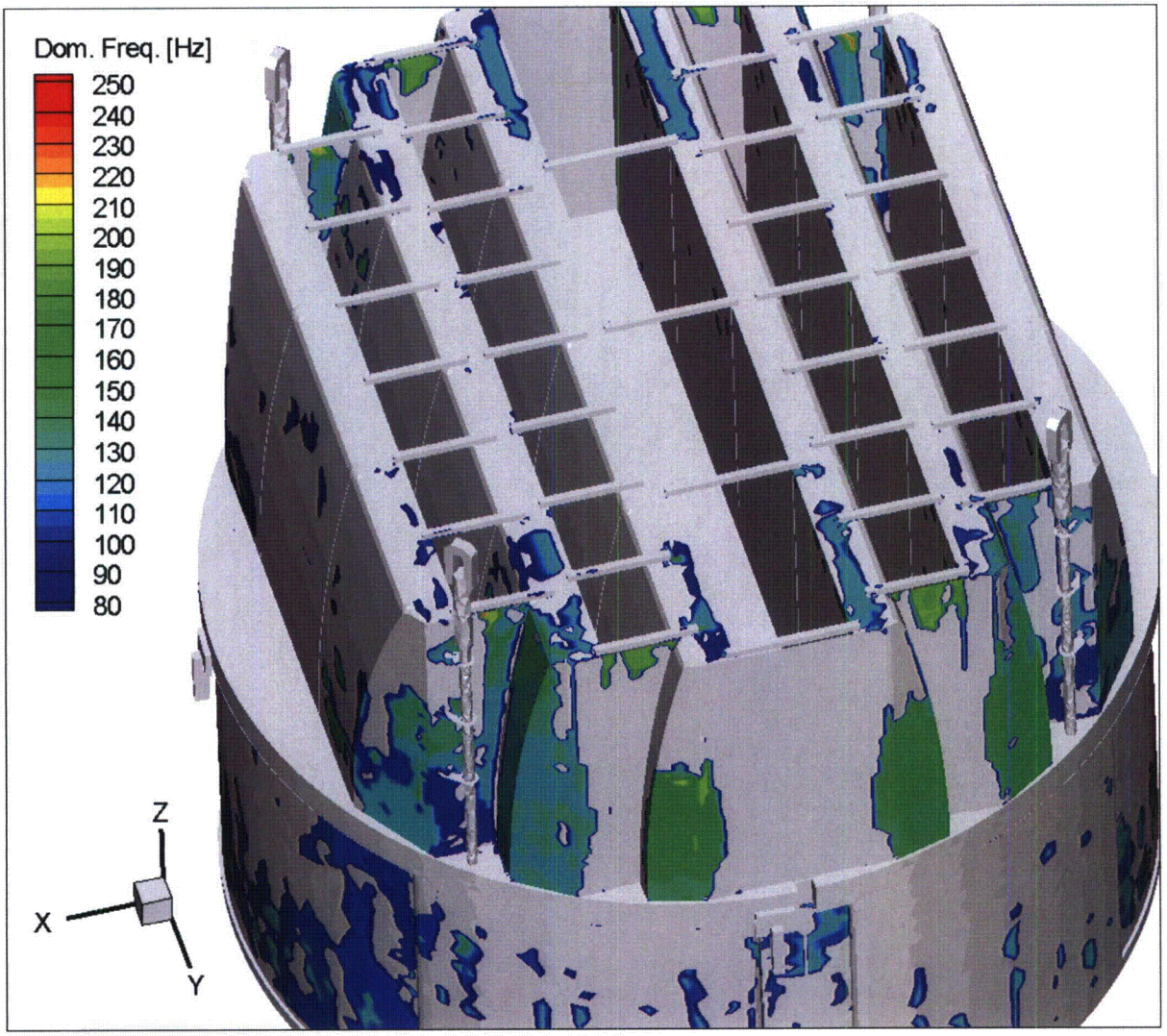

Figure 32c. Contour map showing the dominant frequencies (i.e., the frequency with the largest stress harmonic). This shows locations with dominant frequencies in the range 80-250 Hz.

6.4 Real Time Analysis With (i) 92.5 Hz signal Included and (ii) RCIC Line Closed

As discussed in [5] it was established that during power ascension the MSL B loads were affected by the reactor core isolation cooling (RCIC) steam line configuration. As a result, additional tests and data collections were conducted to define the loads with the RCIC line isolated as described in Appendix C of [5]. In this section the stresses resulting from two additional loads corresponding to different RCIC line configurations are calculated and compared against the baseline EPU loads used in the full steam dryer stress analysis.

The first load adds a 92.5 Hz peak to the baseline 115% CLTP load. This peak was observed in the MSL B data initially collected at 110% CLTP, but was not reproducible in the post-scram recovery. To gage the impact of such a signal at 115% CLTP the peak was scaled and combined with the baseline 115% loads as described in [33]. The second load definition was collected at 115% CLTP with the inboard RCIC valve temporarily closed. This resulted in a narrow peak on MSL B at 89.3 Hz. Both RCIC conditions are considered off-normal conditions corresponding to a short-duration technical specification limiting condition or to a transient loading associated with an unusual steam line drain configuration.

In order to analyze these loads a subset of nodes with smallest stress ratios is selected and stresses re-evaluated at those locations only. The particular set of nodes is selected in a manner similar to that used for real time stress evaluation during power ascension [34]. Specifically the list is comprised of the following nodes:

- All nodes with an EPU alternating stress ratio, SR-a<3.0. There are 41 such nodes on a weld and 7 more located away from a weld.
- The RPS sub-set of nodes with 3.5<SR-a<4 at EPU. There are 36 such nodes on a weld and another 4 away from a weld.
- The RPS set of nodes with SR-P<3 at EPU (skipping those already included in the preceding set). There 18 such nodes on a weld and another node off the weld.

All 107 nodes are processed with three different loads: the baseline EPU loads used in the remainder of this report, the loads with the 92.5 Hz signal artificially added and loads at EPU with the RCIC line closed. The stress intensities are calculated in the same manner as when analyzing the entire dryer and the limiting stresses with frequency shifting included are reported. The resulting stress ratios are summarized in Table 14 together with the dominant frequency.

For most nodes, addition of the 92.5 Hz signal has negligible effect upon the stress intensity. The exceptions occur for those components and limiting locations where the 92.5 Hz signal is the dominant component. The limiting alternating stress ratio is SR-a=2.39.

Closing the RCIC line has a more extended effect where all nodes experience a somewhat different stress with stress changing even when the dominant frequency remains unchanged. The limiting alternating stress ratio is SR-a=2.05.

Table 14. Stresses obtained at 107 locations using: (i) baseline EPU loads; (ii) the same EPU loads with a 92.5 Hz signal added as described in [5, 33] and (iii) at EPU operation with the RCIC line closed.

					EPU			EPU+92.5			RCIC closed		
	node	x	y	z	SR-P	SR-a	freq	SR-P	SR-a	freq	SR-P	SR-a	freq
MINIMUM values over all nodes					**1.25**	**2.49**	**142.0**	**1.25**	**2.39**	**92.5**	**1.27**	**2.05**	**89.3**
All non-weld nodes with SR-a<3													
Inner Hood	81316	-32.4	27.0	72.4	4.86	2.59	60.8	4.85	2.58	60.8	4.42	2.31	52.2
Inner Hood	70703	32.9	-27.2	69.8	5.27	2.66	60.6	5.27	2.66	60.6	4.52	2.25	60.5
Inner Hood	70645	31.7	-31.1	75.6	5.49	2.73	60.6	5.49	2.73	60.6	4.58	2.27	60.5
Inner Hood	70672	32.3	-28.2	73.0	5.26	2.73	60.6	5.25	2.73	60.6	4.51	2.27	60.5
Inner Hood	70588	31.6	-29.0	76.0	5.34	2.75	60.6	5.34	2.75	60.6	4.49	2.30	60.5
Inner Hood	70653	31.8	-33.4	75.1	5.55	2.85	60.6	5.55	2.85	60.6	4.63	2.38	60.5
Inner Hood	70266	31.1	-33.7	78.1	5.83	2.94	60.6	5.82	2.94	60.6	4.88	2.43	60.5
All nodes on weld with SR-a<3													
Vane Bank Plate/Side Plate/End Plate	90170	-24.1	119.0	11.6	4.52	**2.49**	142.0	4.53	2.49	142.0	3.92	2.16	147.4
Hood Support/Outer Cover Plate/Outer Hood	99337	-102.8	-28.4	0.0	2.53	2.54	52.1	2.52	2.53	52.1	2.42	2.51	60.5
Entry Bottom Perf/Side Plate/End Plate	90233	-24.1	119.0	20.0	4.81	2.55	146.1	4.81	2.55	146.1	4.26	2.20	147.4
Hood Support/Outer Cover Plate/Outer Hood	95267	-102.8	28.4	0.0	1.79	2.55	52.1	1.79	2.58	52.1	1.63	2.27	60.5
Entry Bottom Perf/Side Plate/End Plate	90232	-24.1	119.0	21.9	4.80	2.56	146.1	4.80	2.56	146.1	4.23	2.19	147.4
Entry Bottom Perf/Side Plate/End Plate	90234	-24.1	119.0	18.2	4.89	2.58	146.1	4.89	2.58	146.1	4.33	2.22	147.4
Entry Bottom Perf/Side Plate/End Plate	90231	-24.1	119.0	23.7	4.83	2.59	146.1	4.82	2.59	146.1	4.22	2.20	147.4
Side Plate/Top Plate	95617	17.6	0.0	88.0	4.15	2.60	69.4	4.14	2.58	69.4	3.61	2.22	65.2
Side Plate/Top Plate	97693	-49.3	0.0	88.0	4.08	2.60	69.8	4.02	2.56	69.8	3.48	2.13	69.7
Closure Plate/Middle Hood	89317	60.2	-85.2	87.0	2.43	2.60	70.1	2.45	**2.39**	92.5	2.29	2.08	89.3
Side Plate/Top Plate	93031	-80.2	-85.2	88.0	4.57	2.62	69.4	4.50	2.57	69.4	4.18	2.30	69.7
Top Plate/Inner Hood	85512	24.1	-30.6	88.0	5.17	2.67	60.6	5.16	2.67	60.6	4.40	2.20	60.5
Entry Bottom Perf/Side Plate/End Plate	90230	-24.1	119.0	25.6	4.98	2.68	146.1	4.98	2.68	146.1	4.34	2.27	147.4

Entry Bottom Perf/Side Plate/End Plate	90235	-24.1	119.0	16.3	5.14	2.70	146.1	5.14	2.70	146.1	4.49	2.29	147.4
Vane Bank Plate/Entry Bottom Perf/Side Plate/End Plate	90168	-24.1	119.0	14.5	5.14	2.75	146.1	5.14	2.75	146.1	4.44	2.33	147.4
Side Plate/Top Plate	91054	80.2	-85.2	88.0	2.68	2.75	66.0	2.59	2.58	92.5	2.50	2.33	89.3
Side Plate/Top Plate	99455	-80.2	85.2	88.0	2.67	2.78	65.5	2.56	2.58	65.5	2.52	2.40	89.3
Hood Support/Outer Base Plate/Backing Bar	95428	-71.3	0.0	0.0	1.75	2.80	51.2	1.74	2.80	51.2	1.72	2.49	53.8
Top Plate/Inner Hood	99104	-24.1	23.9	88.0	5.66	2.83	60.8	5.66	2.82	60.8	5.32	2.67	52.2
Hood Support/Middle Base Plate Backing Bar/Inner Hood	85723	-39.9	0.0	0.0	1.81	2.84	66.4	1.81	2.74	66.4	1.70	2.36	89.3
Side Plate/Top Plate	85117	-54.0	-54.3	88.0	5.28	2.85	69.4	5.42	2.97	69.4	5.14	2.77	89.3
Entry Bottom Perf/Side Plate/End Plate	90229	-24.1	119.0	27.4	5.19	2.85	146.1	5.19	2.85	146.1	4.56	2.41	147.4
Side Plate/Brace	87633	79.7	-85.2	31.3	3.40	2.86	123.5	3.51	2.83	92.4	3.45	2.66	89.3
Inner Hood/Top Plate	85516	24.1	-23.9	88.0	5.66	2.87	60.6	5.65	2.87	60.6	4.59	2.37	60.5
Inner Hood/Top Plate	90897	24.1	-27.8	88.0	5.16	2.90	60.6	5.16	2.90	60.6	4.66	2.45	60.5
Outer Cover Plate/Outer Hood	95236	-102.8	-1.0	0.0	5.09	2.91	60.6	5.11	2.92	60.6	4.90	2.68	52.2
Outer Cover Plate/Outer Hood	95237	-102.8	1.0	0.0	5.07	2.92	60.6	5.10	2.93	60.6	4.83	2.70	52.2
Top Plate/Inner Hood	99130	-24.1	26.8	88.0	5.55	2.92	60.8	5.55	2.91	60.8	5.26	2.78	61.4
Hood Support/Inner Hood	99540	32.4	0.0	72.5	5.31	2.93	61.3	5.34	2.93	61.3	4.21	2.23	53.8
Top Plate/Inner Hood	99115	-24.1	30.6	88.0	5.71	2.94	60.8	5.75	2.93	60.8	5.27	2.77	52.2
Hood Support/Inner Hood	99541	32.0	0.0	74.4	5.29	2.94	61.3	5.30	2.94	61.3	4.34	2.31	53.8
Vane Bank Plate/Side Plate/End Plate	90169	-24.1	119.0	13.1	5.51	2.94	142.0	5.51	2.94	142.0	4.70	2.49	147.4
Vane Bank Plate/Side Plate/End Plate	90582	24.1	-119.0	11.6	5.17	2.94	147.8	5.18	2.95	147.8	4.67	2.50	148.6
Top Plate/Inner Hood	99132	-24.1	27.8	88.0	5.15	2.95	60.8	5.15	2.94	60.8	4.86	2.78	61.4
Outer Cover Plate/Outer Hood	95238	-102.8	2.9	0.0	5.13	2.95	60.6	5.16	2.95	60.6	4.83	2.73	52.2
Outer Cover Plate/Outer Hood	95234	-102.8	-4.9	0.0	5.24	2.97	60.6	5.24	2.97	60.6	5.10	2.73	52.2
Outer Cover Plate/Outer Hood	95241	-102.8	4.9	0.0	5.13	2.97	60.6	5.16	2.97	60.6	4.78	2.76	52.2
End Plate/Inner Hood	95777	-39.3	115.1	20.5	4.79	2.98	146.1	4.79	2.98	146.1	4.47	2.53	147.4
Tie Bar	137575	17.6	59.8	88.0	2.85	2.98	65.5	2.91	3.02	65.5	2.63	2.29	89.3
Top Plate/Inner Hood	91288	24.1	-26.3	88.0	5.85	2.99	60.6	5.84	2.99	60.6	4.87	2.50	60.5
Tie Bar	138250	17.6	-59.8	88.0	2.88	2.99	69.4	2.90	2.95	92.5	2.64	2.55	89.3

RPS nodes located off weld with 3 < SR-a < 4													
Brace	37811	79.6	85.5	75.8	4.66	3.32	134.3	4.66	3.31	134.3	3.83	2.84	147.4
Inner Hood	70582	31.4	-36.1	77.1	6.72	3.38	60.6	6.71	3.38	60.6	5.67	2.79	60.5
Middle Hood	30488	-64.8	24.8	67.6	7.27	3.68	59.5	7.25	3.68	59.5	5.57	2.76	56.4
Inner Hood	70627	31.8	-16.2	75.4	7.92	3.91	60.6	7.92	3.91	60.6	6.73	3.36	53.8
RPS nodes located on weld with 3 < SR-a < 4													
Outer End Plate/Outer Hood	99213	-97.9	-69.4	58.4	5.74	3.02	69.8	5.82	3.05	69.8	5.62	2.80	69.7
Side Plate/Top Plate	91055	81.1	-85.2	88.0	3.04	3.02	69.5	2.92	2.81	92.5	2.81	2.59	89.3
Outer End Plate/Outer Hood	100731	-101.7	-63.6	27.1	5.67	3.03	91.6	5.34	2.70	92.5	5.49	2.71	89.3
Hood Support/Inner Hood	95645	-36.5	0.0	48.8	5.68	3.04	49.6	5.68	3.04	49.6	4.73	2.47	44.5
Vane Bank Plate/Side Plate/Outer End Plate	90812	87.0	85.2	11.6	3.94	3.15	123.5	4.06	3.22	123.5	3.77	2.82	89.3
Side Plate/Top Plate	103080	49.6	-108.6	88.0	3.11	3.17	92.5	3.21	3.07	92.5	2.39	**2.05**	89.3
Hood Support/Outer Hood	85769	-98.1	-28.4	57.1	6.00	3.20	69.4	5.94	3.17	69.4	5.44	2.90	69.7
Side Plate/Top Plate	101600	-17.6	-119.0	88.0	1.80	3.23	69.8	1.79	3.18	69.8	1.69	2.93	89.3
Hood Support/Inner Hood	90431	-36.8	59.5	46.9	5.89	3.23	49.6	5.90	3.23	49.6	4.75	2.57	52.2
Middle Hood/Top Plate	90947	55.6	-27.9	88.0	5.67	3.24	52.1	5.74	3.26	52.1	5.25	2.76	61.4
Entry Bottom Perf/Side Plate/Outer End Plate	90823	87.0	85.2	29.3	5.88	3.30	96.9	5.94	3.28	96.9	4.78	2.50	89.2
Side Plate/Brace	89650	80.6	85.2	75.8	4.66	3.33	134.3	4.67	3.32	134.3	3.81	2.79	147.4
Hood Support/Middle Hood	98462	63.8	0.0	72.5	6.11	3.33	61.2	6.12	3.34	61.2	6.04	3.38	69.9
Hood Support/Inner Hood	95637	-38.3	0.0	32.9	6.72	3.36	40.3	6.73	3.36	40.3	4.93	2.46	44.5
Outer End Plate/Outer End Plate	95264	95.9	72.4	0.0	6.50	3.37	123.5	6.59	3.37	123.5	5.91	3.18	89.3
Thin Vane Bank Plate/Hood Support/Outer Base Plate	98950	-87.0	-28.4	0.0	3.57	3.40	52.1	3.59	3.47	52.1	3.41	3.72	49.5
Outer Cover Plate/Outer Hood	95251	-102.8	12.7	0.0	5.72	3.43	60.6	5.74	3.43	60.6	5.25	3.24	52.2
Outer End Plate/Outer Hood	94570	100.6	65.3	39.3	6.86	3.44	123.5	6.99	3.50	92.5	5.92	2.95	89.2
End Plate/End Plate Ext	96132	-31.5	117.2	0.0	6.25	3.44	142.0	6.25	3.44	142.0	5.07	2.76	145.5
Hood Support/Outer Hood	91741	-99.8	-28.4	45.3	6.69	3.46	52.1	6.72	3.47	52.1	7.51	3.84	52.2
End Plate/End Plate Ext	96111	-32.7	116.9	0.0	6.48	3.48	142.0	6.47	3.48	142.0	5.23	2.79	145.5
Hood Support/Inner Hood	95821	-32.8	-59.5	70.5	6.73	3.61	60.6	6.73	3.61	60.6	6.83	3.69	60.5

Closure Plate/Middle Hood	91590	-68.7	85.2	42.9	6.72	3.67	69.8	6.62	3.64	69.8	5.67	3.05	69.7
Middle Base Plate/Backing Bar/Inner Hood	84197	-39.9	-108.6	0.0	1.80	3.71	52.1	1.79	3.62	52.1	1.73	2.97	69.7
Hood Support/Inner Hood	99514	39.3	0.0	21.0	7.07	3.71	44.1	7.04	3.71	44.1	6.00	3.07	48.0
Entry Bottom Perf/Side Plate/End Plate	90226	-24.1	119.0	33.0	6.11	3.72	146.1	6.11	3.72	146.1	5.39	3.15	147.4
Hood Support/Middle Hood	98477	68.9	0.0	40.9	7.59	3.74	53.1	7.59	3.75	53.1	6.30	3.16	50.0
Hood Support/Middle Base Plate/Backing Bar/Inner Hood	90468	-39.9	59.5	0.0	2.03	3.77	69.8	2.03	3.75	65.5	1.90	3.34	89.3
Outer End Plate/Outer Hood	99185	-95.7	-72.7	70.1	7.48	3.79	69.8	7.38	3.73	69.8	6.61	3.40	69.7
Top Plate/Inner Hood	99156	-24.1	20.0	88.0	7.58	3.85	60.8	7.57	3.84	60.8	6.94	3.59	52.2
Vane Bank Plate/Hood Support/Middle Base Plate	98968	55.6	-54.3	0.0	2.13	3.87	42.2	2.12	3.85	40.5	2.03	3.21	89.3
Side Plate/Brace	88745	-85.7	-85.2	53.5	7.39	3.91	69.8	7.18	3.59	69.8	6.50	3.29	89.3
Outer End Plate/Outer Hood	94561	102.4	62.5	14.8	7.28	3.96	123.5	7.33	3.88	123.5	6.65	3.31	89.2
Hood Support/Outer Base Plate/Backing Bar	100204	71.3	54.3	0.0	4.16	3.97	147.8	4.17	3.96	147.8	4.02	3.27	53.8
Hood Support/Middle Hood	99416	63.8	54.3	72.5	7.63	3.97	53.1	7.67	3.97	53.1	8.17	4.17	60.5
Vane Bank Plate/Hood Support/Inner Base Plate	85191	24.1	-59.5	0.0	1.82	4.00	52.2	1.77	4.03	92.5	1.67	3.25	89.3
Non weld RPS nodes with SR-P < 3													
Inner Side Plate	37229	3.1	119.0	0.5	2.22	16.78	70.8	2.22	16.16	69.8	2.20	15.56	89.3
RPS nodes located on weld with SR-P < 3													
USR/Support/Seismic Block	113554	-6.9	-122.3	-9.5	1.25	6.15	14.2	1.25	6.12	14.2	1.27	6.48	16.9
Side Plate Ext/Inner Base Plate	94143	16.3	119.0	0.0	1.31	9.65	101.0	1.32	9.95	92.4	1.29	8.02	89.3
Tie Bar	141275	49.3	108.1	88.0	1.45	5.40	91.1	1.45	5.36	92.5	1.38	4.11	89.3
Top Thick Plate/Side Plate/Closure Plate/Top Plate	91558	-47.1	-108.6	88.0	1.56	5.32	195.5	1.57	5.33	191.3	1.58	5.42	190.8
Inner Side Plate/Inner Base Plate	99200	-2.3	-119.0	0.0	1.67	7.67	69.8	1.65	7.33	69.8	1.67	6.97	89.3
Side Plate/Top Plate	91215	17.6	119.0	88.0	1.78	3.46	69.8	1.78	3.31	92.5	1.62	2.40	89.3
Hood Support/Middle Base Plate/Backing Bar/Inner Hood	88639	39.9	0.0	0.0	1.79	3.42	40.5	1.78	3.36	40.5	1.70	2.65	89.2
Vane Bank Plate/Hood Support/Inner Base Plate	99487	-24.1	59.5	0.0	1.81	4.38	44.9	1.76	3.89	92.5	1.73	3.96	53.7
Outer Cover Plate/Outer Hood	94498	102.8	-58.1	0.0	1.91	6.41	10.5	1.91	6.43	10.5	1.88	5.76	10.9
Vane Bank Plate/Hood Support/Inner Base Plate	91888	-24.1	0.0	0.0	2.17	4.33	45.5	2.17	3.97	92.5	2.04	3.36	89.3

Tie Bar	141237	25.0	108.1	88.0	2.32	6.62	70.3	2.36	6.72	92.4	2.24	5.09	89.3
USR/Seismic Block/Support	113508	-122.1	10.2	-9.5	2.38	10.42	52.1	2.38	10.36	52.1	2.28	9.31	89.3
Closure Plate/Inner Hood	95172	28.8	-108.6	87.0	2.38	4.21	66.4	2.32	3.99	92.5	1.90	2.41	89.3
Vane Bank Plate/Hood Support/Outer Base Plate	98956	-87.0	28.4	0.0	2.65	4.02	50.1	2.60	3.97	50.1	2.56	3.94	60.5
Hood Support/Outer Base Plate/Backing Bar	95000	71.3	-54.3	0.0	2.76	4.47	147.8	2.77	4.50	147.8	2.66	3.89	89.3
Submerged Skirt/Drain Channel	95139	91.0	-76.7	-100.0	2.89	4.73	51.5	2.89	4.74	51.5	2.72	3.78	89.3
Tie Bar	140202	-80.8	84.7	88.0	2.93	4.46	65.5	2.81	4.14	65.5	2.66	3.65	89.3
Tie Bar	140238	-56.4	84.7	88.0	2.94	6.42	69.4	2.96	6.57	69.4	3.07	6.75	89.3

7. Conclusions

A stress evaluation of the NMP2 steam dryer with the modifications described in Section 5 and summarized in Table 10 has been carried out using acoustic loads collected at EPU (115% CLTP) conditions. The analysis calculates the stresses arising when the steam dryer is subjected to acoustic loads inferred from strain gage measurements on the main steam lines and a calibrated acoustic circuit model (ACM, Rev. 4.1) that uses these measurements to obtain the acoustic loads on the dryer. The ANSYS FEA package is then used to acquire the dryer stress response resulting from these acoustic loads and the stress results post-processed to obtain the limiting alternating stress ratios. The results account for all biases and uncertainties identified for both the ACM Rev. 4.1 and the FEA harmonic analysis.

The stress evaluation shows that the limiting alternating stress ratio on the dryer with all modifications implemented is SR-a=2.49 and occurs on the inner vane bank welded side plate/end plate junction. The limiting stress ratio due to a maximum stress is SR-P=1.25. These stress estimates represent the limiting values after all frequency shifts in the ±10% frequency range are considered and all end-to-end bias and uncertainties have been imposed.

These stress ratios qualify the steam dryer for EPU operation.

During power ascension testing NMP identified two off-normal loading conditions associated with the operational lineup of the RCIC system that create either a 92.5 Hz (RCIC steam line drains isolated) or a 89.25 Hz content (RCIC steamline isolated)on the MSL B. Therefore a real time analysis is performed using both estimated and measured EPU loads from the test data. The resulting limiting alternating stress ratio is shown to be SR-a=2.39 with 92.5 Hz content and SR-a=2.05 with 89.25 Hz content. In each case the required stress margin is met.

8. References

1. Continuum Dynamics, Inc. (2011) *Stress Evaluation of Nine Mile Point Unit 2 Steam Dryer Using ACM Rev. 4.1 Acoustic Loads*. C.D.I. Report No. 11-04P (Proprietary), Rev. 0, May.
2. Continuum Dynamics, Inc. (2010) *Design and Stress Evaluation of Nine Mile Point Unit 2 Steam Dryer Modifications for EPU Operation*. C.D.I. Report No. 10-12P (Proprietary), July.
3. *ASME Boiler and Pressure Vessel Code, Section III, Subsection NG (2007)*.
4. Continuum Dynamics, Inc. (2011) *ACM Rev. 4.1: Methodology to Predict Full Scale Steam Dryer Loads from In-Plant Measurements (Rev. 3)*. C.D.I. Report No. 10-09P (Proprietary), November.
5. Continuum Dynamics, Inc. (2012) *Acoustic and Low-Frequency Hydrodynamic Loads at 115% CLTP Target Power Level on Nine Mile Point Unit 2 Steam Dryer to 250 Hz Using ACM Rev. 4.1 (Rev. 0)*. C.D.I. Report No. 12-20P (Proprietary), September.
6. Continuum Dynamics, Inc. (2012) *Stress Evaluations of Nine Mile Point Steam Dryer Modifications*. C.D.I. Technical Memo 12-03, Rev. 0, January.
7. Continuum Dynamics, Inc. (2011) *Sub-Modeling in the Nine Mile Point Unit 2 Steam Dryer, Rev. 0*. C.D.I. Report No. 11-03P (Proprietary), June.
8. Continuum Dynamics, Inc. (2007) *Methodology to Predict Full Scale Steam Dryer Loads from In-Plant Measurements, with the Inclusion of a Low Frequency Hydrodynamic Contribution*. C.D.I. Report No. 07-09P (Proprietary).
9. Continuum Dynamics, Inc. (2005) *Methodology to Determine Unsteady Pressure Loading on Components in Reactor Steam Domes (Rev. 6)*. C.D.I. Report No. 04-09 (Proprietary).
10. Continuum Dynamics, Inc. (2010) *Stress Assessment of Nine Mile Point Unit 2 Steam Dryer Using the Acoustic Circuit Model Rev. 4.1*. C.D.I. Report No. 10-11P (Proprietary), June.
11. Continuum Dynamics, Inc. (2010) *Acoustic and Low-Frequency Hydrodynamic Loads at CLTP Power Level on Nine Mile Point Unit 2 Steam Dryer to 250 Hz Using ACM Rev. 4.1 (Rev. 2)*. C.D.I. Report No. 10-10P (Proprietary), January.
12. ANSYS, *Release 10.0 Complete User's Manual Set, (http://www.ansys.com)*.
13. Continuum Dynamics, Inc. (2007) *Response to NRC Request for Additional Information on the Hope Creek Generating Station, Extended Power Uprate*. RAI No. 14.110.
14. Continuum Dynamics, Inc. (2008) *Stress Assessment of Hope Creek Unit 1 Steam Dryer Based on Revision 4 Loads Model, Rev. 4*. C.D.I. Report No. 07-17P (Proprietary).
15. Press, W.H., et al., *Numerical Recipes*. 2 ed. 1992: Cambridge University Press.
16. Structural Integrity Associates, Inc. (2010) *Flaw Evaluation of Indications in the Nine Mile Point Unit 2 Steam Dryer Vertical Support Plates Considering Extended Power Uprate Flow Induced Vibration Loading (Rev. 0)*. SIA Calculation Package No. 1000814.401, July.
17. Continuum Dynamics, Inc. (2009) *Stress Assessment of Nine Mile Point Unit 2 Steam Dryer at CLTP and EPU Conditions, Rev. 1*. C.D.I. Report No. 09-26P (Proprietary), December.

18. Structural Integrity Associates, Inc. (2008) *Flaw Evaluation and Vibration Assessment of the Nine Mile Point Unit 2 Steam Dryer for Extended Power Uprate Operating Conditions*. Report No. 0801273.401.
19. Continuum Dynamics, Inc. (2008) *Stress Assessment of Browns Ferry Nuclear Unit 1 Steam Dryer, Rev. 0*. C.D.I. Report No. 08-06P (Proprietary).
20. O'Donnell, W.J., *Effective Elastic Constants For the Bending of Thin Perforated Plates With Triangular and Square Penetration Patterns*. ASME Journal of Engineering for Industry, 1973. **95**: p. 121-128.
21. de Santo, D.F., *Added Mass and Hydrodynamic Damping of Perforated Plates Vibrating In Water*. Journal of Pressure Vessel Technology, 1981. **103**: p. 175-182.
22. Idel'chik, I E. and E. Fried, *Flow Resistance, a Design Guide for Engineers*. 1989, Washington D.C.: Taylor & Francis. pg. 260.
23. Continuum Dynamics, Inc. (2007) *Dynamics of BWR Steam Dryer Components*. C.D.I. Report No. 07-11P.
24. U.S. Nuclear Regulatory Commission (2007) *Comprehensive Vibration Assessment Program for Reactor Internals During Preoperational and Initial Startup Testing*. Regulatory Guide 1.20, March.
25. Weld Research Council (1998) *Fatigue Strength Reduction and Stress Concentration Factors For Welds In Pressure Vessels and Piping*. WRC Bulletin 432.
26. Pilkey, W.D., *Peterson's Stress Concentration Factors, 2nd ed.* 1997, New York: John Wiley. pg. 139.
27. Lawrence, F.V., N.-J. Ho, and P.K. Mazumdar, *Predicting the Fatigue Resistance of Welds*. Ann. Rev. Mater. Sci., 1981. **11**: p. 401-425.
28. General Electric (GE) Nuclear Energy, *Supplement 1 to Service Information Letter (SIL) 644, "BWR/3 Steam Dryer Failure," September 5*. 2003.
29. Tecplot, Inc. (2004) *Documentation: Tecplot User's Manual Version 10 Tecplot, Inc.*, October.
30. Continuum Dynamics, Inc. (2009) *Compendium of Nine Mile Point Unit 2 Steam Dryer Sub-Models Away From Closure Plates* C.D.I. Technical Note No. 09-16P (Proprietary), August.
31. Structural Integrity Associates, Inc. (2009) *Nine Mile Point Unit 2 Steam Dryer Closure Plates Analysis Results*. SIA Letter Report No. 0900895.401 Revision 0, August 21.
32. Westinghouse (2011) *NMP2 Steam Dryer Modifications and Repairs*. FCN-MODS-NMP2-11, Rev. 1.
33. Continuum Dynamics, Inc. (2012) *Limit Curves with ACM Rev. 4.1 for the 115% Power Level Basis with 92.5 Hz Peak at Nine Mile Point Unit 2 (Rev. 0)*. C.D.I. Technical Note No. 12-28 (Proprietary). September.
34. Continuum Dynamics, Inc. (2012) *Real Time Monitoring of the Nine Mile Point Steam during Power Ascension*. C.D.I. Technical Note No. 12-17P (Proprietary). June.

ATTACHMENT 3

AFFIDAVIT FROM CONTINUUM DYNAMICS, INCORPORATED (CDI) JUSTIFYING WITHHOLDING PROPRIETARY INFORMATION (CDI REPORT NO. 12-18P)

Continuum Dynamics, Inc.

(609) 538-0444 (609) 538-0464 fax 34 Lexington Avenue Ewing, NJ 08618-2302

AFFIDAVIT

Re: C.D.I. Report No. 12-18P "Stress Evaluation of Nine Mile Point Unit 2 Steam Dryer at 115% CLTP," Revision 0

I, Alan J. Bilanin, being duly sworn, depose and state as follows:

1. I hold the position of President and Senior Associate of Continuum Dynamics, Inc. (hereinafter referred to as C.D.I.), and I am authorized to make the request for withholding from Public Record the Information contained in the document described in Paragraph 2. This Affidavit is submitted to the Nuclear Regulatory Commission (NRC) pursuant to 10 CFR 2.390(a)(4) based on the fact that the attached information consists of trade secret(s) of C.D.I. and that the NRC will receive the information from C.D.I. under privilege and in confidence.

2. The Information sought to be withheld, as transmitted to Constellation Energy Group as attachment to C.D.I. Letter No. 12115 dated 17 October 2012, C.D.I. Report No. 12-18P "Stress Evaluation of Nine Mile Point Unit 2 Steam Dryer at 115% CLTP," Revision 0. The proprietary information is identified by its enclosure within pairs of double square brackets ("[[ ]]"). In each case, the superscript notation $^{(3)}$ refers to Paragraph 3 of this affidavit that provides the basis for the proprietary determination.

3. The Information summarizes:

   (a) a process or method, including supporting data and analysis, where prevention of its use by C.D.I.'s competitors without license from C.D.I. constitutes a competitive advantage over other companies;
   (b) Information which, if used by a competitor, would reduce his expenditure of resources or improve his competitive position in the design, manufacture, shipment, installation, assurance of quality, or licensing of a similar product;
   (c) Information which discloses patentable subject matter for which it may be desirable to obtain patent protection.

   The information sought to be withheld is considered to be proprietary for the reasons set forth in paragraphs 3(a), 3(b) and 3(c) above.

4. The Information has been held in confidence by C.D.I., its owner. The Information has consistently been held in confidence by C.D.I. and no public disclosure has been made and it is not available to the public. All disclosures to third parties, which have been limited, have been made pursuant to the terms and conditions contained in C.D.I.'s Nondisclosure Secrecy Agreement which must be fully executed prior to disclosure.

5. The Information is a type customarily held in confidence by C.D.I. and there is a rational basis therefore. The Information is a type, which C.D.I. considers trade secret and is held in confidence by C.D.I. because it constitutes a source of competitive advantage in the competition and performance of such work in the industry. Public disclosure of the Information is likely to cause substantial harm to C.D.I.'s competitive position and foreclose or reduce the availability of profit-making opportunities.

I declare under penalty of perjury that the foregoing affidavit and the matters stated therein are true and correct to be the best of my knowledge, information and belief.

Executed on this 17th day of October 2012.

Alan J. Bilanin
Continuum Dynamics, Inc.

Subscribed and sworn before me this day: October 17 2012

Eileen P. Burmeister, Notary Public

EILEEN P BURMEISTER
NOTARY PUBLIC
STATE OF NEW JERSEY
My Commission Expires May 06 , 2017